NUREG-1824 EPRI 1011999
Final Report

Verification and Validation of Selected Fire Models for Nuclear Power Plant Applications

Volume 2:
Experimental Uncertainty

U.S. Nuclear Regulatory Commission
Office of Nuclear Regulatory Research
Washington, DC 20555-0001

Electric Power Research Institute
3420 Hillview Avenue
Palo Alto, CA 94303

Verification & Validation of Selected Fire Models for Nuclear Power Plant Applications

Volume 2: Experimental Uncertainty

NUREG-1824 **EPRI 1011999**

Final Report

May 2007

U.S. Nuclear Regulatory Commission
Office of Nuclear Regulatory Research (RES)
Two White Flint North, 11545 Rockville Pike
Rockville, MD 20852-2738

U.S. NRC-RES Project Manager
M. H. Salley

Electric Power Research Institute (EPRI)
3420 Hillview Avenue
Palo Alto, CA 94303

EPRI Project Manager
R.P. Kassawara

DISCLAIMER OF WARRANTIES AND LIMITATION OF LIABILITIES

ORGANIZATION(S) THAT PREPARED THIS DOCUMENT:

U.S. Nuclear Regulatory Commission, Office of Nuclear Regulatory Research

Science Applications International Corporation

National Institute of Standards and Technology

NOTE

For further information about EPRI, call the EPRI Customer Assistance Center at 800.313.3774 or e-mail askepri@epri.com.

CITATIONS

This report was prepared by

U.S. Nuclear Regulatory Commission,
Office of Nuclear Regulatory Research (RES)
Two White Flint North, 11545 Rockville Pike
Rockville, MD 20852-2738
Principal Investigators:
K. Hill
J. Dreisbach

Electric Power Research Institute (EPRI)
3420 Hillview Avenue
Palo Alto, CA 94303
Science Applications International Corp (SAIC)
4920 El Camino Real
Los Altos, CA 94022
Principal Investigators:
F. Joglar
B. Najafi

National Institute of Standards and Technology
Building Fire Research Laboratory (BFRL)
100 Bureau Drive, Stop 8600
Gaithersburg, MD 20899-8600
Principal Investigators:
K McGrattan
R. Peacock
A. Hamins

Volume 1, Main Report: B. Najafi, F. Joglar, J. Dreisbach
Volume 2, Experimental Uncertainty: A. Hamins, K. McGrattan
Volume 3, FDT^S: J. Dreisbach, K. Hill
Volume 4, FIVE-Rev1: F. Joglar
Volume 5, CFAST: R. Peacock, P. Reneke (NIST)
Volume 6, MAGIC: F. Joglar, B. Guatier (EdF), L. Gay (EdF), J. Texeraud (EdF)
Volume 7, FDS: K. McGrattan

This report describes research sponsored jointly by U.S. Nuclear Regulatory Commission, Office of Nuclear Regulatory Research (RES), and Electric Power Research Institute (EPRI).

The report is a corporate document that should be cited in the literature in the following manner:

Verification and Validation of Selected Fire Models for Nuclear Power Plant Applications, Volume 2: Experimental Uncertainty, U.S. Nuclear Regulatory Commission, Office of Nuclear Regulatory Research (RES), Rockville, MD, 2007, and Electric Power Research Institute (EPRI), Palo Alto, CA, NUREG-1824 and EPRI 1011999.

ABSTRACT

There is a movement to introduce risk-informed and performance-based analyses into fire protection engineering practice, both domestically and worldwide. This movement exists in the general fire protection community, as well as the nuclear power plant (NPP) fire protection community. The U.S. Nuclear Regulatory Commission (NRC) has used risk-informed insights as part of its regulatory decision marking since the 1990s.

In 2002, the National Fire Protection Association (NFPA) developed NFPA 805, *Performance-Based Standard for Fire Protection for Light-Water Reactor Electric Generating Plants, 2001 Edition.* In July 2004, the NRC amended its fire protection requirements in Title 10, Section 50.48, of the *Code of Federal Regulations* (10 CFR 50.48) to permit existing reactor licensees to voluntarily adopt fire protection requirements contained in NFPA 805 as an alternative to the existing deterministic fire protection requirements. In addition, the NPP fire protection community has been using risk-informed, performance-based (RI/PB) approaches and insights to support fire protection decision-making in general.

One key tool needed to further the use of RI/PB fire protection is the availability of verified and validated fire models that can reliably predict the consequences of fires. Section 2.4.1.2 of NFPA 805 requires that only fire models acceptable to the Authority Having Jurisdiction (AHJ) shall be used in fire modeling calculations. Furthermore, Sections 2.4.1.2.2 and 2.4.1.2.3 of NFPA 805 state that fire models shall only be applied within the limitations of the given model, and shall be verified and validated.

This report is the first effort to document the verification and validation (V&V) of five fire models that are commonly used in NPP applications. The project was performed in accordance with the guidelines that the American Society for Testing and Materials (ASTM) set forth in ASTM E 1355, *Standard Guide for Evaluating the Predictive Capability of Deterministic Fire Models*. The results of this V&V are reported in the form of ranges of accuracies for the fire model predictions.

FOREWORD

Fire modeling and fire dynamics calculations are used in a number of fire hazards analysis (FHA) studies and documents, including fire risk analysis (FRA) calculations; compliance with, and exemptions to the regulatory requirements for fire protection in 10 CFR Part 50; the Significance Determination Process (SDP) used in the inspection program conducted by the U.S. Nuclear Regulatory Commission (NRC); and, most recently, the risk-informed performance-based (RI/PB) voluntary fire protection licensing basis established under 10 CFR 50.48(c). The RI/PB method is based on the National Fire Protection Association (NFPA) Standard 805, *Performance-Based Standard for Fire Protection for Light-Water Reactor Generating Plants*.

The seven volumes of this NUREG-series report provide technical documentation concerning the predictive capabilities of a specific set of fire dynamics calculation tools and fire models for the analysis of fire hazards in postulated nuclear power plant (NPP) scenarios. Under a joint memorandum of understanding (MOU), the NRC Office of Nuclear Regulatory Research (RES) and the Electric Power Research Institute (EPRI) agreed to develop this technical document for NPP application of these fire modeling tools. The objectives of this agreement include creating a library of typical NPP fire scenarios and providing information on the ability of specific fire models to predict the consequences of those typical NPP fire scenarios. To meet these objectives, RES and EPRI initiated this collaborative project to provide an evaluation, in the form of verification and validation (V&V), for a set of five commonly available fire modeling tools.

The road map for this project was derived from NFPA 805 and the American Society for Testing and Materials (ASTM) Standard E 1355, *Standard Guide for Evaluating the Predictive Capability of Deterministic Fire Models*. These industry standards form the methodology and process used to perform this study. Technical review of fire models is also necessary to ensure that those using the models can accurately assess the adequacy of the scientific and technical bases for the models, select models that are appropriate for a desired use, and understand the levels of confidence that can be attributed to the results predicted by the models. This work was performed using state-of-the-art fire dynamics calculation methods/models and the most applicable fire test data. Future improvements in the fire dynamics calculation methods/models and additional fire test data may impact the results presented in the seven volumes of this report.

This document does not constitute regulatory requirements, and NRC participation in this study neither constitutes nor implies regulatory approval of applications based on the analysis contained in this text. The analyses documented in this report represent the combined efforts of individuals from RES and EPRI. Both organizations provided specialists in the use of fire models and other FHA tools to support this work. The results from this combined effort do not constitute either a regulatory position or regulatory guidance. Rather, these results are intended to provide technical analysis of the predictive capabilities of five fire dynamic calculation tools, and they may also help to identify areas where further research and analysis are needed.

Brian W. Sheron, Director
Office of Nuclear Regulatory Research
U.S. Nuclear Regulatory Commission

CONTENTS

FIGURES

TABLES

REPORT SUMMARY

This report documents the verification and validation (V&V) of five selected fire models commonly used in support of risk-informed and performance-based (RI/PB) fire protection at nuclear power plants (NPPs).

Background

Since the 1990s, when it became the policy of the NRC to use risk-informed methods to make regulatory decisions where possible, the nuclear power industry has been moving from prescriptive rules and practices toward the use of risk information to supplement decision-making. Several initiatives have furthered this transition in the area of fire protection. In 2001, the National Fire Protection Association (NFPA) completed the development of NFPA Standard 805, *Performance-Based Standard for Fire Protection for Light-Water Reactor Electric Generating Plants*, 2001 Edition. Effective July 16, 2004, the NRC amended its fire protection requirements in Title 10, Section 50.48(c), of the *Code of Federal Regulations* [10 CFR 50.48(c)] to permit existing reactor licensees to voluntarily adopt fire protection requirements contained in NFPA 805 as an alternative to the existing deterministic fire protection requirements. RI/PB fire protection often relies on fire modeling for determining the consequence of fires. NFPA 805 requires that the "fire models shall be verified and validated," and "only fire models that are acceptable to the Authority Having Jurisdiction (AHJ) shall be used in fire modeling calculations."

Objectives

- To perform V&V studies of selected fire models using a consistent methodology (ASTM I 1335)
- To investigate the specific fire modeling issue of interest to NPP fire protection applications
- To quantify fire model predictive capabilities to the extent that can be supported by comparison with selected and available experimental data.

Approach

This project team performed V&V studies on five selected models: (1) NRC's NUREG-1805 Fire Dynamics Tools (FDTS), (2) EPRI's Fire-Induced Vulnerability Evaluation Revision 1 (FIVE-Rev1), (3) National Institute of Standards and Technology's (NIST) Consolidated Model of Fire Growth and Smoke Transport (CFAST), (4) Electricité de France's (EdF) MAGIC, and (5) NIST's Fire Dynamics Simulator (FDS). The team based these studies on the guidelines of the ASTM E 1355, *Standard Guide for Evaluating the Predictive Capability of Deterministic Fire Models*. The scope of these V&V studies was limited to the capabilities of the selected fire models and did not cover certain potential fire scenarios that fall outside the capabilities of these fire models.

Results

The results of this study are presented in the form of relative differences between fire model predictions and experimental data for fire modeling attributes such as plume temperature that are important to NPP fire modeling applications. While the relative differences sometimes show agreement, they also show both under-prediction and over-prediction in some circumstances. These relative differences are affected by the capabilities of the models, the availability of accurate applicable experimental data, and the experimental uncertainty of these data. The project team used the relative differences, in combination with some engineering judgment as to the appropriateness of the model and the agreement between model and experiment, to produce a graded characterization of each fire model's capability to predict attributes important to NPP fire modeling applications.

This report does not provide relative differences for all known fire scenarios in NPP applications. This incompleteness is attributable to a combination of model capability and lack of relevant experimental data. The first problem can be addressed by improving the fire models, while the second problem calls for more applicable fire experiments.

EPRI Perspective

The use of fire models to support fire protection decision-making requires a good understanding of their limitations and predictive capabilities. While this report makes considerable progress toward this goal, it also points to ranges of accuracies in the predictive capability of these fire models that could limit their use in fire modeling applications. Use of these fire models presents challenges that should be addressed if the fire protection community is to realize the full benefit of fire modeling and performance-based fire protection. Persisting problems require both short-term and long-term solutions. In the short-term, users need to be educated on how the results of this work may affect known applications of fire modeling, perhaps through pilot application of the findings of this report and documentation of the resulting lessons learned. In the long-term, additional work on improving the models and performing additional experiments should be considered.

Keywords

Fire
Fire Modeling
Verification and Validation (V&V)
Performance-Based
Risk-Informed Regulation
Fire Hazard Analysis (FHA)
Fire Safety
Fire Protection
Nuclear Power Plant
Fire Probabilistic Risk Assessment (PRA)
Fire Probabilistic Safety Assessment (PSA)

PREFACE

This report is presented in seven volumes. Volume 1, the Main Report, provides general background information, programmatic and technical overviews, and project insights and conclusions. Volume 2 quantifies the uncertainty of the experiments used in the V&V study of the five fire models considered in this study. Volumes 3 through 7 provide detailed discussions of the verification and validation (V&V) of the fire models:

Volume 3 Fire Dynamics Tools (FDT^{s})

Volume 4 Fire-Induced Vulnerability Evaluation, Revision 1 (FIVE-Rev1)

Volume 5 Consolidated Model of Fire Growth and Smoke Transport (CFAST)

Volume 6 MAGIC

Volume 7 Fire Dynamics Simulator (FDS)

ACKNOWLEDGMENTS

The work documented in this report benefited from contributions and considerable technical support from several organizations.

The verification and validation (V&V) studies for FDT^s (Volume 3), CFAST (Volume 5), and FDS (Volume 7) were conducted in collaboration with the U.S. Department of Commerce, National Institute of Standards and Technology (NIST), Building and Fire Research Laboratory (BFRL). Since the inception of this project in 1999, the NRC has collaborated with NIST through an interagency memorandum of understanding (MOU) and conducted research to provide the necessary technical data and tools to support the use of fire models in nuclear power plant fire hazard analysis (FHA).

We appreciate the efforts of Doug Carpenter and Rob Schmidt of Combustion Science Engineers, Inc. for their comments and contributions to Volume 3.

In addition, we acknowledge and appreciate the extensive contributions of Electricité de France (EdF) in preparing Volume 6 for MAGIC.

We thank Drs. Charles Hagwood and Matthew Bundy of NIST for the many helpful discussions regarding Volume 2.

We also appreciate the efforts of organizations participating in the International Collaborative Fire Model Project (ICFMP) to Evaluate Fire Models for Nuclear Power Plant Applications, which provided experimental data, problem specifications, and insights and peer comment for the international fire model benchmarking and validation exercises, and jointly prepared the panel reports used and referred to in this study. We specifically appreciate the efforts of the Building Research Establishment (BRE) and the Nuclear Installations Inspectorate in the United Kingdom, which provided leadership for ICFMP Benchmark Exercise (BE) #2, as well as Gesellschaft für Anlagen-und Reaktorsicherheit (GRS) and Institut für Baustoffe, Massivbau und Brandschutz (iBMB) in Germany, which provided leadership and valuable experimental data for ICFMP BE #4 and BE #5. In particular, ICFMP BE #2 was led by Stewart Miles at BRE; ICFMP BE #4 was led by Walter Klein-Hessling and Marina Rowekamp at GRS, and R. Dobbernack and Olaf Riese at iBMB; and ICFMP BE #5 was led by Olaf Riese and D. Hosser at iBMB, and Marina Rowekamp at GRS. Simo Hostikka of VTT, Finland also assisted with ICFMP BE#2 by providing pictures, tests reports, and answered various technical questions of those experiments. We acknowledge and sincerely appreciate all of their efforts.

We greatly appreciate Paula Garrity, Technical Editor for the Office of Nuclear Regulatory Research, and Linda Stevenson, agency Publications Specialist, for providing editorial and publishing support for this report. Lionel Watkins and Felix Gonzalez developed the graphics

for Volume 1. We also greatly appreciate Dariusz Szwarc and Alan Kouchinsky for their assistance finalizing this report.

We wish to acknowledge the team of peer reviewers who reviewed the initial draft of this report and provided valuable comments. The peer reviewers were Dr. Craig Beyler and Mr. Phil DiNenno of Hughes Associates, Inc., and Dr. James Quintiere of the University of Maryland.

Finally, we would like to thank the internal and external stakeholders who took the time to provide comments and suggestions on the initial draft of this report when it was published in the *Federal Register* (71 FR 5088) on January 31, 2006. Those stakeholders who commented are listed and acknowledged below.

Janice Bardi, ASTM International

Moonhak Jee, Korea Electric Power Research Institute

U.S. Nuclear Regulatory Commission, Office of Nuclear Reactor Regulation Fire Protection Branch

J. Greg Sanchez, New York City Transit

David Showalter, Fluent, Inc.

Douglas Carpenter, Combustion Science & Engineering, Inc.

Nathan Siu, U.S. Nuclear Regulatory Commission, Office of Nuclear Regulatory Research

Clarence Worrell, Pacific Gas & Electric

LIST OF ACRONYMS

AGA	American Gas Association
AHJ	Authority Having Jurisdiction
ASME	American Society of Mechanical Engineers
ASTM	American Society for Testing and Materials
BE	Benchmark Exercise
BFRL	Building and Fire Research Laboratory
BRE	Building Research Establishment
BWR	Boiling-Water Reactor
CDF	Core Damage Frequency
CFAST	Consolidated Fire Growth and Smoke Transport Model
CFD	Computational Fluid Dynamics
CFR	Code of Federal Regulations
CSR	Cable Spreading Room
EdF	Electricité de France
EPRI	Electric Power Research Institute
FDS	Fire Dynamics Simulator
FDT^s	Fire Dynamics Tools (NUREG-1805)
FHA	Fire Hazard Analysis
FIVE-Rev1	Fire-Induced Vulnerability Evaluation, Revision 1
FM/SNL	Factory Mutual & Sandia National Laboratories
FMRC	Factory Mutual Research Corporation
FPA	Foote, Pagni, and Alvares
FRA	Fire Risk Analysis
GRS	Gesellschaft für Anlagen-und Reaktorsicherheit (Germany)
HGL	Hot Gas Layer

HRR	Heat Release Rate
IAFSS	International Association of Fire Safety Science
iBMB	Institut für Baustoffe, Massivbau und Brandschutz
ICFMP	International Collaborative Fire Model Project
IEEE	Institute of Electrical and Electronics Engineers
IPEEE	Individual Plant Examination of External Events
MCC	Motor Control Center
MCR	Main Control Room
MQH	McCaffrey, Quintiere, and Harkleroad
MOU	Memorandum of Understanding
NBS	National Bureau of Standards (now NIST)
NFPA	National Fire Protection Association
NIST	National Institute of Standards and Technology
NPP	Nuclear Power Plant
NRC	U.S. Nuclear Regulatory Commission
NRR	Office of Nuclear Reactor Regulation (NRC)
PMMA	Polymethyl-methacrylate
PWR	Pressurized Water Reactor
RCP	Reactor Coolant Pump
RES	Office of Nuclear Regulatory Research (NRC)
RI/PB	Risk-Informed, Performance-Based
SBDG	Stand-By Diesel Generator
SDP	Significance Determination Process
SFPE	Society of Fire Protection Engineers
SNL	Sandia National Laboratory
SWGR	Switchgear Room
TC	Thermocouple
V&V	Verification & Validation

1
MODEL EVALUATION APPROACH*

The purpose of this volume is to provide a means for quantitative comparison of model simulations and measurements. The methodology employed follows the guidelines outlined in ASTM E 1355, *Standard Guide for Evaluating the Predictive Capability of Deterministic Fire Models* [1], for verification and validation (V&V) of the selected fire models. That guide outlines four parts of model evaluation:

1. Define the model and scenarios for which the evaluation is to be conducted.
2. Assess the appropriateness of the theoretical basis and assumptions used in the model.
3. Assess the mathematical and numerical robustness of the model.
4. Validate a model by quantifying the accuracy of the model results in predicting the course of events for specific fire scenarios.

This volume describes the methodology used to addresses the fourth part of the ASTM model evaluation process. The other parts are found in Volumes 1 and 3 through 7 of this report series.

Traditionally, model validation studies report the comparison of model results with experimental data. There are various ways of expressing the difference between the two, but there are no widely accepted criteria for judging whether the agreement is satisfactory or not. ASTM E 1355 [1] does not explicitly define how model validation should be accomplished, nor does it provide criteria regarding what constitutes "reasonable" agreement between models and experiments. Section 11.3.2.4 of ASTM E 1355 states that, "Where data are available, model predictions should be viewed in light of the variability of the full-scale test results and model sensitivity." No further guidance is supplied by ASTM E 1355 on the details of how experiments might be used to validate fire models.

In this study, the results are presented in the form of relative differences between fire model predictions and experimental measurements for 13 fire modeling attributes important to NPP fire modeling applications (e.g., plume temperature). The relative differences sometimes show general agreement, and sometimes show under-prediction or over-prediction. The relative differences are attributable to a number of factors, including the capabilities and limitations of the predictive models, and the accuracy of the experimental measurements. In this study, the relative differences between the model predictions and the experimental measurements are compared to a *combined uncertainty*. This comparison allowed the determination of a graded characterization of a fire model's capability to predict attributes important to NPP fire modeling applications.

* Certain trade names and company products are mentioned in the text to specify adequately the experimental procedure and equipment used or to identify types of currently available commercial products. In no case does such identification imply recommendation or endorsement by the National Institute of Standards and Technology, nor does it imply that the products are necessarily the best available for the purpose.

The combined uncertainty includes the *model input uncertainty*, which is derived from experimental measurements and the experimental *measurement uncertainty* associated with each of the key quantities of interest (see Section 1.2). This metric allows quantification of the level of agreement between the model predictions and the experimental measurements.

The objective of this volume is not to provide a comprehensive description of the selected fire experiments. That information can be obtained in the original test reports, which are cited in the text. Rather, this volume serves as a link between the experiments and the models, especially with regard to experimental uncertainties, which are often not reported in the original test reports. Here, estimates of the experimental uncertainties are provided, based on engineering judgment. Also, certain parameters required as input by the fire models, like the radiation loss from the fire, are often not provided in the original test reports, because these quantities have not been measured. Here, estimates of these quantities are provided, based on engineering judgment. This document provides information that cannot be found in the original test reports for implementing the models and comparing the model results to experimental measurements. In summary, this volume provides information on the model evaluation process, and the various forms of uncertainty that play a role in that process.

1.1 Fire Experiments and Test Selection

This volume contains descriptions of the six sets of fire experiments that are being used in the evaluation of the selected models considered in this report series. A number of the experiments were designed for model validation, other were not.

In general, the experiments established steady fires burning in simple compartment geometries. The decision to include or exclude a particular test from a particular experimental series was made for a variety of reasons and is described below. Table 1-1 summarizes the experiments selected for the validation study in terms of the number of tests, the number of experimental quantities or parameters used for model evaluation (see Section 1.2), as well as aspects of the fire and the compartment, including the fire heat release rate ($\dot{Q}$), the compartment volume (V) and compartment height (H).

Table 1-1: Overview of the Experiments Used for Model Evaluation

Series	Number of Tests	Number of Measurement Parameters	$\dot{Q}$ (kW)	*V* (m^3)	*H* (m)
FM/SNL	3	4	500	1400	6.1
NBS	3	2	100	15	2.4
ICFMP BE #2	3	2	1800-3600	5900	19
ICFMP BE #3	15	8	400-2300	580	3.8
ICFMP BE #4	1	3	3500	74	5.7
ICFMP BE #5	1	4	400	73	5.6

The six fire experiments are introduced below, approximately in chronological order:

1. FM/SNL Test Series: 25 fire experiments conducted for the NRC by Factory Mutual Research Corporation (FMRC) in 1985, under the direction of Sandia National Laboratories (SNL) [2]. The primary purpose of these tests was to provide data with which to evaluate fire models used in hazard assessments of NPP enclosures. The results of three of these experiments have been used in the current validation study.

   The FM/SNL series involved a large number of measurements made during a long test series, but much of the data was never thoroughly analyzed. In particular, uncertainties were not provided. The three experiments selected were described in greater detail than the others, and these same three experiments have been used in a variety of prior validation studies.

2. NBS Multi-Compartment Test Series: 45 fire experiments, representing 9 different sets of test conditions, with multiple replicates of each set, that were conducted in a three-room suite at the National Bureau of Standards in 1985 (NBS, now the National Institute of Standards and Technology or NIST) [3]. The primary purpose of these experiments was to evaluate fire models under development at NBS at that time, in particular, the zone model CFAST. The results of three of these experiments have been used in the current validation study. Estimates of uncertainty were determined from the test reports, the data itself, and supporting information. Tests for this study were selected based on confidence in the data quality[1]. The selected tests represented three different geometric configurations. Estimates of uncertainty were determined from the test reports, the data itself, and supporting information, including conversations with one of the experimentalists.

3. ICFMP Benchmark Exercise (BE) #2: A series of 8 fire experiments, representing 3 different sets of test conditions, that were conducted within a 19 m high test hall at VTT, the Finnish National Testing Laboratory during 1998 and 1999 [4]. The test results were contributed to the International Collaborative Fire Model Project (ICFMP). All three cases, representing average results from the 8 tests, have been used in the current validation study.

4. ICFMP BE #3: A series of 15 fire experiments were conducted at NIST in 2003, which were partially funded by the U.S. NRC and NIST as part of the ICFMP. The results of all of the experiments have been used in the current study. Analysis of the heat release rate data led to a report [5], which includes a detailed explanation of the heat release rate uncertainty estimate.

5. ICFMP BE #4: A series of small compartment kerosene pool fire experiments, conducted at the Institut für Baustoffe, Massivbau und Brandschutz (iBMB) of Braunschweig University of Technology in Germany in 2004 [6]. The results of two of these experiments (Tests 1 and 3) were contributed to the ICFMP, of which one has been used in the current V&V study. A malfunction in the measurement of the fuel mass loss rate was reported in Test 3, implying a level of uncertainty that is unacceptable for the current study. The results from Test 1 were considered here.

6. ICFMP BE #5: A series of fire experiments in 2004 that involved realistically routed cable trays inside the same concrete enclosure at iBMB as BE #4 [7]. The results of four tests were contributed to the ICFMP, of which one has been used in the current V&V study.

   BE #5 was conducted primarily for the evaluation of cable ignition and flame spread. The results were erratic, and no replicate experiments were performed. Given the primitive

[1] Peacock, R., National Institute of Standards and Technology, Gaithersburg, MD, *personal communication*, 2005.

nature of the ignition and spread algorithms within the models, it was decided that only a qualitative analysis would be possible with the data from three of the four experiments. However, in one experiment, the first 20 minutes involved a fairly well-characterized ethanol pool fire burning on the opposite side of the compartment from the cable tray. This part of the experiment has been used as part of the model evaluation.

1.2 Measurements

For comparison to the models, 13 key experimental quantities or parameters were selected for comparison with the model predictions. Section 2.4 of Volume 1 describes the rationale for the selection of these parameters, which was based on their relevance to typical nuclear power plant fire modeling applications.

The experiments did not provide data for all of the measurement parameters. Table 1-2, similar to Table 2-3 in Volume 1 of this report, summarizes the measurements from each set of experiments that were used for comparison with the models. About 45 of the 78 (or 60%) of the cells in Table 1-2 have entries that say, "no data," which means that either the measurement was conducted, or that the data were flawed or otherwise suspect. Some of the tests provided more information than others, but none of the tests provided information for all of the parameters of interest. Reliable data for some of the parameters (i.e., smoke, compartment pressure, radiant and total heat flux, etc.) are difficult to find in the literature. The limited amount of data in the table is a reflection of the experimental data sets used in this study and, in general, the availability of reliable data in the literature. Because the data used to evaluate each parameter is different, the generality of each of the results is correspondingly limited. If more data becomes available in the future, it should be used to check the consistency of the results in this report series.

The graphical comparisons of measured and calculated results for each of the five fire models are presented in Appendix A of Volumes 3 through 7 of this report series. Chapter 3 of this volume provides a basic description of the experiments and provides some details about the decision to use, or exclude, a given measurement in the model evaluation process.

This study evaluates the model predictions for the following 13 key experimental quantities or parameters:

1. hot gas layer temperature
2. hot gas layer height
3. ceiling jet temperature
4. plume temperature
5. flame height
6. oxygen concentration
7. smoke concentration
8. compartment pressure
9. radiated heat flux to target

10. total heat flux to target

11. target temperature

12. total heat flux to walls

13. wall temperature

Often, the documentation associated with these six experimental studies did not completely address measurement uncertainty. In those cases, measurement uncertainty was estimated here using engineering judgment. For example, each of the experiments provided data that was used to characterize the fire heat release rate. More often than not, however, the uncertainty in the heat release rate was not reported. Since this parameter drives the thermal environment in a fire, and the model calculation results are particularly sensitive to uncertainty in this parameter, engineering judgment was used to provide a reasonable estimate for this parameter.

Table 1-2: Summary of the Test Series, Experiments, and Instrumentation Used for the Model Evaluation

Fire Modeling Parameters	Selected Test Series/Experiments/Instrumentation					
	FM/SNL	NBS	ICFMP BE #2	ICFMP BE #3	ICFMP BE #4	ICFMP BE #5
	Tests 4,5, & 21	100A, 100O, 100Z	Part I, Cases 1, 2, 3	Tests 1-5, 7-10, 13-18	Test 1	Test 4
1. HGL temperature	Vertical arrays of thermocouples (Type K and aspirated)	Vertical arrays of thermocouples (Type K)	Vertical arrays of thermocouples (Type K)	Vertical arrays of thermocouples (Type K and aspirated)	Vertical arrays of thermocouples (Type K)	Vertical arrays of thermocouples (Type K)
2. HGL depth	Vertical arrays of thermocouples (Type K and aspirated)	Vertical arrays of thermocouples (Type K)	Vertical arrays of thermocouples (Type K)	Vertical arrays of thermocouples (Type K and aspirated)	Vertical arrays of thermocouples (Type K)	Vertical arrays of thermocouples (Type K)
3. Ceiling jet temperature	Thermocouple (Type K)	No Data	No Data	Thermocouple (Type K)	No Data	No Data
4. Plume temperature	Thermocouple (Type K and aspirated)	No Data	Thermocouple	No Data	No Data	No Data
5. Flame height	No Data	No Data	Photos	Photos	No Data	No Data
6. Gas concentrations	No Data	No Data	No Data	Paramagnetic oxygen analyzer	No Data	Paramagnetic oxygen analyzer
7. Smoke concentration	No Data	No Data	No Data	Laser transmission	No Data	No Data
8. Compartment pressure	No Data	No Data	No Data	Differential transducer	No Data	No Data
9. Radiant heat flux to target	No Data	No Data	No Data	Large view angle radiometers	No Data	No Data
10. Total heat flux to targets	No Data	No Data	No Data	Schmiddt-Boelterr gauges	Heat flux gauges	Heat flux gauges
11. Target surface temperature	No Data	No Data	No Data	Thermocouples (Type K)	Thermocouples (Type K)	Thermocouples (Type K)
12. Total heat flux to walls	No Data	No Data	No Data	Uncooled heat flux gauges	No Data	No Data
13. Wall surface temperature	No Data	No Data	No Data	Thermocouples (Type K)	Thermocouples (Type K)	Thermocouples (Type K)

1.3 Fire Models

Section 2.2 of Volume 1 describes the selection of the fire models considered in this study. The models represent a wide range of capabilities and computational sophistication. They included two libraries of engineering calculations, two two-zone models, and one field model, as follows:

- Two libraries of engineering spreadsheet calculations: FDT^s and FIVE-Rev1
- Two two-zone models: CFAST and MAGIC
- One field model: FDS

Volumes 3 through 7 of this report describe these models in detail. Table 2-2 in Volume 1 lists the output provided by each of the fire models. While two of the models provide output for all of the 13 parameters listed above, the other three models considered in this study do not. Applicability of the method outlined here is not limited to the models considered in this study.

1.4 Uncertainty and Sensitivity

In the appendices to Volumes 3 through 7, there are hundreds of graphs comparing time histories of experimental measurements and model predictions. The curves rarely lie exactly on top of each other, which raises the question as to how well the models predict the experimental measurements. One can imagine numerous ways of quantifying the "closeness" of the agreement. In practice, there are many kinds of applications, and the degree to which the curves ought to match depends on the application. For example, knowing the gas temperature within a few degrees might be important if the application is detection, but it may be an order of magnitude larger if the interest is the prediction of flashover. Fire protection engineers performing a hazard analysis are often content to demonstrate merely that the model is consistently "conservative"; that is, that a safety factor is implicit in the model formulation. Forensic experts, however, require the model to be as accurate as possible, with no built-in bias. In either case, model accuracy needs to be quantified. This means comparing model predictions to experimental measurements, as is done throughout Volumes 3 through 7, and then quantifying the differences between the two. The agreement between measurements and models is considered here in terms of the combined measurement and model input uncertainties.

1.4.1 Types of Uncertainty

For model evaluation, the impact of experimental uncertainty on the comparison of model simulations and the experiments is considered. The experimental uncertainty is considered in two ways. First, the uncertainty associated with parameters derived from experimental measurements that are used as model input is considered. Second, the uncertainty associated with the experimental measurements themselves (for those quantities that are model output) is considered. The former type of uncertainty is referred to here as *model input uncertainty*. The uncertainty in model input parameters may include uncertainty in the thermal properties of solid surfaces, in the chemical properties of the fuel, in the yields of the various products of combustion, and most importantly, in the heat release rate of the fire.

Beyond the input uncertainty, uncertainty associated with the experimental measurements is also considered in the model evaluation process. Measurements by thermocouples, heat flux gauges and gas analyzers all have a certain degree of uncertainty related to their operation, calibration, *etc*. This is referred to as *measurement uncertainty*. A measurement result is fully documented only when accompanied by a quantitative statement of its uncertainty. There are two types of measurement uncertainty: instrument uncertainty and repeatability [Refs. 8, 9]. When these components of the measurement uncertainty are quantified, they are pooled into a combined uncertainty value that is a better representation of the total measurement uncertainty. The uncertainty is often expressed in terms of an expanded uncertainty, in which the confidence level that the measurement falls within the expanded bounds is high. The size of the expanded bounds is described by an expansion factor. For an expansion factor of two, the uncertainty is related to two standard deviations ($2 \cdot \sigma$) and the confidence level corresponds to 95%. References 8 and 9 discuss types of measurement uncertainty and ways to quantify them.

Typically, it is possible to provide rational estimates of the experimental *measurement uncertainty* and the experimental *model input uncertainty*. Both are related to measurements. Another type of uncertainty, the model *intrinsic uncertainty*, is far more difficult to quantify. Model *intrinsic uncertainty* is uncertainty associated with the physical and mathematical assumptions and methods that are an intrinsic part of the model formulation and its implementation. This uncertainty is not part of the *model input uncertainty*. A methodology for examining this type of uncertainty is described in reference 10. Examples of *intrinsic uncertainty are* the two-layer assumption in a zone fire model, the description of turbulence in a CFD fire model, or the grid size used in a CFD fire model. We do not attempt to quantify model *intrinsic uncertainty* in this study. In this sense, only a portion of the total uncertainty in the model simulation results is considered here. However, a sense of the size of the *intrinsic uncertainty* of the models can be ascertained from the results of this study.

The purpose of this volume is to develop a methodology to determine the level of agreement between the models and measurements. The next section goes into the details of the methodology.

1.4.2 Methodology for Evaluating the Models

This section describes the methodology used to compare the model and measurement results. NFPA 805 and ASTM E 1355 offer some suggestions, but do not specify one method over another for comparison of models and measurements. The method developed here is distinct in many ways from the methods suggested by those documents. In this report, the predictive capability of each of the models is determined through comparison with quantitative experimental results. The detailed plots of the comparisons are presented for each of the models in Appendix A to Volumes 3 through 7 of this report series. The fire models are used to simulate the experiments, and then the effects of experimental measurement uncertainty and the model sensitivity to model input uncertainty are considered as possible sources of the difference between the model calculation results and the measurements.

As an example, Figure 1-1 shows the measured and the simulated temperature as a function of time for a hypothetical scenario. For simplicity, experimental measurements and model simulations are compared at the time of their respective maximum values. This approach is suggested in ASTM E 1355. In the case shown in Figure 1-1, the maxima occurs nearly 600 s

after ignition, albeit at somewhat different times. In Figure 1-1, there are finite differences between the peak value (M_p) of the model prediction and the peak value of the experimental measurement (E_p). In this report, model evaluation is considered in terms of the uncertainty in these quantities, that is, in the uncertainty of the experimental measurements, and the uncertainty in the simulations that arise as a result of sensitivity to uncertainty in values of model input parameters. The bulk of this volume is spent estimating the uncertainty bars associated with the peak value (M_p) of the model prediction and the peak value of the experimental measurement (E_p).

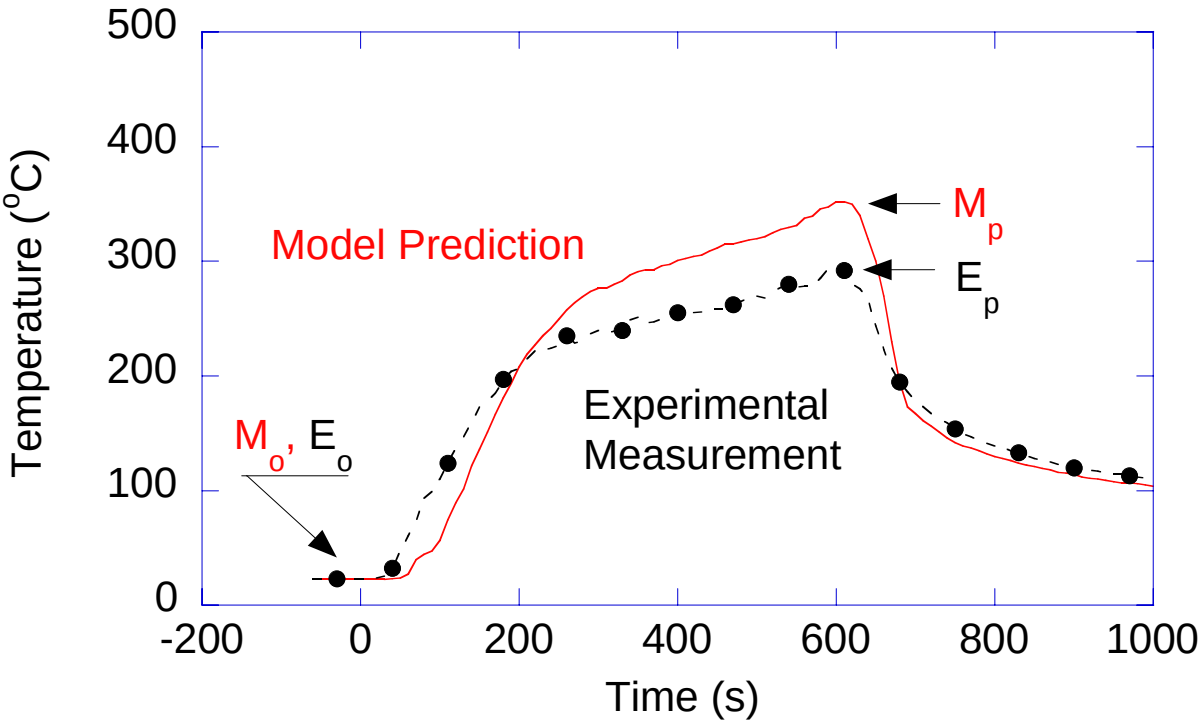

Figure 1-1: Comparison of typical experimental measurements (filled points and broken line) and model predictions (solid line) of temperature in the hot upper layer of a compartment fire as a function of time. The initial and peak values of the predictions and measurements are also shown.

Hundreds of model predictions and measurements were compared as part of the evaluation of the models (see Volume 3 through 7) in this report series. To facilitate assessment of model strengths and weaknesses for the 13 quantities tested (see Section 1.2), relative differences (percent differences) rather than absolute differences are considered, which puts all comparisons on the same basis and avoided the use of different units for each parameter of interest.

For each comparison, a relative difference is defined as follows:

$$\varepsilon = \frac{\Delta M - \Delta E}{\Delta E} = \frac{\left(M_p - M_o\right) - \left(E_p - E_o\right)}{\left(E_p - E_o\right)} \qquad (1.1)$$

where ΔM is the difference between the peak value of the model prediction (M_p) and its baseline value (M_o), and ΔE is the difference between the peak value of the experimental measurement (E_p) and its baseline value (E_o). The parameter ε is a non-dimensional quantity that represents the relative difference between the model predictions and the measurements. If ε is equal to

zero, then the models and measurements are in exact agreement. Typically, the difference is small, but non-zero. To determine if a value of a relative difference, ε, is significantly different from its expected statistical variation about zero, a statistical significance test may be carried out. CFD code validation studies have considered a similar methodology [11]. The distribution of ε can be approximated using the first terms of a Taylor series expansion:

$$\varepsilon \approx \left(\frac{\partial \varepsilon}{\partial \Delta M}\right)\Delta M + \left(\frac{\partial \varepsilon}{\partial \Delta E}\right)\Delta E \qquad (1.2)$$

This expression assumes that other contributors to the distribution are small. This approximation is subsequently considered through interpretation of the results that compare ε with its variance. Following Eq. 1.2, the statistical distribution of ε is assumed to be normal with a mean of zero and variance given by:

$$u_\varepsilon^2 \approx \left(\frac{\partial \varepsilon}{\partial \Delta M}\right)^2 u_M^2 + \left(\frac{\partial \varepsilon}{\partial \Delta E}\right)^2 u_E^2 + 2\left(\frac{\partial \varepsilon}{\partial \Delta M}\right)\left(\frac{\partial \varepsilon}{\partial \Delta E}\right) u_{EM}^2 \qquad (1.3)$$

where u_M^2 and u_E^2 are the variances of ΔM and ΔE, respectively, and the third term, u_{EM}^2, is the covariance term involving products of deviations of ΔM and ΔE simultaneously. This covariance term is taken as negligible, as the fluctuations in ΔM and ΔE are assumed to be uncorrelated [12]. Equation 1.3 is just the propagation of error formula [12]. Using the definition of ε from Eq. 1.1, Eq. 1.3 can be rewritten as follows:

$$u_\varepsilon^2 \approx \frac{1}{\Delta E^2} u_M^2 + \left(\frac{-\Delta M}{\Delta E^2}\right)^2 u_E^2 \qquad (1.4)$$

Rearranging terms leads to the following expression:

$$u_\varepsilon^2 = \frac{\Delta M^2}{\Delta E^2}\left(\frac{u_M^2}{\Delta M^2} + \frac{u_E^2}{\Delta E^2}\right) \qquad (1.5)$$

Rewriting this expression in terms of the relative, rather than the absolute, uncertainties, $\tilde{u}_M = u_M / \Delta M$ and $\tilde{u}_E = u_E / \Delta E$, yields the following expression for u_ε :

$$u_\varepsilon = (1 + |\varepsilon|)\left(\tilde{u}_M^2 + \tilde{u}_E^2\right)^{1/2} \qquad (1.6)$$

where the vertical bars represent the absolute value of the function, and are included because only positive values of ε are allowed. Rewriting Eq. 1.6 in terms of the expanded value of u_ε, that is U_ε (= $2u_\varepsilon$), leads to the following expression:

$$U_\varepsilon = (1 + |\varepsilon|)\left(\tilde{U}_M^2 + \tilde{U}_E^2\right)^{1/2} \qquad (1.7)$$

where $\tilde{U}_M$ (= $2\tilde{u}_M$) and $\tilde{U}_E$ (= $2\tilde{u}_E$) are the relative expanded uncertainties.

The normal significance test says to reject the assumption that the mean deviation of ε from zero is caused by random statistical variation, at the 95% significance level [13], if

$$\left| \varepsilon \right| > 1.96\ u_{\varepsilon} \tag{1.8}$$

Assessment of the agreement between a particular comparison of model and experimental measurement can be made using Eq. 1.8.

If the expanded relative uncertainty, U_{ε}, is considered, ($U_{\varepsilon} = 2u_{\varepsilon}$), then Eq. 1.8 is rewritten as follows:

$$\left| \varepsilon \right| > 0.98\ U_{\varepsilon} \tag{1.9}$$

and approximately

$$\left| \varepsilon \right| > U_{\varepsilon} \tag{1.10}$$

The level of agreement between models and measurements is considered by comparing the value of ε with its variance, U_{ε}, as represented by the combined absolute expanded experimental uncertainty in Eq. 1.10. As described above, U_{ε} does not account for model *intrinsic uncertainty*.

For most of the model/measurement comparisons in this study, $|\varepsilon|$ takes on values between 0.01 and 0.2. In some cases, it is larger, occasionally reaching values between 0.2 and 1, and in some cases, $|\varepsilon| > 1$. When $|\varepsilon| << 1$, then the term $(1 + |\varepsilon|)$ in Eq. 1.7 is about equal to one, so Eq. 1.7 is rewritten as follows:

$$U_{\varepsilon} \approx \left(\tilde{U}_M^2 + \tilde{U}_E^2\right)^{1/2} \tag{1.11}$$

and Eq. 1.10 asks if the following is true:

$$\left| \varepsilon \right| > \left(\tilde{U}_M^2 + \tilde{U}_E^2\right)^{1/2} \tag{1.12}$$

If $|\varepsilon|$ is not small, then neglecting its contribution makes Eq. 1.10 less likely. Seeking simplification in the presentation of the hundreds of comparisons of model predictions with experimental measurements, Eq. 1.11 is used in place of Eq. 1.7. In terms of model validation, this approximation does not impact the conclusions. The simplification is graphically illustrated in Figure 1-2 in which the domain of "disagreement" between models and experimental predictions is expanded when Eq. 1.11 is considered in place of Eq. 1.7, especially for values of $|\varepsilon| > 0.2$. In this manner, use of Eq. 1.11 rather than Eq. 1.7 is conservative, and "agreement" between models and measurements is more demanding and less likely.

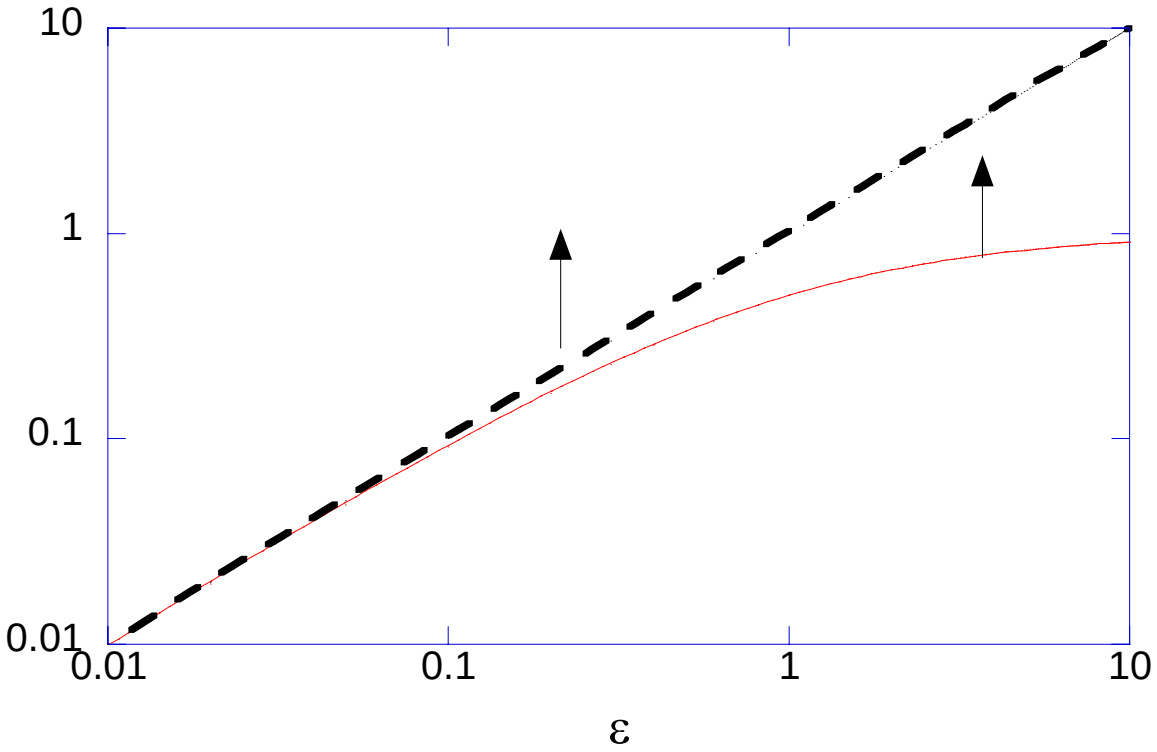

Figure 1-2: Consideration of the inequality defined by Eq. 1.10 using the definition in Eqs. 1.7 and 1.11. Models and measurements are considered to disagree in the regions above the curves.

In this study, evaluation of the inequality in Eq. 1.12 requires knowledge of ΔE, ΔM, and U_ε. Assessment of Eq. 1.12 is analogous to determining if the expanded uncertainty bars about the peak values in Figure 1-1 overlap. To illustrate this point, the data in Figure 1-1 are replotted with the measurement and model results and associated expanded uncertainty bars shown in Figure 1-3. The values of ΔM and ΔE are approximately 330 °C and 270 °C, respectively. From Eq. 1.1, the value of ε is equal to 0.22. The experimental *measurement uncertainty* ($\tilde{U}_E$) and the *model input uncertainty* ($\tilde{U}_M$) are also shown as a function of time in the figure, represented by the bars about the curves. The values of the relative expanded *measurement and model input uncertainties*, $\tilde{U}_M$ and $\tilde{U}_E$, are approximately ±20% and ±10% about their respective peaks, so that the combined relative uncertainty from Eq. 1.11 gives U_ε = 0.22.

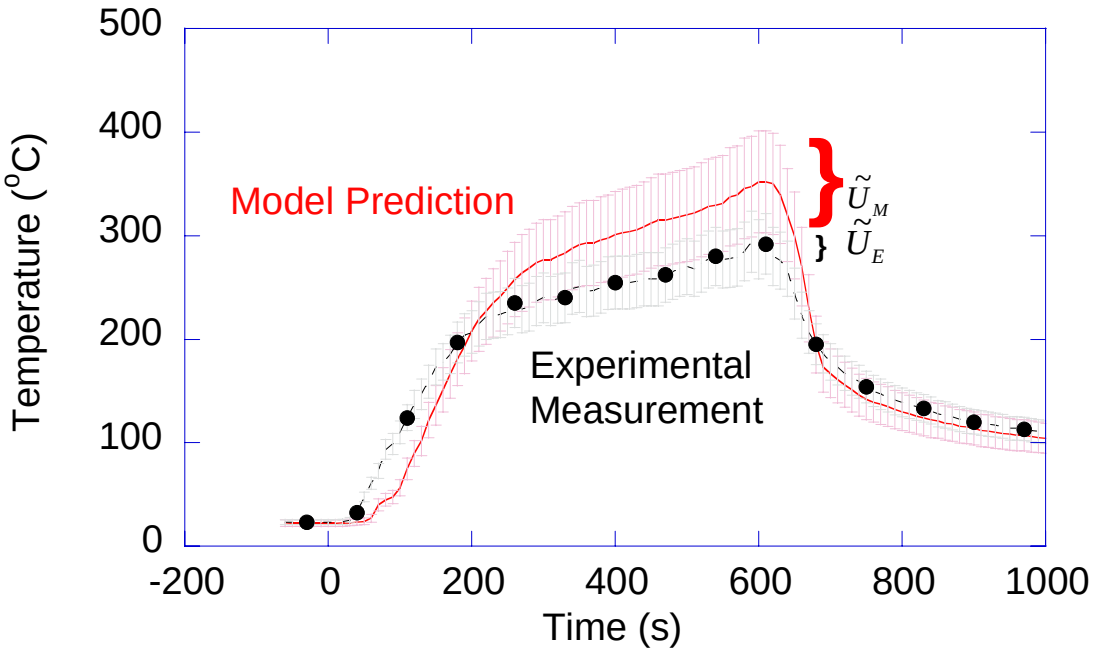

Figure 1-3: Comparison of typical experimental measurements (filled points and broken line) and model predictions (line) of temperature in the hot upper layer of a compartment fire as a function of time. The uncertainty associated with the model predictions and the experimental measurements are indicated by the uncertainty bars.

If Eq. 1.12 does not hold, then the difference between the model and the measurement is within the uncertainty bounds defined by U_ε, and model and measurement are in agreement. By contrast, if Eq. 1.12 holds, then the difference between model and measurement is not within the bounds defined by U_ε, and model and measurement are not in agreement. This may be the case for a variety of reasons. Alternatively, the magnitude of the disagreement may be interpreted as providing an estimate of the terms unaccounted for in the determination of U_ε, involving the model *intrinsic uncertainty*, for example.

Figure 1-4 illustrates the approach used here to compare the model and measurements. In the figure, the data from Figure 1-3 is plotted in terms of ε as a function of time. Its value is initially negative as ΔE is greater than ΔM (see Eq. 1.1). Its value then becomes positive, and finally steady toward the end of the experiment. The figure also shows the relative combined uncertainty (U_ε) at 600 s, which is the time of the peak values of ΔM and ΔE. If the lower value of the uncertainty bar defined by U_ε extends beyond ε=0, then model and measurement are considered to be in agreement. In the example shown in Figure 1-4, the uncertainty bar is just touching ε=0, and the agreement between the model and measurement should be considered borderline.

In this report series, hundreds of measurements and model results are compared, and the results are presented in Volume 3 through 7. For simplicity, a value of U_ε is estimated for each of the measured quantities of interest (see Section 1.2) for each experimental series, not for each of the

tests that comprise a series. While some differences in the values of U_ε may exist from test to test within each of the six test series, the differences are relatively insignificant when the accuracy of the uncertainty estimate is considered. Finally, using the U_ε for each test series, a single representative value of U_ε is determined from a weighted average.

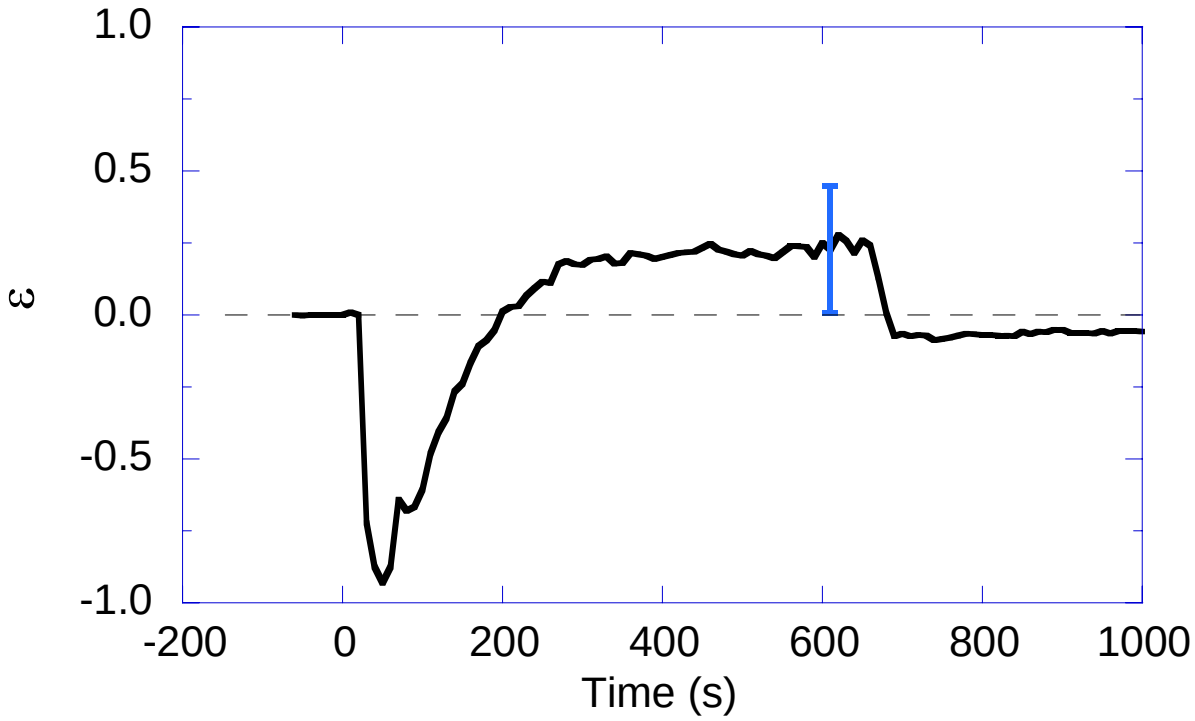

Figure 1-4: The data in Figure 1-3 replotted in terms of ε . The combined expanded uncertainty U_ε at 600 s, the time of the peak values of ΔM and ΔE, is also shown.

1.5 Organization of this Volume

This study highlights the use of experimental uncertainty as a criterion to assess the level of agreement between models and measurements. The objective of this volume is to describe this methodology, and show how experimental uncertainty associated with measurement results and model predictions can be combined and used as a basis for model evaluation. Although other means to judge the reasonableness of model validation may be possible, the method developed here provides a quantitative and rigorous approach that emphasizes the importance of experimental quality and measurement accuracy in the evaluation of fire models.

This volume is organized as follows:

- Chapter 2 discusses each of the six experimental series considered in this report (see Table 1-1). The input data used by the models to simulate the six experiments is provided.
- Chapter 3 defines the heat release rate and the radiative fraction, and discusses uncertainty in these measurements, which is important the determination of the *model input uncertainty* ($\tilde{U}_M$, see Section 1.4.2) discussed in Chapter 5.
- Chapter 4 addresses the uncertainty in the experimental measurements, which is important in model evaluation and the determination of the *combined uncertainty* ($\tilde{U}_E$, see Section 1.4.2).
- Chapter 5 discusses the value of the model input uncertainty ($\tilde{U}_M$) for relevant measurements. For each parameter of interest, a simple analytic description of the sensitivity of that parameter to the fire heat release rate is given. The model input uncertainty ($\tilde{U}_M$) is estimated based on uncertainty in the experimental heat release rate, and a number of other parameters. The magnitude of this uncertainty plays an important role in the evaluation of model accuracy through consideration of Eqs. 1.7 and 1.10, above.
- Chapter 6 summarizes the experimental ($\tilde{U}_E$) and model ($\tilde{U}_M$) uncertainties taken from Chapters 4 and 5, respectively, and uses these values to calculate the combined uncertainty (see Eqs. 1.7 and 1.10). The combined uncertainties are weighted and used to determine a representative uncertainty for comparison with ε, the relative difference between the measurements and the models.
- Chapter 7 presents a list of references.
- Appendix A presents a series of calculations, investigating effects associated with the selection of the interval used to time-average the data.

2
TEST SERIES DESCRIPTION AND MODEL INPUT DATA

In this chapter, each of the six experimental series is briefly described. The experimental arrangement is described, and model input parameters involving the fire, the ventilation (mechanical, natural, and leakage, if available), the compartment (detailed layout), ambient conditions (if available), and target position and orientation are given. Information necessary to reproduce the model calculations is presented for each of the experiments. Schematic diagrams are presented for each of the experiments, and tables are provided that summarize the information used as input for the model simulations including data on the compartment, fire, ventilation, and ambient conditions.

Some of the measurement methods are highlighted, including measurements of the heat release rate ($\dot{Q}$) and the radiative fraction. These parameters varied from experiment to experiment, as did their uncertainty. Because measurement uncertainty was not documented for many of the experiments, engineering judgment is used, in this and the following chapter, to estimate its value. Measurement uncertainty varies from experiment to experiment, and for each attribute being measured. Accurate determination of experimental uncertainty is challenging, and characterization of the uncertainty in experiments conducted by others is even more so. A good faith effort is made here to quantify measurement uncertainty, but the uncertainty determinations provided in this document should be regarded as estimates and the uncertainty bounds should be regarded as guidelines to assist in the evaluation of the predictive capabilities of the models. Some factors that contribute to experimental uncertainty were not considered here, but may be important. For measurements, systematic error may have been present, but may not have been identified. The potential for human error is always present in the implementation of instrumentation and interpretation of measurement results. In this sense, it is recognized that the uncertainty values presented here are not necessarily all-inclusive or definitive. This highlights the importance of expert judgment in the interpretation of the agreement between measurements and models.

The term “specified” or “prescribed” heat release rate ($\dot{Q}$) is used in this section when referring to the average heat release rate during the steady-burn period in the experiments. It is the input value that is used in the model simulations. The prescribed $\dot{Q}$ in the compartment typically differs from the measured value in the exhaust hood because of mixing in the upper layer of the compartment, which effectively adds a time-delay and a time constant attributable to mixing. For some of the experiments considered here, the prescribed $\dot{Q}$ was inferred from the calorimetric measurement made in the exhaust hood. In these cases, as expected, the measured $\dot{Q}$ increased slowly with time, and then approached a steady value.

The data from all but one of the experimental series were time-averaged over a 10 s interval for use in this study. The data in the NBS data set were acquired every 10 s with a 6 s time-average.

A nearly uniform value for the time-averaging interval establishes consistency among the various experimental data sets. The value of this interval is selected based on a balance between the need to reduce the impact of experimental noise on the determination of ε (see Section 1.4.2), and the need to minimize data smoothing, which may lead to the loss of information. Appendix A provides example calculations regarding this issue.

2.1 FM/SNL Test Series

The Factory Mutual and Sandia National Laboratories (FM/SNL) test series was a series of 25 fire tests conducted in 1985 for the NRC by Factory Mutual Research Corporation (FMRC), under the direction of Sandia National Laboratories (SNL). The primary purpose of these tests was to provide data with which to validate computer models for various types of NPP compartments. The experiments were conducted in an enclosure measuring 18 m long x 12 m wide x 6 m high (60 ft x 40 ft x 20 ft), constructed at the FMRC fire test facility in Rhode Island. Figure 2-2 shows detailed schematic drawings of the compartment from various perspectives. References 2, 14, and 15 provide a detailed description of the FM/SNL test series, including the types and locations of measurement devices, as well as some results.

All of the tests involved forced ventilation to simulate typical NPP installation practices. Four of the tests were conducted with a full-scale control room mockup in place. Parameters varied during the experiments included fire intensity, enclosure ventilation rate, and fire location.

The current study used data from three experiments (Tests 4, 5, and 21). In these tests, the fire source was a propylene gas burner with a diameter of approximately 0.9 m (36 in), with its rim located approximately 0.1 m (4 in) above the floor. For Tests 4 and 5, a round 0.3 m (1 ft) diameter burner was centered along the longitudinal axis centerline, 6.1 m (20 ft) laterally from the nearest wall. For Test 21, the fire source was placed within a simulated benchboard electrical cabinet. Table 2-1 summarizes the information that was used as input for all of the models in the simulation of the FM/SNL tests, including the test duration and information on the compartment, the fire, and the ventilation.

2.1.1 Heat Release Rate

The value of $\dot{Q}$ was determined using oxygen consumption calorimetry in the exhaust stack with a correction applied for the carbon dioxide (CO_2) in the upper layer of the compartment. The uncertainty of the fuel mass flow was not documented. All three tests selected for this study had the same target peak heat release rate ($\dot{Q}$) of 516 kW followed by a 4 min "t-squared" growth profile. The test report contains time histories of the measured $\dot{Q}$, for which the average sustained $\dot{Q}$ following the ramp up for Tests 4, 5, and 21 have been estimated as 510 kW, 480 kW, and 470 kW, respectively. Once reached, the peak $\dot{Q}$ was maintained essentially constant during a steady-burn period of 6 min in Tests 4 and 5, and 16 min in Test 21. Figure 2-1 shows the specified and the measured $\dot{Q}$ [15] as a function of time during Test 21 of the FM/SNL test series. The specified curves are used in the model calculations rather than the measured time-dependent curves, because the fuel flow was maintained a constant and fluctuations in $\dot{Q}$ are expected from calorimetry measurements. Also, there was some concern with the quality of the

heat release rate measurement as the test report notes that during Tests 4, 5, and 21 there was a downward bias in the measured $\dot{Q}$ because of "significant" loss of effluent from the exhaust hood. This bias was treated as an additional uncertainty, and the relative combined expanded uncertainty was assumed to equal ±20%, which is somewhat larger than typical calorimetric measurement uncertainty. The uncertainty in $\dot{Q}$ is discussed further in Chapter 3.

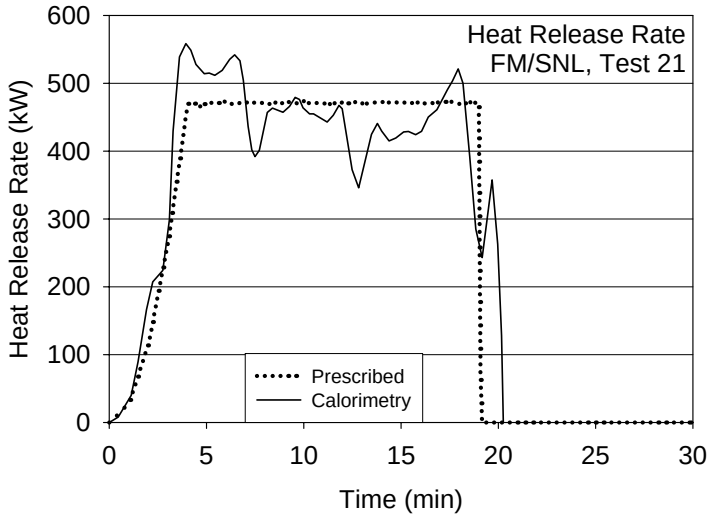

Figure 2-1: Prescribed (dotted line) and measured (solid line) heat release rate as a function of time during Test 21 of the FM/SNL test series

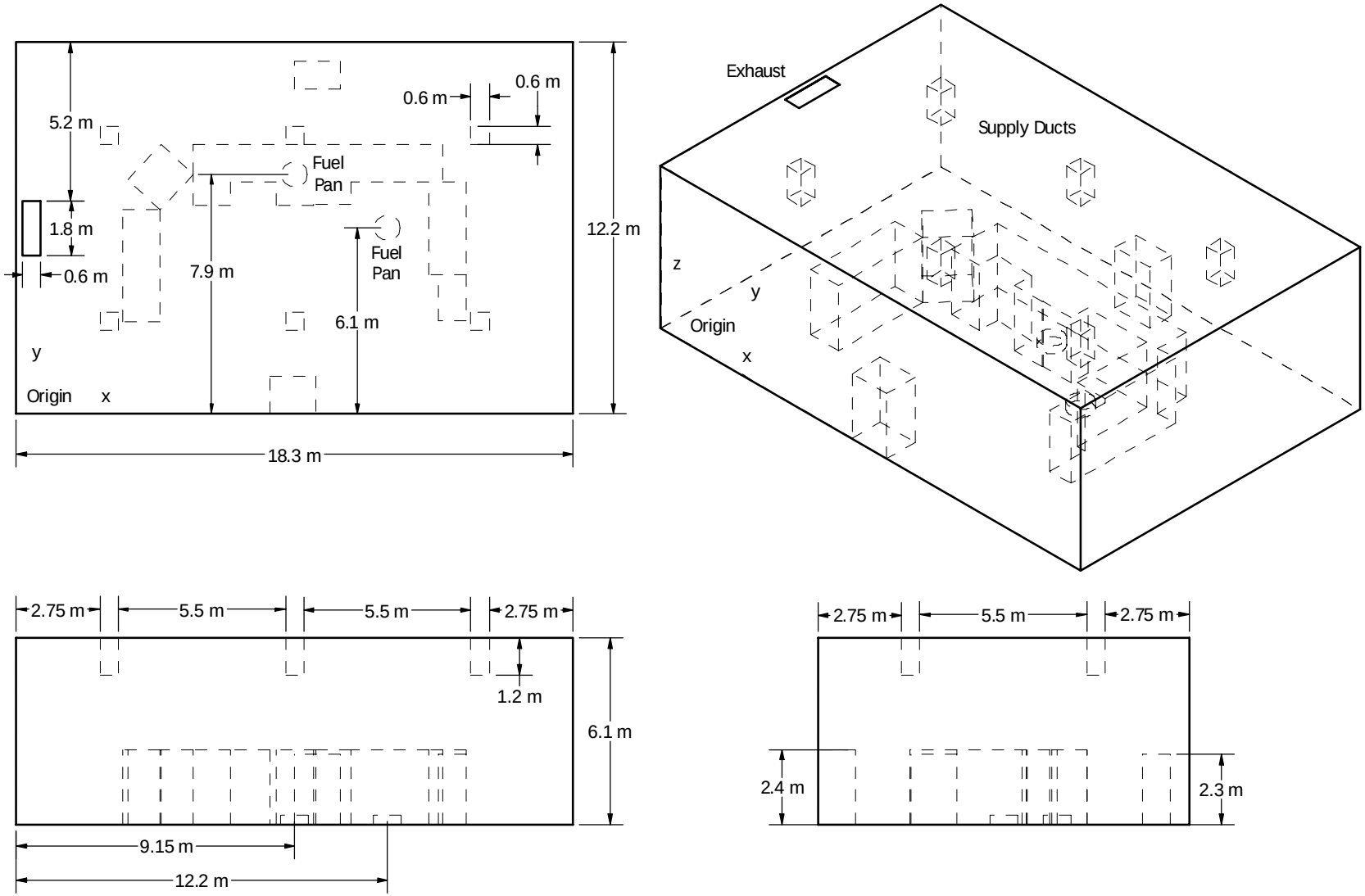

Figure 2-2: Detailed plan, side, and perspective schematic drawings of the FM/SNL experimental arrangement, including the supply and exhaust ducts, and the fuel pan

Table 2-1: Input for Calculation of the FM/SNL Tests

Simulation Time = 900 s

Compartment					
Size			**Position**		
X (Width) (m)	**Y (Depth)** (m)	**Z (Height)** (m)	**X (Width)** (m)	**Y (Depth)** (m)	**Z (Height)** (m)
18.3	12.2	6.1	0	0	0

Compartment Materials (Inside Layer)*		
Ceiling	**Floor**	**Walls**
Marinite (25 mm)	Concrete	Marinite (25 mm)

Fire Description								
Test	**Fuel**	**Fire Area** (m^2)	**Position X(m),Y(m)**	$\dot{Q}$ **(kW)**	**Radiative Fraction**	**Ramp-Up Time (s)**	**Steady-Burn Period (s)**	**Ramp-Down Time (s)**
Test 4	Propylene	1.08	12, 6.1	510	0.35	240	360	10
Test 5	Propylene	2.01	12, 6.1	480	0.35	240	360	10
Test 21	Propylene	2.01		470	0.35	240	900	10

Ventilation			
Openings			
From	**To**	**Area** (m^2)	**Position**
Fire Room	Outside	1.08	Ceiling
Mechanical Vents			
From	**To**	**Area** (m^2)	**Height** (m)
Outside	Fire Room	0.66	4.9

Forced Ventilation		
Test	**Mechanical Ventilation**	**Inflow** (m^3/s)
Test 4	On	0.38
Test 5	On	3.78
Test 21	On	0.38

2.1.2 Radiative Fraction

The radiative fraction (see definition in Chapter 3) was not measured during the experiment, but in this study it is assumed to equal 0.35, which is typical for a smoky hydrocarbons [16, 17]. The expanded uncertainty in this value was taken as ±20%, a value typical of reported uncertainty [18, 19]. It was further assumed that the radiative fraction was about the same in Test 21 as the other tests, as fuel burning must have occurred outside of the electrical cabinet in which the burner was placed. The radiative fraction and its uncertainty are discussed further in Chapter 3.

2.1.3 Other Measurements

Four types of measurements were conducted during the FM/SNL test series that are used in the current model evaluation study, including the HGL temperature and depth, and the ceiling jet and plume temperatures. Aspirated thermocouples (TCs) were used to make all of the temperature measurements. Generally, aspirated TC measurements are preferable to bare-bead TC measurements, as systematic radiative exchange measurement error is reduced. For the relatively low temperatures observed (<100 °C), however, the differences are expected to be small.

Aspirated Thermocouples: Aspirated TC measurements for the range of temperatures measured are typically accurate to a few degrees (°C); see the discussion of thermocouple uncertainty in Chapter 4. The temperatures were measured using the aspirated TCs in Sectors 1, 2 and 3 of the compartment. In addition, there were some near-ceiling TCs placed directly above the burner in Tests 4 and 5.

HGL Depth and Temperature: Data from all of the vertical TC trees were used when reducing the HGL height and temperature. For the FM/SNL Tests 4 and 5, Sectors 1, 2, and 3 were used, all weighted evenly. For Test 21, Sectors 1 and 3 were used, evenly weighted. Sector 2 was partially within the fire plume in Test 21.

2.2 NBS Multi-Compartment Test Series

The National Bureau of Standards (NBS, which is now called the National Institute of Standards and Technology, NIST) Multi-Compartment Test Series consisted of 45 fire tests representing 9 different sets of conditions were conducted in a three-room suite. The experiments were conducted in 1985 and are described in detail in reference 3. The suite consisted of two relatively small rooms, connected via a relatively long corridor. The fire source, a gas burner, was located against the rear wall of one of the small compartments as seen in Figure 2-3 for a 100 kW fire. Figure 2-4 presents the experimental arrangement in the form of plan, side and perspective schematic drawings of the compartments. Fire tests of 100 kW, 300 kW and 500 kW were conducted. For the current V&V study, only three 100 kW fire experiments have been used, including Test 100A from Set 1, Test 100O from Set 2, and Test 100Z from Set 4. The selected data are also available in reference 20. Table 2-2 summarizes information used as model input for simulation of the NBS tests, including information on the compartment, the fire, the ventilation, and ambient conditions.

For the NBS Multi-room series, Tests 100A, 100O and 100Z were selected for study, because they were constructively used in the previous EPRI study [20], and because these tests had the steadiest values of measured heat release rate during the steady-burn period. The data in the NBS data set was acquired every 10 s with a 6 s time-average. This time-averaging interval was somewhat smaller than all of the other experimental series, which were time-averaged over a 10 s interval.

Figure 2-3: Photo of a 100 kW fire with the burner located against the rear wall of one of the small compartments. Photo provided by Rick Peacock, NIST.

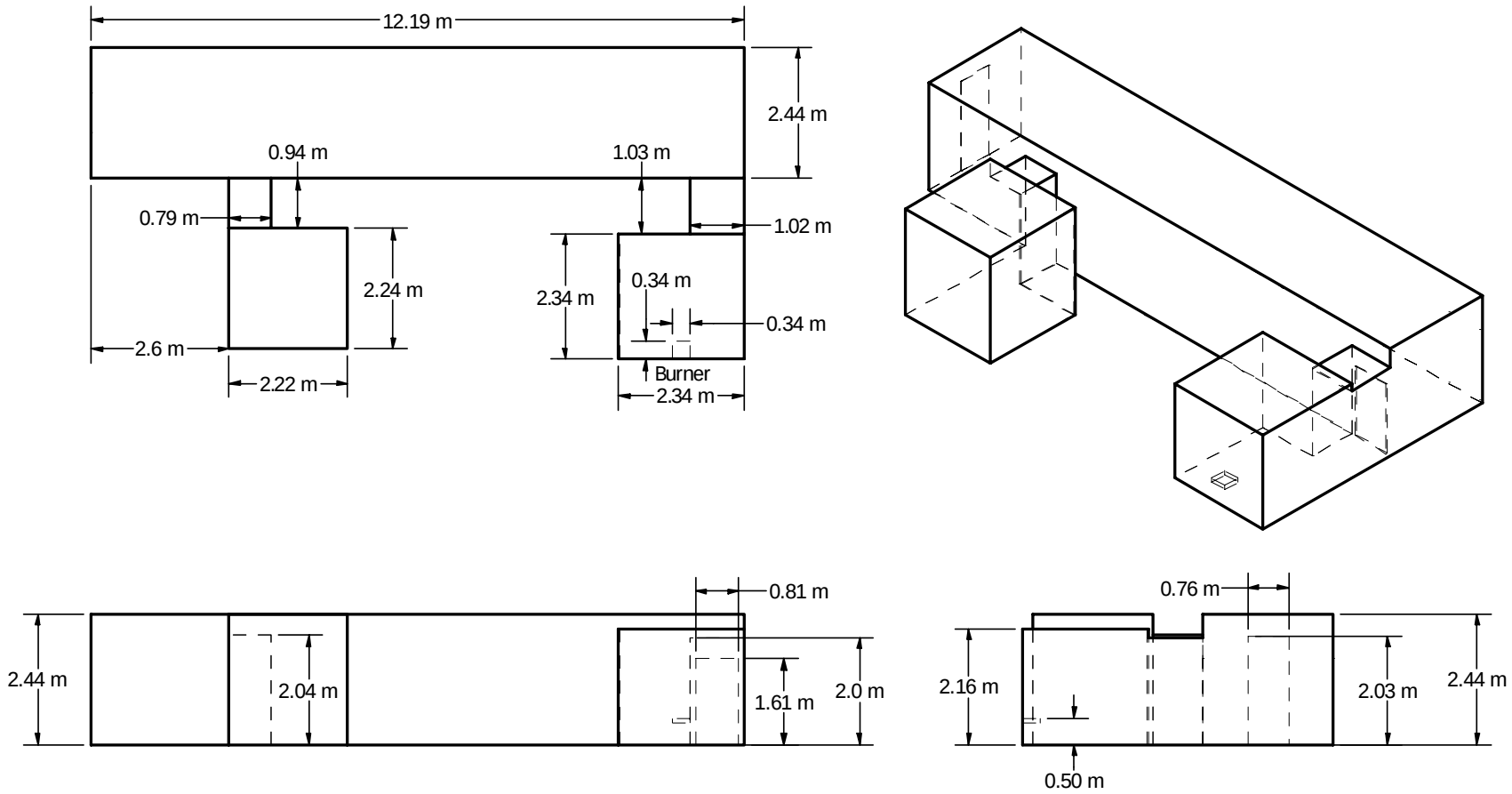

Figure 2-4: Plan, side, and perspective schematic drawings of the NBS experimental arrangement, including the burner

Table 2-2: Input for Calculation of NBS Tests

Simulation Time = 1200 s

Compartment

Compartment	Size			Reference Position		
	X (Width) (m)	Y (Depth) (m)	Z (Height) (m)	X (Width) (m)	Y Depth) (m)	Z (Height) (m)
Fire Room	2.34	2.34	2.16	9.85	0.00	0.00
Fire Stub Corridor	1.03	1.02	2.00	11.16	2.34	0.00
Corridor	12.19	2.44	2.44	0.00	3.36	0.00
Target Room	2.22	2.24	2.43	2.07	0.33	0.00
Target Stub Corridor	0.94	0.79	2.04	2.07	2.57	0.00

Compartment Materials (Inside Layer)

Compartment	Ceiling	Floor	Walls
Fire Room	Ceramic Fiber (113 mm)	Fire Brick (20 mm)	Ceramic Fiber (113 mm)
Fire Stub Corridor	Marinite (12.7 mm)	Gypsum (12.7 mm)	Marinite (12.7 mm)
Corridor	Marinite (12.7 mm)	Gypsum (12.7 mm)	Marinite (12.7 mm)
Target Room	Gypsum (12.7 mm)	Concrete (102 mm)	Gypsum (12.7 mm)
Target Stub Corridor	Gypsum (12.7 mm)	Concrete (102 mm)	Gypsum (12.7 mm)

Fire Description

Test	Fuel	Fire Area (m²)	Position X(m),Y(m)	$\dot{Q}$ (kW)	Radiative Fraction
MV100A	Natural Gas	-	1.17, 0	110	0.2
MV100O	80% Natural Gas + 20% Acetylene	-	1.17, 0	110	0.3
MV100Z	80% Natural Gas + 20% Acetylene	-	1.17, 0	110	0.3

Test	Ramp-up Time		Steady-Burn Period		Ramp Down Time	
	Period (s)	End time (s)	Period (s)	End time (s)	Period (s)	End time (s)
MV100A	5	5	900	905	5	910
MV100O	5	5	900	905	5	910
MV100Z	5	5	900	905	5	910

Openings

From	To	Width (m)	Height (m)	Sill (m)	Area (m²)	Position (m)	Face
Fire Room	Fire Stub Corridor	0.81	1.6	0	-	1.42	-
Fire Stub Corridor	Corridor	0.81	1.6	0	-	0.11	-
Corridor	Outside	0.76	2.03	0	-	0.84	-
Corridor	Target Stub Corridor	0.79	2.04	0	-	2.14	-
Target Stub Corridor	Target Room	0.79	2.04	0	-	0.075	-

Test	Ambient Conditions	
	Temperature (°C)	Rh (%)
MV100A	23	-

MV100O	21	45
MV100Z	22	62

2.2.1 Heat Release Rate

Figures 2-5 and 2-6 show the experimentally measured $\dot{Q}$ as a function of time during Tests 100A and 100 Z, respectively, of the NBS multi-room test series. In these two tests, for which the door was open, the $\dot{Q}$ during the steady-burn period measured via oxygen consumption calorimetry was about 110 kW ±17 kW (±15%). The combined relative expanded (2σ) uncertainty in the calorimetric $\dot{Q}$ is assigned a value of ±15%, consistent with the replicate measurements made during the experimental series and the uncertainty typical of oxygen consumption calorimetry. This value is also consistent with the measurement variation evident in the figures. It was assumed that the closed door test (Test 100O) had the same $\dot{Q}$ as the open door tests.

The specified or prescribed $\dot{Q}$ is also shown in the figures (see page 2-1 for a description of this term). The mass flow of the fuel (natural gas in Test 100 A, or natural gas mixed with acetylene in Tests 100O and 100Z) was not metered; rather, the effluent was captured in a hood mounted above the open door in the corridor and the $\dot{Q}$ was measured using oxygen consumption calorimetry. The manner by which the fuel flow was controlled is not documented. In Test 100A, candles were used to increase smoke in the upper layer to promote visualization. In Tests 100O and 100Z, acetylene was used (about 20% by volume) to produce smoke. In those tests, the flow of natural gas and acetylene were adjusted to obtain approximately the same $\dot{Q}$ as in Test 100A. The addition of acetylene increased the radiative fraction of the fire. This is discussed in the next section. The value of $\dot{Q}$ and its uncertainty are further discussed in Chapter 3.

2.2.2 Radiative Fraction

For practical reasons, piped natural gas supplied by large utility companies is often used in fire experiments. While its composition may vary from day to day, there is little change expected in the value of the radiative fraction. As mentioned above, natural gas was used as the fuel in Test 100A. In Tests 100O and 100Z, acetylene was added to the natural gas to increase the smoke yield, and as a consequence, the radiative fraction increased. The radiative fraction of natural gas has been studied previously, whereas the radiative fraction of the acetylene/natural gas mixture has not been studied. The radiative fraction for the natural gas fire was assigned a value of 0.20, whereas a value of 0.30 was assigned for the natural gas/acetylene fires [19].

The relative combined expanded (2σ) uncertainty in this parameter was assigned a value of ±20% in Test 100A and ±30% in 100O and 100Z. The 20% expanded deviation value is consistent with typical values of the deviation reported in the literature for the measured radiative fraction. The 100O and 100Z tests had a 50% larger value assigned, because the effect on the radiative fraction of adding acetylene to the natural gas was not measured. The radiative fraction and its uncertainty are discussed further in Chapter 3.

2.2.3 Other Measurements

Measurements made during the NBS test series included gas and surface temperature, pressure, smoke and major gas species concentration, and doorway gas velocity. As seen in Table 1-2, only two types of measurements conducted during the NBS test series were used in the evaluation considered here, because there was less confidence in the other measurements. The measurements considered here were the HGL temperature and depth, in which bare bead TCs were used to make these measurements. Single point measurements of temperature within the burn room were not used in the evaluation of plume or ceiling jet algorithms. This is because the geometry was not consistent in either case with the assumptions used in the model algorithms of plumes or jets. Specifically, the burner was mounted against a wall, and the room width-to-height ratio was less than that assumed by the various ceiling jet correlations.

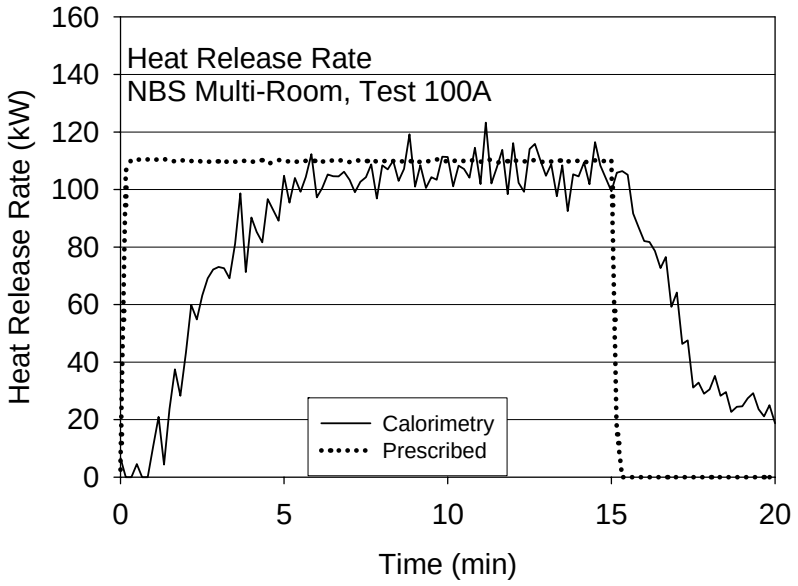

Figure 2-5: Prescribed and measured heat release rate as a function of time during Test 100A of the NBS multi-room test series

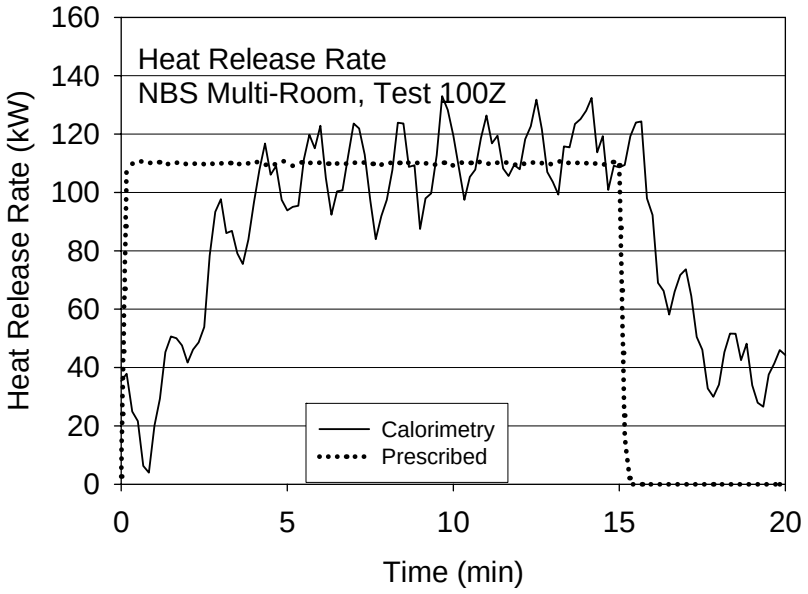

Figure 2-6: Prescribed and measured heat release rate as a function of time during Test 100Z of the NBS multi-room test series

2.3 ICFMP Benchmark Exercise #2

The experiments are described in Reference 4. Benchmark Exercise #2 (BE #2) consisted of eight experiments conducted in 1998 and 1999. The experiments represented three sets of conditions, and were undertaken to study the movement of smoke in a large hall with a sloped ceiling. The results of the experiments were contributed to the International Collaborative Fire Model Project (ICFMP) for use in evaluating model predictions of fires in large volumes representative of turbine halls in NPPs. The tests were conducted inside the VTT Fire Test Hall, with dimensions of 19 m high x 27 m long x 14 m wide (62 ft x 89 ft x 46 ft). Figure 2-7 shows detailed plan, side, and perspective schematic diagrams of the experimental arrangement. Each test involved a single heptane pool fire, ranging from 2 MW to 4 MW. Figure 2-8 is a photo of a 2 MW heptane fire in the facility.

As seen in Table 1-2, four types of measurements conducted during the VTT test series (BE #2) were used in the evaluation considered here, including the HGL temperature and depth, average flame height, and plume temperature. Three vertical arrays of TCs, plus two TCs in the plume, were compared to model simulation results. The HGL temperature and height were reduced from an average of the three TC trees using the standard algorithm [21]. The ceiling jet temperature was not considered, because the ceiling in the test hall is not flat, and the standard model algorithm is not appropriate for these conditions.

2.3.1 Supplementary Information

The VTT test report lacks some information needed to model the experiments, so some information was based on private communications with the principal investigator.[2] The information used to conduct the model simulations is presented in Table 2-3, including information on the fire, compartment, and ventilation.

Surface Materials: The walls and ceiling of the test hall consist of a 1-mm (0.04-in) thick layer of sheet metal on top of a 5-cm (2-in) layer of mineral wool. The floor was constructed of concrete. The report does not provide thermal properties of these materials. Thermophysical properties of the materials that were used in the simulations are given in Chapter 3.

Natural Ventilation: In Cases 1 and 2, all doors were closed, and ventilation was restricted to infiltration through the building envelope. Precise information on air infiltration during these tests is not available. The scientists who conducted the experiments recommend a leakage area of about 2 m^2 (20 ft^2), distributed uniformly throughout the enclosure. By contrast, in Case 3, the doors located in each end wall (Doors 1 and 2, respectively) were open to the external ambient environment. These doors are each 0.8 m wide x 4 m high (2.6 ft x 5 ft), and are located such that their centers are 9.3 m (30.5 ft) from the south wall.

Mechanical Ventilation: The test hall had a single mechanical exhaust duct, located in the roof space, running along the center of the building. This duct had a circular section with a diameter of 1 m (40 in), and opened horizontally to the hall at a distance of 12 m (39 ft) from the floor and 10.5 m (34.4 ft) from the west wall. Mechanical exhaust ventilation was operational for Case 3, with a constant volume flow rate of 11 m^3/s drawn through the 1 m (40 in) diameter exhaust duct.

HGL Height and Temperature: All of the vertical TC trees were used to compute the HGL depth and temperature using the standard two-layer reduction algorithm [21], with all of the trees assigned equal importance or weighting.

[2] Hostikka, Simo, VTT, Helsinki, Finland. Telephone conversation on May 2005 discussing the surface materials used during BE #2.

Table 2-3: Input for Calculation of BE #2

Simulation Time = 900 s

Compartment

Size				Position		
X (Width) (m)	**Y (Depth)** (m)	**Area** (m^2)	**Z (Height)** (m)	**X (Width)** (m)	**Y (Depth)** (m)	**Z (Height)** (m)
13.8	27	372.6	19	0	0	0
1.9	27	51.3	19			
1.9	27	51.3	19			
Cross-sectional area varies as a function of height						

Compartment Materials (Inside Layer)*

Ceiling	Floor	Walls
Steel	Concrete	Steel

Fire Description

Test	Fuel	Fire Area (m^2)	Position X(m),Y(m)	$\dot{Q}$ (kW)	Radiative Fraction	Main Door
Case 1	Heptane	1.08	7.2, 16	Profile	0.35	Closed
Case 2	Heptane	2.01	7.2, 16	Profile	0.35	Closed
Case 3	Heptane	2.01	7.2, 16	Profile	0.35	Open

Ventilation

Openings

From	To	Width (m)	Height (m)	Sill (m)	Position (m)	Face
Fire Room	Outside	0.8	4.0	0	8.90	Front
Fire Room	Outside	0.8	4.0	0	8.90	Rear
Fire Room	Outside	0.71	0.71	0	6.55	Left
Fire Room	Outside	0.71	0.71	12	6.55	Left
Fire Room	Outside	0.71	0.71	0	6.55	Right
Fire Room	Outside	0.71	0.71	12	6.55	Right

Mechanical Vents

From	To	Area (m^2)	Height (m)	Case
Fire Room	Outside	3.14	12.0	Case 3 only
Fire Room	Outside			Case 3 only
Fire Room	Outside			Case 3 only
Fire Room	Outside			Leakage
Fire Room	Outside			Leakage
Fire Room	Outside			Leakage
Fire Room	Outside			Leakage

2.3.2 Heat Release Rate

Each test used a single fire source with its center located 16 m (52 ft) from the west wall and 7.4 m (24.3 ft) from the south wall. For all tests, the fuel was heptane in a circular steel pan that was partially filled with water. The pan had a diameter of 1.17 m (46.0 in) for Case 1 and 1.6 m (63 in) for Cases 2 and 3. In each case, the fuel surface was 1 m (40 in) above the floor. The trays were placed on load cells, and the $\dot{Q}$ was calculated from the mass loss rate (see definition in Chapter 3). For the three cases, the fuel mass loss rate was averaged from individual replicate tests.

In the $\dot{Q}$ estimation, the heat of combustion (taken as 44.6 kJ/g) and the combustion efficiency (χ_a) for n-heptane was used. Hostikka [4] suggests a value of 0.8 for the combustion efficiency. Bundy estimates the efficiency of a 500 kW heptane pool fire to be equal to 0.97[3]. Tewarson reports a value of 0.93 for a 10 cm pool [17]. The magnitude of the combustion efficiency is a complicated function of fire size, ventilation, and other effects. Consideration of the chemical structure of a fire suggests that the combustion efficiency should decrease as the fire size grows. Available data confirms this [22]. The size of a compartment may also impact this parameter, but there is little information in the fire literature that addresses this point. In summary, there is little certainty in the actual value of the combustion efficiency in this experiment. In this report, a combustion efficiency of 0.85 ±0.12 (or ±14%) is recommended for the BE #2 pool fire tests, based on engineering judgment. Because of the relatively large value of the uncertainty associated with χ_a, the uncertainty in $\dot{Q}$ is dominated by the uncertainty in the combustion efficiency. Uncertainty in the mass loss rate measurement also contributed to the overall uncertainty, and the uncertainty in $\dot{Q}$ was estimated as 15%. Figures 2-9 through 2-11 show the prescribed $\dot{Q}$ as a function of time during Cases 1 through 3, respectively. Tables 2-4 through 2-6 represent the mass loss and estimated $\dot{Q}$ associated with Figures 2-9 through 2-11, respectively.

2.3.3 Radiative Fraction

The radiative fraction was assigned a value of 0.35, similar to many smoky hydrocarbons [19]. The relative combined expanded (2σ) uncertainty in this parameter was assigned a value of ±20%, which is typical of uncertainty values reported in the literature for this parameter.

[3] Bundy, Matthew, NIST, Gaithersburg, MD. Conversation at NIST during May, 2005 on determination of the combustion efficiency and the heat release rate in heptane spray flames in the NIST Large Fire Laboratory. Considering stoichiometry of the combustion and measurements in the exhaust hood, a combustion efficiency of 0.97 was determined for a 500 kW heptane spray fire.

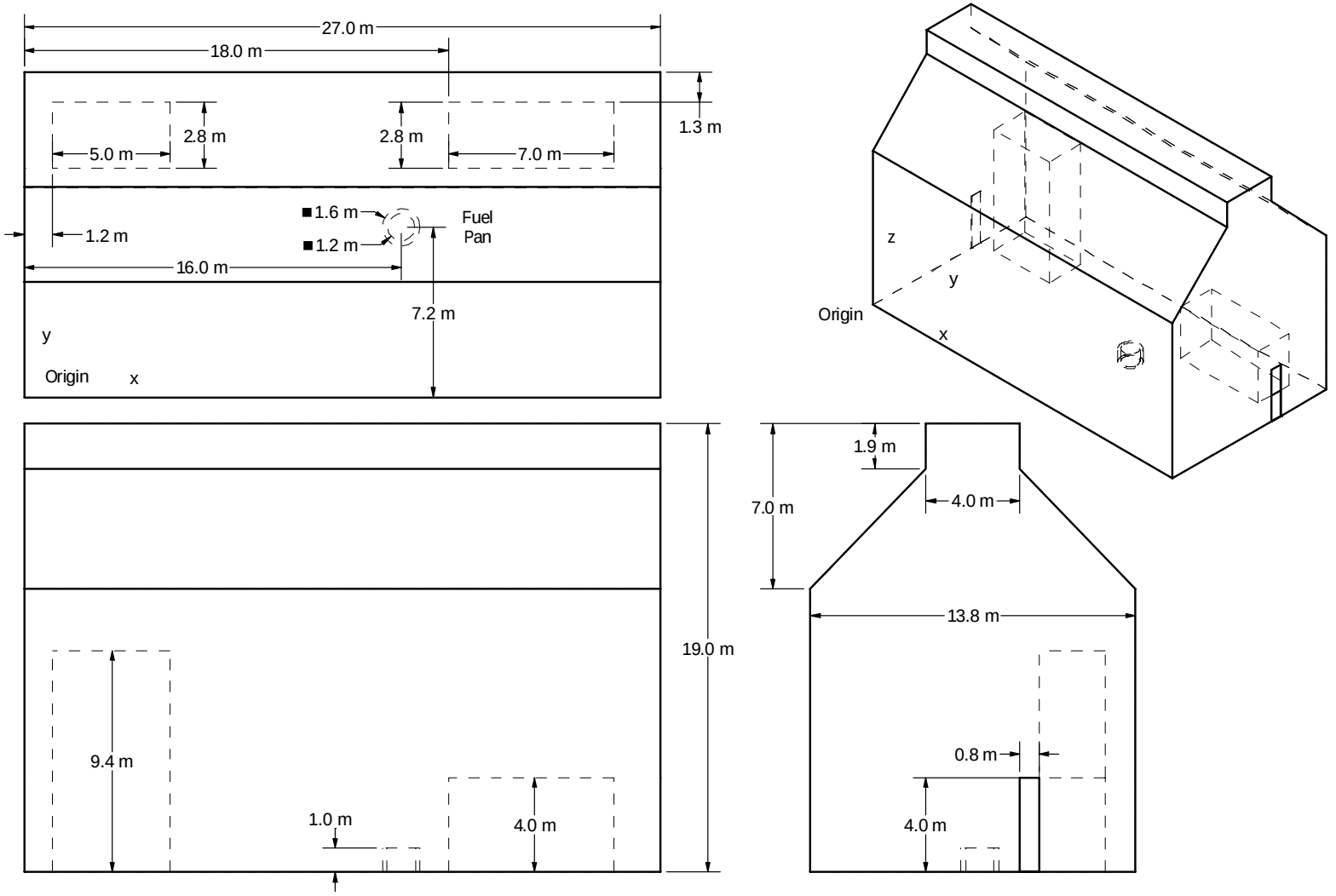

Figure 2-7: Plan, side, and perspective schematic drawings of the experimental arrangement of the BE #2 large hall fire tests, including the fuel

pan 

Figure 2-8: Photo of a 2 MW heptane fire during the BE #2 tests. Photo provided by Simo Hostikka, VTT

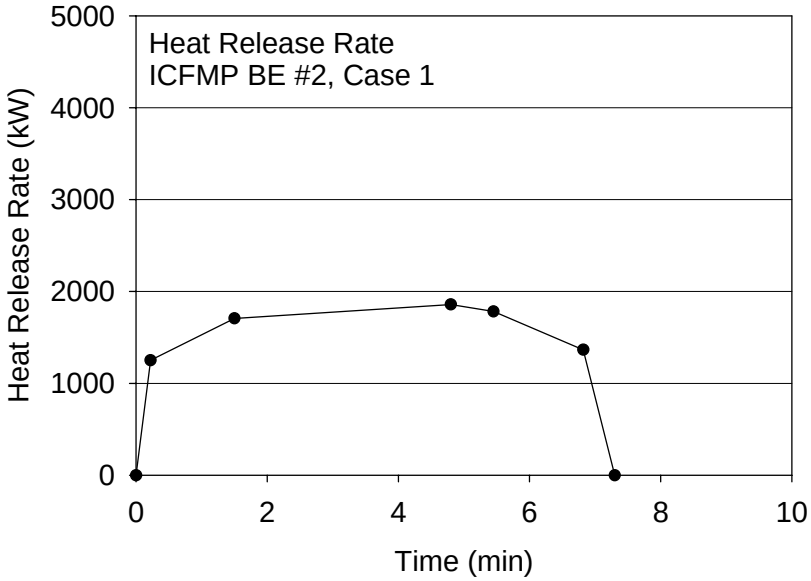

Figure 2-9: Prescribed heat release rate as a function of time for Case 1

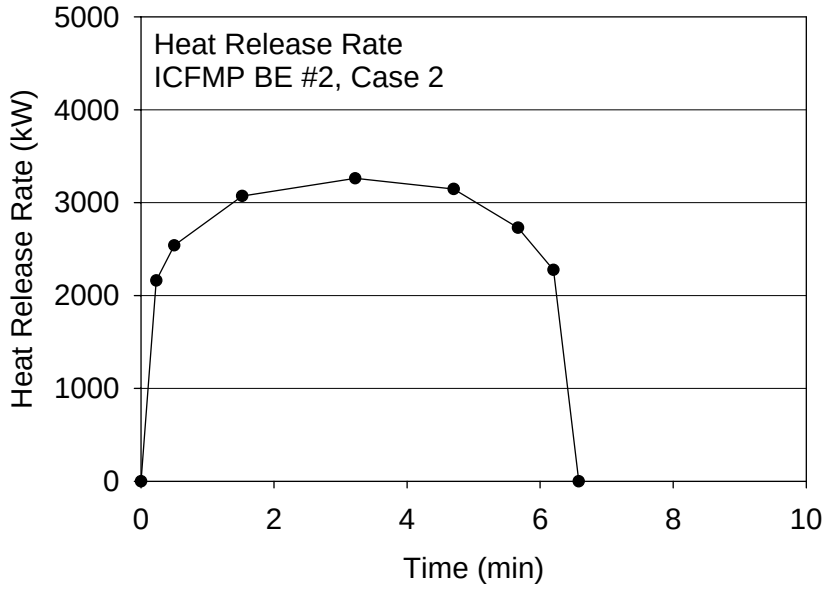

Figure 2-10: Prescribed heat release rate as a function of time for Case 2

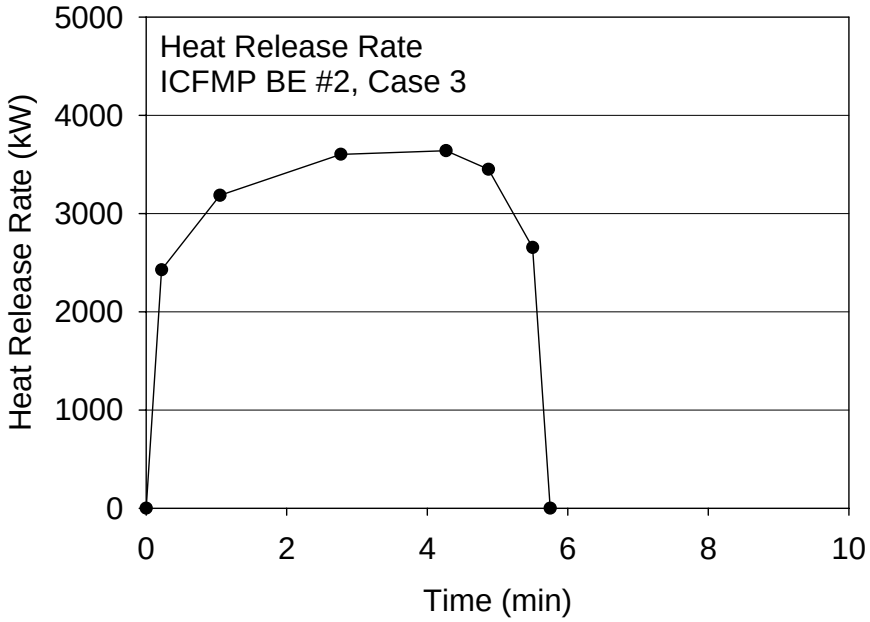

Figure 2-11: Prescribed heat release rate as a function of time for Case 3

Table 2-4: Mass Loss ($\dot{m}$) and Heat Release Rate ($\dot{Q}$) for Case 1

Time (s)	$\dot{m}$ (kg/s)	$\dot{Q}$ (kW)
0	0	0
13	0.033	1245
90	0.045	1709
288	0.049	1858
327	0.047	1783
409	0.036	1356
438	0	0

Table 2-5: Mass Loss ($\dot{m}$) and Heat Release Rate ($\dot{Q}$) for Case 2

Time (s)	$\dot{m}$ (kg/s)	$\dot{Q}$ (kW)
0	0	0
14	0.057	2151
30	0.067	2542
91	0.081	3063
193	0.086	3259
282	0.083	3129
340	0.072	2737
372	0.060	2275
395	0	0

Table 2-6: Mass Loss ($\dot{m}$) and Heat Release Rate ($\dot{Q}$) for Case 3

Time (s)	$\dot{m}$ (kg/s)	$\dot{Q}$ (kW)
0	0	0
13	0.064	2426
63	0.084	3184
166	0.095	3601
256	0.096	3639
292	0.091	3450
330	0.070	2654
345	0	0

2.4 ICFMP Benchmark Exercise #3

Benchmark Exercise #3 (BE #3), conducted as part of the International Collaborative Fire Model Project (ICFMP) and sponsored by the NRC, consisted of 15 large-scale experiments performed at NIST in June 2003. All 15 tests were considered in this study. The experiments are documented in Reference 5. The fire sizes ranged from 350 kW to 2.2 MW in a compartment with dimensions of 21.7 m x 7.1 m x 3.8 m high (71.2 ft x 23.3 ft x 2.5 ft), designed to represent a compartment in an NPP containing power and control cables. A photo of the fire seen through the compartment doorway is shown in Figure 2-12. Walls and ceiling were covered with two layers of marinate boards, each layer 0.0125 m (0.5 in) thick. The floor was covered with one layer of 0.0125-m (0.5-in) thick gypsum board on top of a 0.0183-m (23/32-in) layer of plywood. Thermophysical and optical properties of the marinate and other materials used in the compartment are given in Chapter 3 and reference 5. The room had one door and a mechanical air injection and extraction system. Ventilation conditions, the fire size, and fire location were varied. Numerous measurements (approximately 350 per test) were made including gas and surface temperatures, heat fluxes and gas velocities. Detailed schematic diagrams of the experimental arrangement are shown in Figure 2-13. Table 2-7 lists information associated with the fuel including the fuel type, the steady heat release rate, the pan position and duration of the ramp-up, ramp-down and steady-burn periods. Other information used to conduct the model simulations is presented in Tables 2-8 and 2-9, including information on the fire, compartment, ventilation, targets, and ambient conditions.

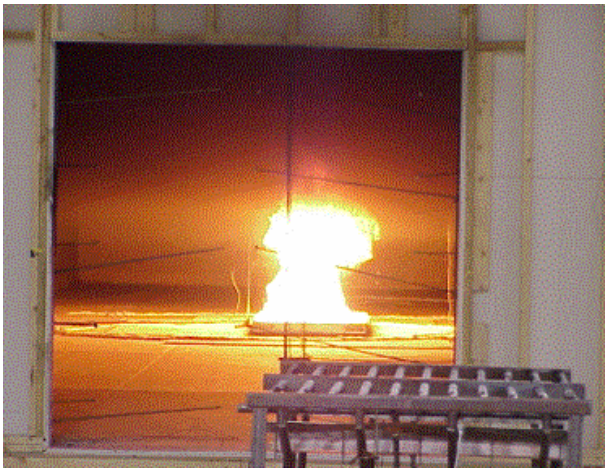

Figure 2-12: Photograph of a 1 MW heptane fire seen through the open doorway. Photo provided by Anthony Hamins, NIST

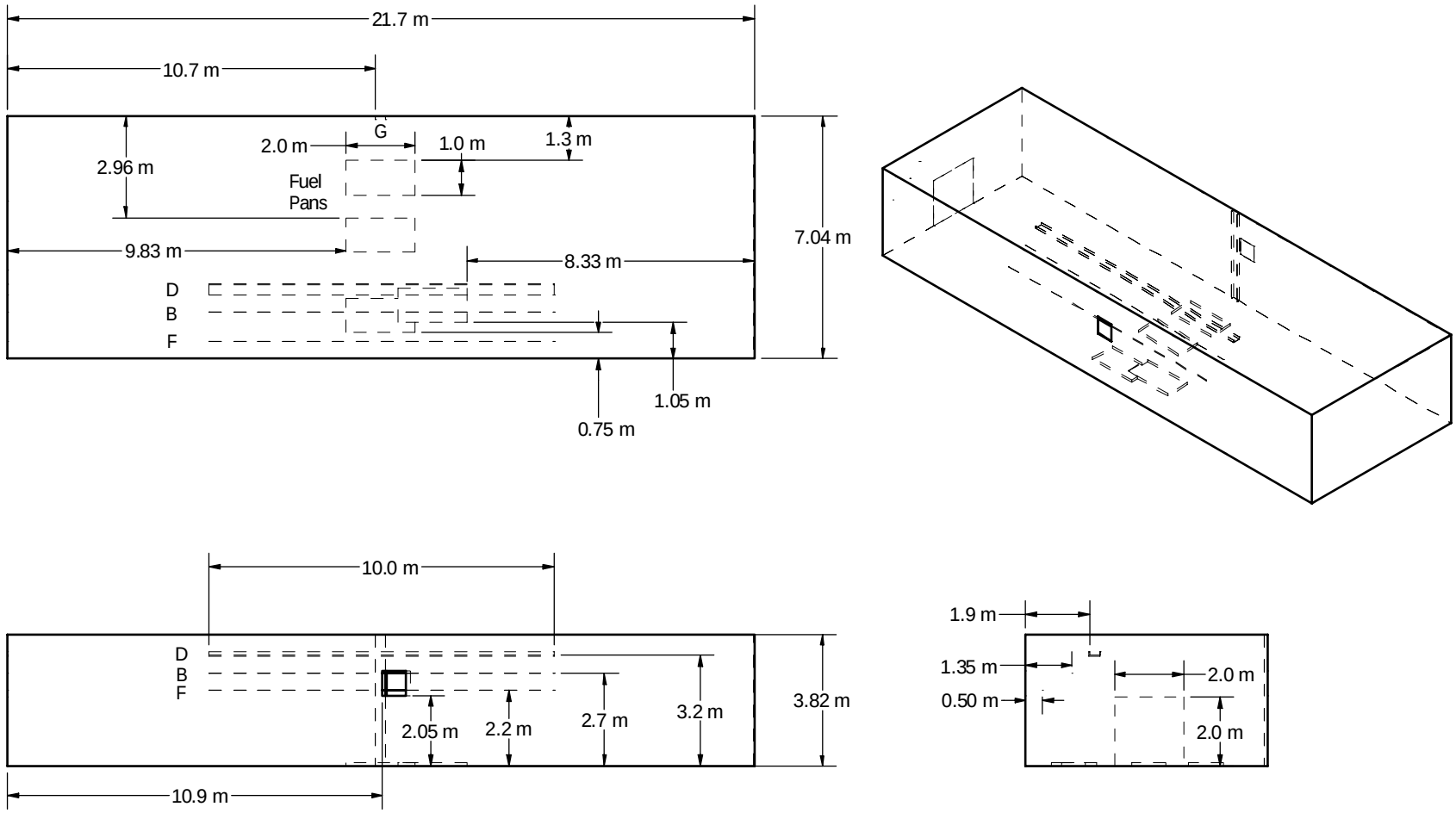

Figure 2-13: Plan, side, and perspective schematic drawings of the ICFMP BE #3 experimental arrangement. The fuel pan and cables B, D, F, and G (dotted lines) are also shown.

Table 2-7: Fire Character, Including Fuel Type; Pan Position; and Duration of the Ramp-Up, Ramp-Down, and Steady-Burn Periods

Test	Fuel	Fuel Pan Position	$\dot{Q}$	Ramp-up Time		Steady-Burn Period		Ramp Down Time	
		x (m), y (m)	(kW)	(s)	End time (s)	(s)	End time (s)	(s)	End time(s)
1	Heptane	Center	410	148	148	1202	1350	150	1500
2	Heptane	Center	1190	180	180	445	625	1	626
3	Heptane	Center	1190	178	178	1201	1379	183	1562
4	Heptane	Center	1200	178	178	636	814	1	815
5	Heptane	Center	1190	178	178	1201	1379	183	1562
6	test not conducted								
7	Heptane	Center	400	129	129	1203	1332	128	1460
8	Heptane	Center	1190	176	176	434	610	1	611
9	Heptane	Center	1170	175	175	1201	1376	184	1560
10	Heptane	Center	1190	176	176	650	826	1	827
11	test not conducted								
12	test not conducted								
13	Heptane	Center	2330	177	177	187	364	1	365
14	Heptane	10.83, 5.21	1180	176	176	1205	1381	186	1567
15	Heptane	10.83,1.25	1180	180	180	1200	1380	187	1567
16	Heptane	Center	2300	177	177	205	382	1	383
17	Toluene	Center	1160	181	181	91	272	1	273
18	Heptane	12.33,1.55	1180	178	178	1202	1380	187	1567

Table 2-8: Input for Calculation of BE #3

Simulation Time = 1800 s

Compartment					
Size			**Position**		
X (Width) (m)	**Y (Depth) (m)**	**Z (Height) (m)**	**X (Width) (m)**	**Y (Depth) (m)**	**Z (Height) (m)**
21.7	7.04	3.82	0	0	0

Compartment Materials (Inside Layer)*		
Ceiling	**Floor**	**Walls**
Marinite (25 mm)	Gypsum (25 mm)	Marinite (25 mm)

Ventilation

Openings

From	To	Width (m)	Height (m)	Sill (m)	Area (m^2)	Position (m)	Face
Fire Room	Outside	2	2	0	4	2.58	Left

Mechanical Vents

From	To	Area (m^2)	Height (m)
Outside	Fire Room	0.49	2.4

Ventilation and Leakage Conditions

Test	Door	Forced Ventilation			Leakage	
		Mechanical Ventilation	Inflow (m^3/s)	Outflow (m^3/s)	Area (cm^2)	Width (m)
1	Closed	Off	na	na	593	5.93
2	Closed	Off	na	na	580	5.8
3	Open	Off	na	na	na	na
4	Closed	On	1.70	0.90	580	5.8
5	Open	On	1.70	0.90	na	na
6	test not conducted					
7	Closed	Off	na	na	712	7.12
8	Closed	Off	na	na	645	6.45
9	Open	Off	na	na	na	na
10	Closed	On	1.70	0.90	712	7.12
11	test not conducted					
12	test not conducted					
13	Closed	Off	na	na	833	8.33
14	Open	Off	na	na	na	na
15	Open	Off	na	na	na	na
16	Closed	On	1.70	0.90	712	7.12
17	Closed	Off	na	na	712	7.12
18	Open	Off	na	na	na	na

Table 2-9: Target and Ambient Data for BE #3

Targets									
Target	**Position**			**Face**	**Normal Vector**			**Material**	**Target**
	x (m)	**y (m)**	**Z (m)**		**x(m)**	**y(m)**	**z(m)**		
Surface Flux N1	3.91	7.04	1.49	Rear	0	-1	0	Marinite	1
Surface Flux N4	12.15	7.04	1.87	Rear	0	-1	0	Marinite	2
Surface Flux S1	3.91	0	1.49	Front	0	1	0	Marinite	3
Surface Flux S3	9.55	0	1.87	Front	0	1	0	Marinite	4
Surface Flux S4	12.15	0	1.87	Front	0	1	0	Marinite	5
Surface Flux E1	21.7	1.59	1.12	Right	-1	0	0	Marinite	6
Surface Flux E2	21.7	1.59	2.43	Right	-1	0	0	Marinite	7
Surface Flux E3	21.7	5.76	1.12	Right	-1	0	0	Marinite	8
Surface Flux E4	21.7	5.76	2.43	Right	-1	0	0	Marinite	9
Surface Flux C1	3.04	3.59	3.82	Ceiling	0	0	-1	Marinite	10
Surface Flux C2	9.11	5.97	3.82	Ceiling	0	0	-1	Marinite	11
Surface Flux C4	10.85	2.39	3.82	Ceiling	0	0	-1	Marinite	12
Surface Flux C5	10.85	5.17	3.82	Ceiling	0	0	-1	Marinite	13
Surface Flux C7	13.02	5.97	3.82	Ceiling	0	0	-1	Marinite	14
Surface Flux F1	3.04	3.59	0	Floor	0	0	1	Gypsum	15
Surface Flux F2	9.11	2.00	0	Floor	0	0	1	Gypsum	16
Surface Flux F4	10.85	2.39	0	Floor	0	0	1	Gypsum	17
Cable Tray Control D	10.85	2.00	3.20	Down	0	0	-1	XLP Control	18
Cable Control E	10.85	1.25	2.70	Down	0	0	-1	PVC Control	19
Cable Control B	10.55	1.30	2.80	Down	0	0	-1	XLP Control	20
Cable Power F	10.85	0.50	2.20	Down	0	0	-1	XLP Power	21
Cable Tray Control G33	10.80	6.8	1.75	Rear	0	-1	0	XLP Control	22

Test	**Ambient Conditions**	
	Temp (°C)	**Rh (%)**
1	22	32
2	26	36
3	30	34
4	27	44
5	28	37
6	test not conducted	
7	24	58
8	25	63
9	27	62
10	27	63
11	test not conducted	
12	test not conducted	
13	31	52
14	28	61
15	18	95
16	26	55
17	29	45
18	27	40

2.4.1 Ventilation

Natural Ventilation: The compartment had one door with dimensions of 2 m x 2 m (6.6 ft x 6.6 ft) in the middle of the west wall. Some of the tests had a closed door and no mechanical ventilation (Tests 2, 7, 8, 13, and 17), and in those tests, the measured compartment leakage was an important consideration. Reference 5 reports leakage area based on measurements performed prior to Tests 1, 2, 7, 8, and 13. For the closed door tests, the leakage area used in the simulations ought to be based on the last available measurement. It should be noted that the chronological order of the tests differed from the numerical order [5]. For Test 4, it is recommended that the leakage area measured before Test 2 be used. For Tests 10 and 16, it is recommended that the leakage area measured before Test 7 be used.

Mechanical Ventilation: The mechanical ventilation and exhaust was used during Tests 4, 5, 10, and 16, providing about 5 air changes per hour. The door was closed during Test 4 and open during Tests 5, 10, and 16. The supply duct was positioned on the south wall, about 2 m (6.6 ft) off the floor. An exhaust duct of equal area to the supply duct was positioned on the opposite wall at a comparable location. The flow rates through the supply and exhaust ducts were measured in detail during breaks in the testing, in the absence of a fire.

During the tests, the flows were monitored with single bidirectional probes during the tests themselves. A bidirectional probe was positioned in the center of the exhaust duct, and its velocity was recorded under the column header "BP Exhaust Vent" in the BE #3 experimental data sets. Its value varied between 3 m/s (10 ft/s) and 4 m/s (13 ft/s) for the four ventilated tests. The supply and exhaust volume flow rates and other pertinent information can be found in reference 5. This is usually expressed as the vent area times an average velocity. Another bidirectional probe was positioned in the supply duct, 30 cm (1 ft) from the bottom of the duct during Tests 4 and 5, and 15 cm from the bottom of the duct for Tests 10 and 16. In the data sets, this measurement is listed under the column header "BP Supply Vent-16." Its value was between 3 m/s (10 ft/s) and 4 m/s (13 ft/s) for Tests 4 and 5, and was as high as 10 m/s (33 ft/s) during Tests 10 and 16.

The exhaust duct profile was relatively uniform, whereas the supply was not. Most of the air was blown out of the bottom third of the supply duct. The single point measurements during the fire tests indicated that the flow field changed from its ambient values. The measured supply volume flow rate of 1.06 m^3/s (37.4 ft^3/s) pre-test decreased to 0.9 m^3/s (31 ft^3/s) during testing. For the exhaust, the measured volume flow rate of 1.03 m^3/s (36.4 ft^3/s) pretest increased to about 1.7 m^3/s (60 ft^3/s) during testing. The uncertainties during the fires are substantially higher than the uncertainties in the ambient measurements (±0.2 m^3/s or 7 ft^3/s). Doubling this value is appropriate.

The ventilation system affected the compartment pressure, HGL temperature, and the surface temperature of various cable targets. The cable surface TCs were just outside of the direct path of the supply fan. In the absence of a fire, blowing was observed to flow upwards at about a 35° angle.

Fire: The fire was located at floor level in the center of the compartment for most of the tests (Tests 1–13, 16, and 17). In Test 14, the fire was centered 1.8 m (72 in) from the North wall. In Test 15, the fire was centered 1.25 m (50 in) from the South wall. In Test 18, the fire was centered 1.55 m (62 in) from the South wall. Physically, the fuel pan was 2 m long x 1 m wide x

0.1 m deep (80 in x 40 in x 4 in). A single nozzle was used to spray liquid hydrocarbon fuels onto a fire pan with dimensions of 1 m long x 2 m wide x 0.02 m deep (40 in x 80 in x 1 in). The test plan originally called for the use of two nozzles to provide the fuel spray. Experimental observation suggested that the fire was less unsteady with the use of a single nozzle. In addition, it was observed that the actual extent of the liquid pool was well-approximated by a 1 m (40 in) circle in the center of the pan. The uncertainty in the location of the liquid fuel was about ±0.1 m (± 4 in). For safety reasons, the fuel flow was terminated when the lower-layer oxygen concentration dropped to approximately 15% by volume.

2.4.2 Heat Release Rate

The fuel used in 14 of the tests was heptane, while toluene was used for one test (see Test 17 in Table 2-7). The $\dot{Q}$ was determined using oxygen consumption calorimetry. The uncertainty in the $\dot{Q}$ measurement was documented in reference 5. The recommended uncertainty values were 17% for all of the tests (also see Table 3-1). Figure 2-14 shows the measured and prescribed $\dot{Q}$ as a function of time during Test 3. Reference 5 discusses the shape of the prescribed $\dot{Q}$ curve in detail.

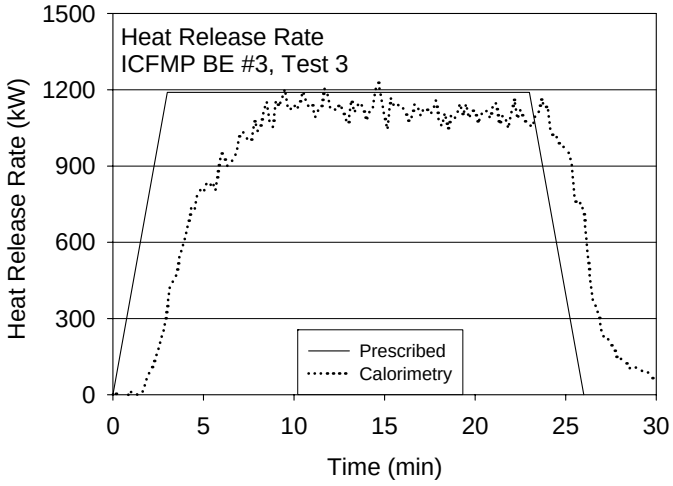

Figure 2-14: Measured and prescribed heat release rate as a function of time during Test 3 of the ICFMP #3 test series

2.4.3 Radiative Fraction

The radiative fraction was measured in an independent study for the same fuels using the same spray burner as used in the BE #3 test series [18]. The value of the radiative fraction and its uncertainty were reported as 0.44 ±16% and 0.40 ±23% for heptane and toluene, respectively (also see Table 3-1).

2.4.4 Other Measurements

As seen in Table 1-2, measurements made during the NIST test series (BE #3) included the 13 parameters considered in this study, except the plume temperature. The vertical TC trees were used to determine the HGL depth and temperature, except Tree 4, which had a faulty TC. The TC data were weighted because the TC trees were not evenly distributed within the compartment. The weighting factors considered the relative location of the TCs and assigned weighting factors based on representative floor area subtended by each tree. Table 2-10 shows the relative weightings used in this study. Trees 1 and 7 were weighted 0.3 each, Tree 2 was weighted 0.2, Tree 3 was weighted 0.1, and the others were weighted 0.05. Calculations of the upper layer depth and temperature showed that a simple average of the TC trees yielded results nearly identical to the weighted results (within 2%).

Table 2-10: Relative Weighting of the Calculation of HGL

Thermocouple Tree	Relative Weight
1	0.3
2	0.2
3	0.1
4	0
5	0.05
6	0.05
7	0.3

2.5 ICFMP Benchmark Exercise #4

Benchmark Exercise (BE) #4 consisted of kerosene pool fire experiments conducted at the Institut für Baustoffe, Massivbau und Brandschutz (iBMB) of the Braunschweig University of Technology in Germany. The results of two experiments were contributed to the International Collaborative Fire Model Project (ICFMP) and documented in the report, *Evaluation of Fire Models for Nuclear Power Plant Applications: Fuel Pool Fire inside a Compartment* [6]. These experiments involved relatively large fires in a relatively small [3.6 m x 3.6 m x 5.7 m (12 ft x 12 ft x 19 ft)] concrete enclosure. Figure 2-15 shows plan, side and perspective schematic drawings of the experimental arrangement, including the location of the fuel pan, which was located at the center of the compartment.

Only a portion of Test 1 was selected for consideration in the present study, because a significant amount of data was lost in Test 1, and the measured $\dot{Q}$ during Test 3 exhibited significant amounts of fluctuation. As seen in Table 1-2, five types of measurements that were conducted during the BE #4 test series were used in the model evaluation reported here. These included the HGL temperature and depth, the temperature of targets and compartment surfaces, and heat flux. Table 2-11 list the inputs used for this experiment.

Table 2-11: Input for Calculation of BE #4

Simulation Time = 2100 s					
Compartment					
Size			**Position**		
X (Width) (m)	**Y (Depth)** (m)	**Z (Height)** (m)	**X (Width)** (m)	**Y (Depth)** (m)	**Z (Height)** (m)
3.6	3.6	5.7	0	0	0

Compartment Materials (Inside Layer)*		
Ceiling	**Floor**	**Walls**
Concrete	Concrete	Light Concrete

Fire Description					
Test	**Fuel**	**Fire Area (m²)**	**Position X(m),Y(m)**	$\dot{Q}$ **(kW)**	**Radiative Fraction**
Test 1	Jet fuel	1	1.8, 1.8	Profile	0.35

Openings							
From	**To**	**Width (m)**	**Height (m)**	**Sill (m)**	**Area (m²)**	**Position (m)**	**Face**
Fire Room	Outside	0.7	3.0	0.6	2.1	1.80	Front door
Fire Room	Outside	3.63	0.42	5.7	1.52	Ceiling	Mechanical ventilation ducts
Fire Room	Outside	3.63	0.42	5.7	1.52	Ceiling	Mechanical ventilation ducts

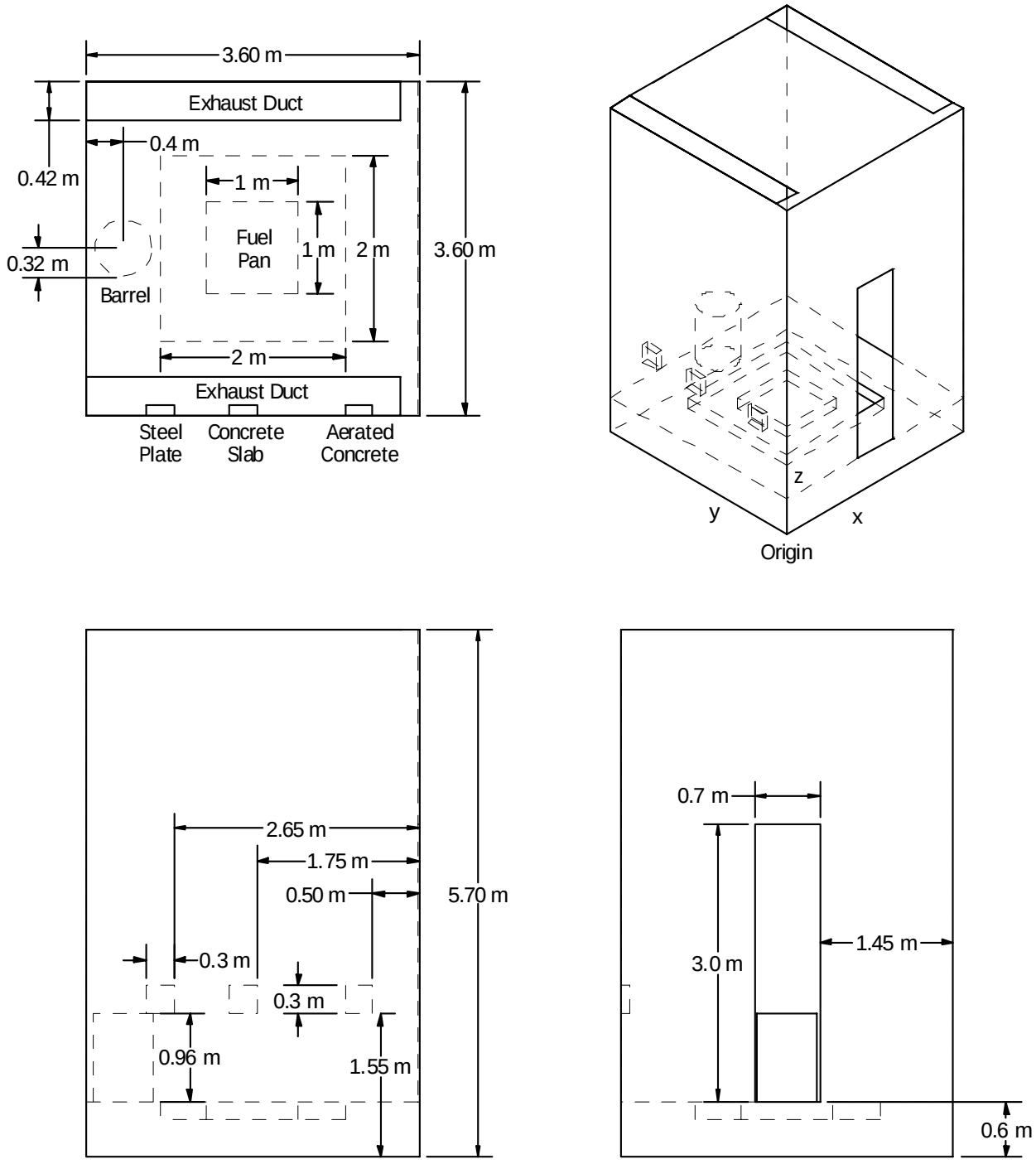

Figure 2-15: Plan, side and perspective schematic drawings of the ICFMP BE #4 experimental arrangement, including the fuel pan

2.5.1 Heat Release Rate

The fire in Test 1 was a 1 m x 1 m (40 in x 40 in) square pan of jet fuel, type A-1. The test report [6] states that the fuel was a mixture of hydrocarbons with a summary formula given by $C_{11.64}H_{25.29}$, and that the thermophysical properties of the jet fuel were similar to dodecane.

Figure 2-16 shows the heat release rate, which was estimated from the mass loss rate measurement. Table 2-12 lists the measured mass loss rate, as well as the calculated $\dot{Q}$ (for an explanation of this calculation, see Chapter 3). In this calculation, the heat of combustion and the combustion efficiency were taken as 42.8 MJ/kg and 1, respectively, as suggested by Reference 6. There were several reported difficulties in measuring the mass loss rate, including data loss attributable to an instrument malfunction and significant fluctuations in the measured mass loss rate. Because of these measurement issues and because the combustion efficiency was not well-characterized, the $\dot{Q}$ uncertainty was assigned a relatively large expanded uncertainty of ±25%. The value of $\dot{Q}$ and its uncertainty are discussed further in Chapter 3.

Table 2-12: Measured Mass Loss Rate and Calculated Heat Release Rate

Time (s)	Mass Loss Rate (kg/s)	$\dot{Q}$ (kW)
0	0	0
92	0.0028	120
180	0.037	1584
260	0.0613	2624
600	0.0747	3197
822	0.0783	3351
870	0.079	3382
1368	0.0822	3518
1395	0	0

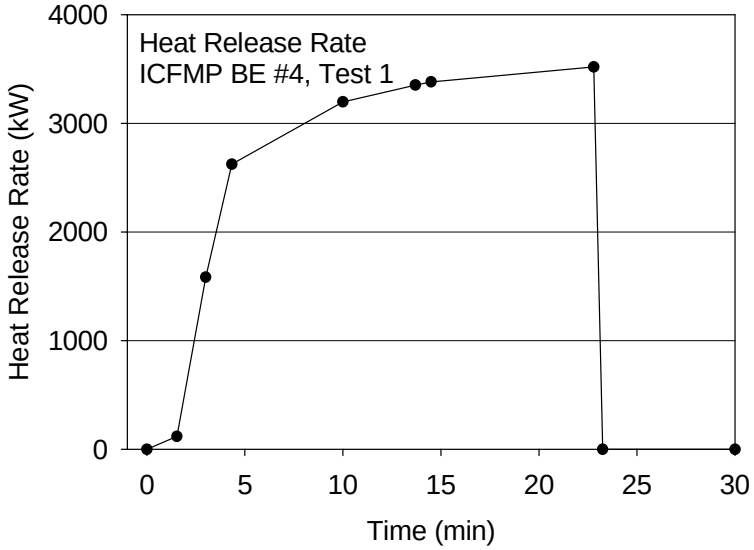

Figure 2-16: The estimated heat release rate in Test 1 based on the mass loss rate

2.5.2 Radiative Fraction

The radiative fraction of the jet fuel was taken as 0.35, similar to other smoky hydrocarbons [16, 17, 19]. The relative combined expanded uncertainty in this parameter was assigned a value of ±20%, consistent with typical values reported in the literature for the measured radiative fraction [18, 19]. The radiative fraction and its uncertainty are discussed further in Chapter 3.

2.6 ICFMP Benchmark Exercise #5

Benchmark Exercise (BE) #5, conducted under the International Collaborative Fire Model Project (ICFMP), was comprised of four large-scale tests inside a concrete enclosure with realistically routed cable trays [7]. This test series was conducted in the same facility as Benchmark Exercise #4, which was at the Institut für Baustoffe, Massivbau und Brandschutz (iBMB) of the Braunschweig University of Technology in Germany. The compartment was configured slightly differently, and the height was 5.6 m (18.4 ft) in BE #5. Test 4 of the BE #5 test series was selected for the quantitative evaluation of models reported here. A schematic diagram from plan, side, and perspective views of the experimental arrangement is shown in Figure 2-17.

As seen in Table 1-2, six types of measurements conducted during the BE #5 test series were used in the evaluation conducted here, including the HGL temperature and depth, oxygen gas concentration, the temperature of targets and compartment surfaces, and heat flux. Table 2-13 lists the input data used for this experiment.

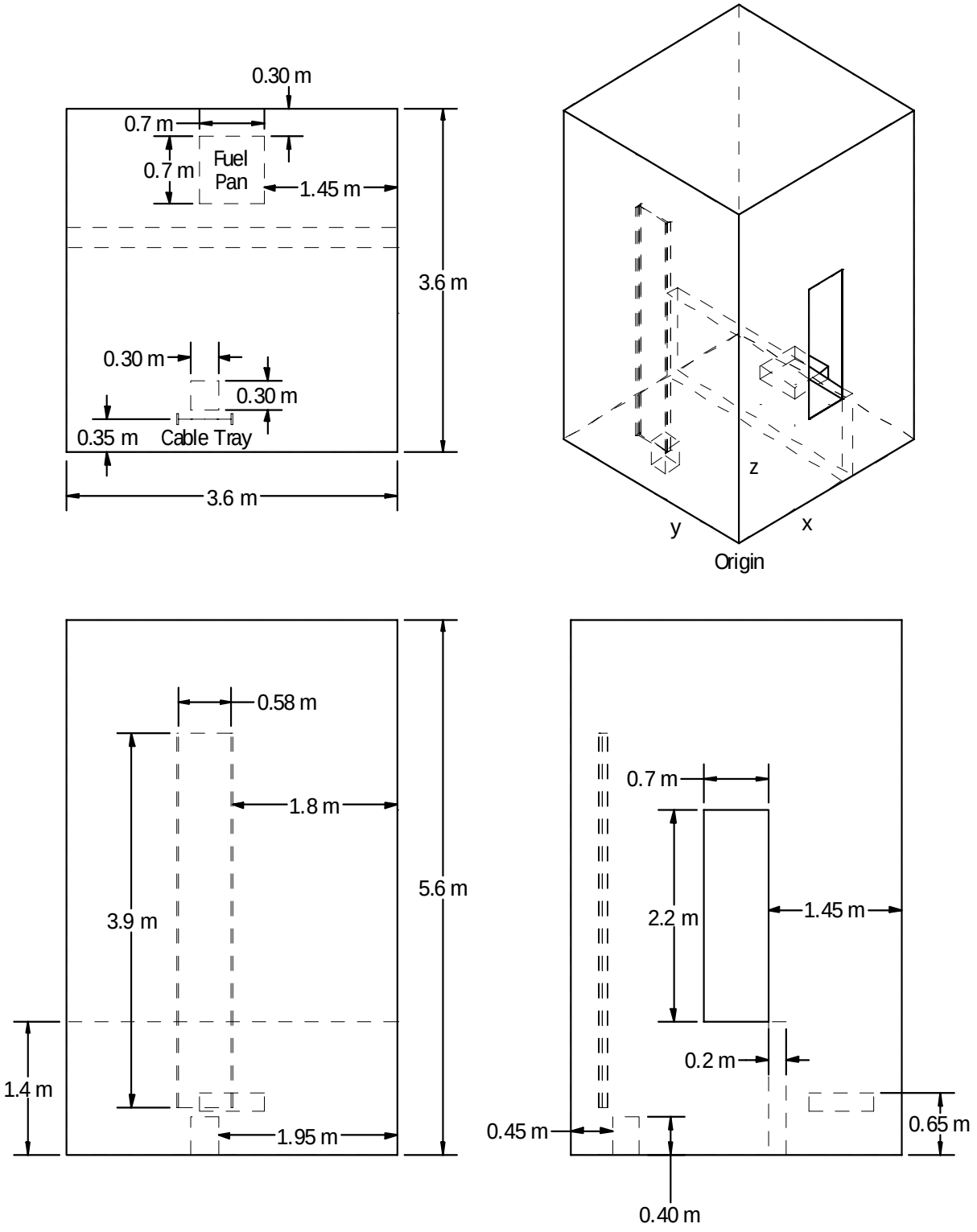

Figure 2-17: Plan, side, and perspective schematic drawings of the ICFMP BE #5 experimental arrangement, including the fuel pan and cable tray

Table 2-13: Input for Calculation of BE #5

Simulation Time = 1800 s

Compartment

Size			Position		
X (Width) (m)	Y (Depth) (m)	Z (Height) (m)	X (Width) (m)	Y (Depth) (m)	Z (Height) (m)
3.6	3.6	5.6	0	0	0

Compartment Materials (Inside Layer)*

Ceiling	Floor	Walls
Concrete	Concrete	Light Concrete

Fire Description

Test	Fuel	Fire Area (m^2)	Position X(m),Y(m)	$\dot{Q}$ (kW)	Radiative Fraction
Test 4	Jet Fuel	0.09	2.05,1.75	Profile	0.35
	Ethanol pan fire	0.49		Profile	0.20

Openings

From	To	Width (m)	Height (m)	Sill (m)	Area (m^2)	Position (m)	Face
Fire Room	Outside	0.7	2.2	1.4	1.54	1.80	Front door
Fire Room	Outside	0.6	0.7	0.7	0.42	1.80	Left side wall

Targets

Target	Position			Face	Normal Vector			Material	Target
	x (m)	y (m)	z (m)		x(m)	y(m)	z(m)		
Heat Flux Meter WS1	0.41	2.13	1.2	Left	1	0	0	Concrete	1
Heat Flux Meter WS2	0.41	2.13	2	Left	1	0	0	Concrete	2
Heat Flux Meter WS3	0.41	2.13	2.8	Left	1	0	0	Concrete	3
Heat Flux Meter WS4	0.41	2.13	3.6	Left	1	0	0	PVC Power	4
Heat Flux Meter WS5	0.41	2.13	4.4	Left	1	0	0	PVC Power	5
Power Cable TCO 1-1	0.44	2.24	1.2	Left	1	0	0	PVC Power	6
Power Cable TCO 1-2	0.44	2.24	1.6	Left	1	0	0	PVC Power	7
Power Cable TCO 1-3	0.44	2.24	2	Left	1	0	0	PVC Power	8
Power Cable TCO 1-4	0.44	2.24	2.4	Left	1	0	0	PVC Power	9
Power Cable TCO 1-5	0.44	2.24	2.8	Left	1	0	0	PVC Power	10
Power Cable TCO 1-6	0.44	2.24	3.2	Left	1	0	0	PVC Power	11
Power Cable TCO 1-7	0.44	2.24	3.6	Left	1	0	0	PVC Power	12
Power Cable TCO 1-8	0.44	2.24	4	Left	1	0	0	PVC Power	13
Power Cable TCO 1-9	0.44	2.24	4.4	Left	1	0	0	PVC Power	14
Power Cable TCO 3-1	0.44	2.05	1.2	Left	1	0	0	PVC Control	15
Power Cable TCO 3-2	0.44	2.05	1.6	Left	1	0	0	PVC Control	16
Power Cable TCO 3-3	0.44	2.05	2	Left	1	0	0	PVC Control	17
Power Cable TCO 3-4	0.44	2.05	2.4	Left	1	0	0	PVC Control	18
Power Cable TCO 3-5	0.44	2.05	2.8	Left	1	0	0	PVC Control	19
Power Cable TCO 3-6	0.44	2.05	3.2	Left	1	0	0	PVC Control	20
Power Cable TCO 3-7	0.44	2.05	3.6	Left	1	0	0	PVC Control	21
Power Cable TCO 3-8	0.44	2.05	4	Left	1	0	0	PVC Control	22
Power Cable TCO 3-9	0.44	2.05	4.4	Left	1	0	0	PVC Control	23

2.6.1 Heat Release Rate

The scenario selected for study was a large fire in a relatively small enclosure. The first part of the test consisted of preheating the cable trays in the room with a 1 m^2 (11 ft^2) round pan on the floor filled with ethanol (ethyl alcohol) used as the preheating source, and a propane gas burner was used as the fire source after pre-heating.

Exhaust products were collected in an exhaust duct and the $\dot{Q}$ was measured using the oxygen calorimetry. For the purpose of this V&V study, the measured $\dot{Q}$ was used as direct input to the various fire models. The first 20 min of data were used for the model evaluation. After 20 min, the $\dot{Q}$ became relatively noisy. At 33 min, thermoplastic cables located in the compartment began to burn and contribute to the $\dot{Q}$. Figure 3-15 depicts the measured $\dot{Q}$ profile. The relative combined expanded uncertainty in this parameter was assigned a value of ±15%, consistent with typical values of this parameter [23, 24]. Tables 2-14 and 2-15 lists the measured $\dot{Q}$ for both the ethanol and the propane burner.

2.6.2 Radiative Fraction

The radiative fractions for the ethanol pool fire and the propane fire were taken as 0.20 and 0.35, respectively. The relative combined expanded uncertainty in this parameter was assigned a value of ±20%, which is consistent with typical values reported for this parameter [16, 17, 19].

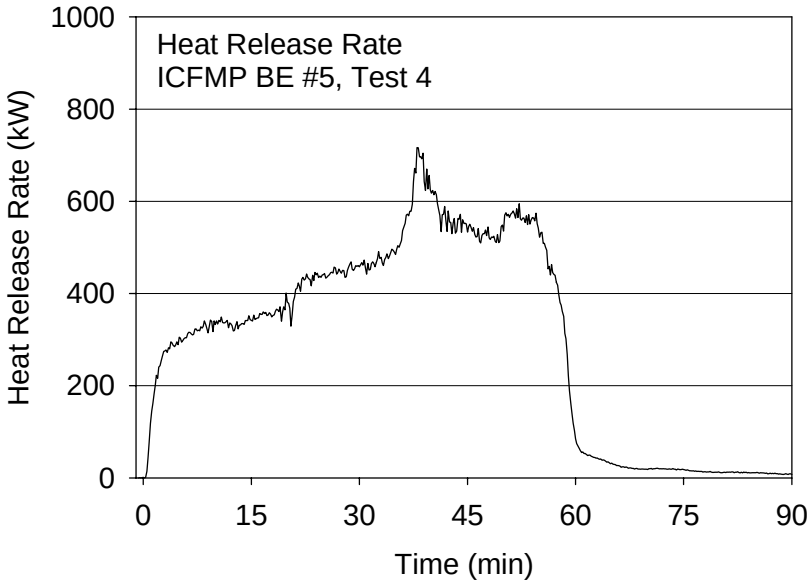

Figure 2-18: The heat release rate as a function of time during Test 4 of the BE #5 test series. Only the first 30 min (1800 s) of the test were used for model evaluation.

Table 2-14: Heat Release Rate of the Ethanol Pan Fire

Time (s)	$\dot{Q}$ (kW)
0	0
60	120
120	220
180	280
240	290
300	300
480	320
600	330
900	340
1800	360

Table 2-15: Heat Release Rate of the Propane Gas Burner

Time (s)	$\dot{Q}$ (kW)
0	0
1200	0
1201	50
2100	50

3
HEAT RELEASE RATE, RADIATIVE FRACTION, AND THEIR UNCERTAINTY

This chapter summarizes the discussion of model input and its uncertainty that was initiated in Chapter 2. The measurement and uncertainty of the heat release rate ($\dot{Q}$), the radiative fraction (χ_{rad}), and thermophysical material properties are considered here.

The fire $\dot{Q}$ is the single most important parameter in terms of characterizing a fire, and its uncertainty is the most significant *model input uncertainty.* The magnitude of $\dot{Q}$ controls the thermal impact of a fire on its environment. The current generation of fire models cannot accurately predict the transient value of $\dot{Q}$, and for the fire model evaluations considered in this report, the value of $\dot{Q}$ is prescribed (that is, $\dot{Q}$ is an input parameter, rather than an output parameter that is calculated by a model). The sensitivity of model output to the uncertainty in $\dot{Q}$ is an important part of the model evaluation in this report series and is discussed in detail in Chapter 5.

The actual heat release rate of a fire ($\dot{Q}$) is a function of the mass loss rate of fuel ($\dot{m}$), the heat of combustion (H_c), and the combustion efficiency (χ_A):

$$\dot{Q} = \chi_A \cdot \dot{m} \cdot H_c \tag{3.1}$$

The value of $\dot{m} \cdot H_c$ is sometimes referred to as the idealized heat release rate. The idealized heat release rate is always greater than or equal to the actual heat release rate $\dot{Q}$ as the value of χ_A is always less than or equal to 1.0.

In the fire models considered in this report, the radiative fraction of the fire, like $\dot{Q}$, is prescribed. Since the radiative fraction was not reported in the documentation of the experiments considered in this report, this chapter suggests values for use in the model evaluation considered in this report series. The radiative fraction provides information on how the energy from a fire is distributed between the sensible enthalpy convected by the plume and the heat transferred to the surroundings by radiation. In a compartment fire, the value of the radiative fraction has little impact on the upper layer temperature, which depends on $\dot{Q}$, but it does affect, for example, the radiative flux to a nearby target. The radiative fraction, χ_{rad}, is based on the idealized heat release rate of a fire ($\dot{m} \cdot H_c$) and is defined as:

$$\dot{Q}_r = \chi_{rad} \cdot \dot{m} \cdot H_c \tag{3.2}$$

where $\dot{Q}_r$ is the radiative emission from a fire to its surroundings. As used in the fire literature (e.g., reference 14), the radiative fraction of a fire does not consider radiative exchange with walls or a hot upper layer.

3.1 Heat Release Rate Measurement Uncertainty

In the experiments considered in this report, the heat release rate was determined by measuring the mass loss rate of fuel or by oxygen consumption calorimetry.

Calorimetric measurements typically involve dozens of independent measurements [23], and a combined uncertainty analysis can be quite elaborate. Measurement uncertainty depends on the exact instrument types, details of the flow and sampling hardware, experimental procedures, and application details. Reference 23 provides a survey of the few studies that address uncertainty of the $\dot{Q}$ measurement by oxygen consumption calorimetry. These studies considered completely different situations including various types of instrumentation, different levels of the $\dot{Q}$, and detail of the analysis, including several versions of the $\dot{Q}$ equation. Reference 24 estimated the $\dot{Q}$ measurement uncertainty for the measurement as conducted in the Single Burning Item Test and the Room Corner Test (ISO 9705). The relative expanded uncertainty estimates ranged from 0.07 to 0.14, depending on the apparatus and the $\dot{Q}$. The uncertainty of the oxygen concentration measurement, followed by the heat of combustion factor and the mass flow rate measurement were identified as the major sources of uncertainty. Details on the uncertainty of the oxygen and the mass flow rate measurements were presented. The study notes that for larger oxygen deficits the combined uncertainty of the $\dot{Q}$ measurement is less. Reference 25 reports an analytical estimate of the $\dot{Q}$ measurement uncertainty for the cone calorimeter. Specifically, that reference estimated relative expanded uncertainty values from 0.10 to 0.12, depending on the $\dot{Q}$. The greatest sources of uncertainty were identified as the heat of combustion factor, the combustion expansion factor, and the oxygen measurement. Reference 26 reports an uncertainty analysis for experiments conducted in a compartment with a controlled energy supply. The volume flow rate and oxygen measurement were identified as majors source of uncertainty, and a relative expanded uncertainty of 0.12 was reported under conditions when the exhaust volume flow rate was optimized for the fire size. The oxygen depletion measurement and the exhaust mass flow rate measurement have been consistently identified as major sources of uncertainty. However, reference 27 reviewed the results of the $\dot{Q}$ round-robin tests and highlighted the uncertainty attributable to random effects, such as material and burning variability, environmental effects, operator error, and measurement bias between laboratories.

For some of the experiments considered here, the $\dot{Q}$ was estimated through measurement of the fuel flow rate. In these cases, the $\dot{Q}$ was calculated based on the heat of combustion and an assumed combustion efficiency (Eq. 3.1). While the mass flow rate measurements typically have low uncertainties, the uncertainty in the combustion efficiency is not necessarily small. Inside a compartment, even less is known about combustion efficiency as the fire plume is partially engulfed in a hot upper layer and the oxygen volume fraction in the lower layer is vitiated.

3.2 Radiative Fraction

The radiative fraction is typically determined through single or multiple location measurements of the radiative flux in conjunction with measurement of $\dot{Q}$, or the mass burning rate, $\dot{m}$. Assuming symmetry, χ_{rad} can be determined either through single or multiple-location heat flux measurements at a suitable distance from the fire source. The radiative fraction of burning pools of hydrocarbons, such as those used in the experiments considered here, vary with fuel type [16, 17] and scale of the fire [19].

3.3 Summary of Heat Release Rate and Radiative Fraction Model Input Values

The values of the $\dot{Q}$ varied from experiment to experiment, depending on the nature of the experimental conditions. This information is available in the test reports [2, 3–7] and is summarized in Table 3-1. The $\dot{Q}$ listed in the table refers to the average heat release rate during the steady-burn period, and is the value specified for use by the models in this report series. Table 2-1 also presents the values of the estimated uncertainty of the $\dot{Q}$ for the experiments, which varied from 15% to 25%. For two of the experiments (BE #2 and BE #4), the $\dot{Q}$ was estimated through the fuel flow rate measurement results. In those experiments, the $\dot{Q}$ was calculated based on Eq. 3.1 using information on the heat of combustion and an estimate of the combustion efficiency. Whereas the mass flow rate measurement typically has low uncertainty, the uncertainty in the combustion efficiency is not small. Inside a compartment, even less is known about combustion efficiency as the fire plume may be partially engulfed in a hot upper layer and the oxygen volume fraction in the lower layer may be vitiated. The table also lists values of the radiative fraction, and its uncertainty. Discussion of the table entries is given in detail in Chapter 2 for each of the six experimental test series.

Table 3-1: Summary of the Heat Release Rate and the Radiative Fraction During the Steady-Burn Period

Series	Test	Fire	$\dot{Q}$ (kW) *	Radiative Fraction
FM/SNL Ref. 2	Test 4	Propylene 0.9 m round sand burner	510 ±20%	0.35 ±20%
	Test 5		480 ±20%	
	Test 21		470 ±20%	
NBS Ref.3	100A	natural gas	110 ±15%	0.20 ±20%
	100O	natural gas/acetylene	110 ±20%	0.30 ±30%
	100Z		110 ±20%	0.30 ±30%
BE #2 Ref. 5	Case 1	heptane on water round 1.17 m pan	Mass loss Uncertainty: ±15%	0.35 ±20%
	Case 2	heptane on water round 1.60 m pan		
	Case 3			
BE #3 Ref. 6	15 tests	heptane & toluene (1 test) spray 1 m ±0.1 m round pool	400-2300; see Chap. 2 ±17% uncertainty	heptane: 0.44 ±16% toluene: 0.40 ±23%
BE #4 Ref. 7	Test 1	jet fuel	Mass loss Uncertainty: ±25%	0.35 ±20%
BE #5 Ref. 8	Test 4	propane gas burner	see Fig. 3-9 Uncertainty: ±15%	0.35 ±20%
		ethanol pan fire		0.20 ±20%

* determination of $\dot{Q}$ involved oxygen consumption calorimetry for all experiments, except for BE #2 and BE #4, which used mass loss and Eq. 3.1.

3.4 Summary of Material Property Information

Table 3-2 summarizes the material property information that was used in the model calculations, including the material thermal conductivity, specific heat, density, and emissivity. The material thickness is also given. In addition, the thickness of the compartment surfaces is given. This is important for consideration of heat losses via conduction through compartment surfaces. The information was obtained from a number of sources, mostly from the test reports or the model documentation as noted in the footnotes of the table. Uncertainty in these values has small impact on the modeling results as confirmed by a sensitivity analysis conducted using the CFAST and FDS models (see Volumes 5 and 7 of this report series). For this reason, uncertainties of material properties are not explicitly considered in this report series.

Table 3-2: Summary of Material Property Information

Test	Material	Thermal Conductivity (W/m °C)	Specific Heat (J/kg °C)	Density (kg/m^3)	Thickness (m)	Emissivity
BE #2 [A]	Mineral Wool	0.2	150	500	0.05	0.95
	Steel	54	425	7850	0.001	0.95
	Concrete	2	900	2300	0.15	0.95
BE #3 [B]	Marinite (two ½ in layers)	0.12	1250	737	0.0254	0.8
	Gypsum (two ½ in layers)	0.16	900	790	0.0254	0.9
	F XPE Cable	0.21	1560	1375	0.01	0.95
	PVC Slab	0.147	1469	1380	0.01	0.95
	F XPE Cable	0.21	1560	1375	0.191	0.95
	PVC Slab	0.147	1469	1380	0.191	0.95
BE #4 & #5 [C]	Steel (ICFMP BE #4 only)	44.5	480	7743	0.02	0.95
	Concrete	2.1	880	2400	0.25	0.95
	Lightweight Concrete	0.75	840	1500	0.30	0.95
	PVC Power Cable	0.134	1586	1380	0.015	0.8
	PVC Control Cable	0.134	1586	1380	0.007	0.8
FM/ SNL [D]	Marinite	0.12	1250	720	0.025	0.95
	Concrete	1.8	1040	2280	0.15	0.95
NBS [E]	Fire Brick	0.36	1040	750	0.113	0.8
	Ceramic Fiber	0.09	1040	128	0.05	0.97
	Marinite	0.12	1250	720	0.0127	0.83
	Gypsum	0.17	1090	930	0.0127	0.95
	Concrete	1.8	1040	2280	0.102	0.95

A. Ref. 30
B. Ref. 6
C. Refs. 7, 8
D. Ref. 2
E. Ref. 3

4
MEASUREMENT UNCERTAINTY

For many of the experiments and most of the measurements considered in this report, the experimental uncertainty was not documented. In this chapter, estimates of measurement uncertainty based on engineering judgment are provided. Quantifying uncertainty in measured quantities provides a basis for evaluation of model results through consideration of Eqs. 1.1 through 1.4. Documentation of the measurement uncertainty produces a consistent set of data for use in the evaluation of the models considered in this report. The uncertainty of each of the 13 measurement quantities considered in the model evaluation is provided here (see Section 1.2 for a list of parameters, which included the hot gas layer temperature and depth, the ceiling jet and plume temperature, etc.). The relative uncertainty was defined in Section 1.4.2 as $\tilde{u}_M = u_M / \Delta M$ and $\tilde{u}_E = u_E / \Delta E$, or in terms of the expanded relative uncertainties $\tilde{U}_M = 2\tilde{u}_M$ and $\tilde{U}_E = 2\tilde{u}_E$, where ΔE.and ΔM are equal to the difference between the baseline or initial values and the peak values, that is (E_p-E_o) and (M_p-M_o), respectively. The analysis presented here, then considers the uncertainty in the difference between the baseline and the peak values. In practice, the uncertainty in the peak value is a good approximation is to the uncertainty in this difference.

The uncertainty estimates provided here are limited by knowledge of the details associated with each of the experiments. For this reason, the uncertainty values provided here should be thought of as rough estimates, rather than precise determinations of measurement uncertainty. Even for the experimentalists themselves, the accuracy of an uncertainty analysis is often limited by incomplete understanding. For example, in heat flux gauges, the uncertainty attributable to soot deposition on the face of the gauge is difficult to quantify. The amount of soot deposition depends on many parameters, such as the location of the gauge, the flow field and the temperature field near the gauge, the duration of the test, and the local soot volume fraction. Unexpected events or poor understanding limits the accuracy of an uncertainty analysis.

In general, measurement uncertainty depends on many issues, including the exact type of instrumentation, the experimental procedure, and the details of the measurement scenario. The uncertainty in many of the experimental measurements is difficult to accurately estimate, because most of the test reports do not provide uncertainties for the individual measurements. For this reason, the values are inferred based upon engineering judgment and experience with similar instrumentation.

4.1 Hot Gas Layer Depth and Temperature

The gas phase temperature was measured using bare bead or aspirated TCs in all six of the experiments considered in this report. Bare bead TCs were used in all of the experiments considered in this report except the BE #3 and FM/SNL tests in which bare and aspirated TCs were used. The HGL temperatures and depths were determined using the two-layer reduction

method described in reference 21. To determine the uncertainty in the layer depth and temperature, a propagation of error analysis was conducted considering the form of the reduction method and the uncertainty in the position and the measured value of each of the temperature measurements. The uncertainty in the temperature measurement is considered in Section 4.1.1. In Section 4.1.2, the uncertainty in the calculated HGL temperature and depth are described.

4.1.1 Temperature Measurement Uncertainty

The interpretation of a bare bead TC signal must consider several possible sources of error. TC measurement error can occur because of the breakdown of the TC insulation at high temperatures, corrosion from acid combustion byproducts, de-calibration at high temperatures, inherent measurement accuracy limited by materials effects, and measurement error attributable to radiative exchange effects. The latter requires attention for the experiments considered in this report.

Blevins [28] reported on the development of a model to compute TC error attributable to radiative exchange effects. Radiative exchange between the TC and walls, flame gases, soot, and the ambient environment were considered. In the same document, report of soot accumulation on the TC bead or sensing junction and changing of its thermophysical properties may also contributing to error. Variability in the convective heat transfer between the sample gas and the TC junction is also cited as a source of error.

There are several ways to handle radiative exchange effects on TC measurements. A correction may be applied to the signal to improve measurement accuracy. This is burdensome, because the radiative exchange correction may depend on the character of the TC, such as its diameter, material composition, and surface emissivity, as well as the details of its application, involving the local temperature, radiation, and flow fields. Thus, the correction depends on local conditions, and each TC should be independently analyzed. Typically, not enough experimental information is available to perform an accurate radiation correction. In such a case, it may be more practical to expand the uncertainty bounds for the measurement to encompass radiative exchange effects that are estimated based on simplified assumptions. This approach is used here and described below.

A completely different measurement approach involves the use of an aspirated TC as the measurement device, in which radiative exchange effects are minimized. Aspirated TCs are constructed such that the TC junction is within two concentric steel tubes. A mechanical pump draws gas extracted from the sampling location through a tube, engulfing the TC sensing junction with the sample gas, while the tubes protect the TC sensing junction from impinging thermal radiation. The error associated with the aspirated probe measurement itself depends on the application conditions and the results are a strong function of the aspiration velocity as well as a number of other parameters [28,29]. Aspirated TCs provide accurate temperature information, but are typically used sparingly, because of their relatively high cost compared to bare bead TCs. FM/SNL used aspirated TCs in the experiments considered in this report and BE #3 used aspirated TCs to assess the accuracy of the bare bead TC results.

In a hot upper layer of a compartment with lots of soot, a TC reading may be fairly accurate and not need to be corrected for radiative exchange effects. This is because the environment in such a scenario is nearly optically thick, for which radiative exchange effects are minimized. Many reports, including references. 2, 28, and 29, have examined the magnitude of the TC measurement error attributable to radiative exchange by comparing bare bead TC measurements

to measurements by nearby aspirated TCs in well-developed hot [60 °C to 800 °C (140 °F to 1500 °F)] smoky upper layers of compartment fires. For the fires considered in this report, it is assumed that the upper layer in all of the tests had a high opacity at the time of the peak temperature readings. This is a reasonable assumption for the types of fuels being used in the experiments considered here with the exception of NBS Test 100A in which natural gas was used as a fuel. For the other tests, Table 2-1 shows that the fuels included smoky fuels such as toluene, heptane, propylene, jet fuel, and propane. Estimation of the uncertainty in the bare bead TC measurements involves determination of the uncertainty of the various components of the measurement and the effect that each component has on the overall uncertainty. Computation of the overall uncertainty considers the measurement error attributable to radiative exchange, the inherent uncertainty associated with a bare-bead TC, and the error associated with use of an aspirated TC. The manufacturer reported accuracy for Type K TCs is 1.1 °C (2.0 °F) for temperatures of 0 °C to 293 °C (32 °F to 560 °F), and 0.4% for temperatures of 293 °C to 1250 °C (560 °F to 2280 °F), interpreted here as the expanded uncertainty [30]. These values are listed in Table 4-1 as U_w for a number of temperatures. The expanded uncertainty associated with aspirated probe measurements (U_a) is taken as approximately 4% for an aspiration velocity of 15 to 20 m/s (49.2 to 65.6 ft/s) as used in BE #3 [28]. The value of U_a, listed in Table 4-1, also includes the inherent TC uncertainty. The contribution of the uncertainty attributable to radiative exchange on a bare bead TC is estimated from the results of Refs. 2, 28, and 29. In those experiments, the measurement results of bare bead TCs were within 3 °C to 15 °C (5 °F to 27 °F) of nearby aspirated TCs. In the three FM/SNL tests [2], for example, a bare bead TC in the upper layer was within 5 °C to 6 °C (9 °F to 11 °F) of a nearby aspirated TC, for upper layer temperatures of about 60 °C (140 °F). In the hot upper layer of a heptane fire [31], bare bead TCs in the HGL were within 12 °C (22 °F) of nearby aspirated TCs, for various tests in which the upper layer temperatures ranged from 400 °C to 800 °C (750 °F to 1500 °F). Intermediate temperatures were estimated based on linear interpolation between the higher and lower temperature results. Contributions to the uncertainty associated with radiative exchange are listed as U_r in Table 4-1. The component expanded uncertainties were used to compute the combined expanded uncertainty for a bare bead TC (see Table 4-1). The largest contributor to the overall uncertainty at high temperatures was the uncertainty in the aspirated TC measurement, while at low temperatures, the contribution of uncertainty in the radiative exchange was relatively more important.

In the lower layer of compartment fires with a smoky, high-opacity upper layer, radiative gain attributable to flux from the hot upper layer may lead to erroneously high TC readings. This is not considered a significant problem for the model evaluation considered here, as the lower layer information is directly used only to determine the HGL depth. It is assumed that the uncertainty in the layer depth calculation is not significantly impacted by erroneously high lower layer TC readings, since the layer calculation seeks locations of significant temperature change, rather than, for example, the absolute value of that difference. Neglecting uncertainty in the lower layer temperature measurement reduces the total uncertainty, and in this sense is a conservative approach for model validation. The most significant contributor to the uncertainty of the upper layer depth and the temperature is the physical distance between TCs, which is the spatial resolution of the measurement.

Table 4-1: Expanded Measurement Uncertainty of a Bare Bead Thermocouple in the Hot Smoky Upper Layer of a Compartment Fire

Gas Temperature °C (°F)	U_w °C (°F)	U_r °C (°F)	U_a °C (°F)	U_E, Combined Expanded Uncertainty °C (°F)
0 (32)	2 (4)	0 (0)	2 (4)	3 (5)
60 (140)	2 (4)	5	3 (5)	6 (11)
120 (250)	2 (4)	6 (11)*	4 (7)	8 (14)
150 (300)	2 (4)	6 (11)*	5 (9)	8 (14)
300 (570)	2 (4)	9 (16)*	12 (22)	15 (27)
500 (930)	4 (7)	12 (22)	20 (36)	24 (43)
800 (1500)	6 (11)	12 (22)	32 (58)	35 (63)
* based on linear interpolation between the higher and lower temperature results.				

4.1.2 Uncertainty in the Calculated Upper Layer Depth and Temperature

Upper layer temperature (T_u) and depth (z_{int}) was determined using the two-layer reduction method [21]. A propagation of error analysis was performed to determine the uncertainty associated with this calculation. The two-layer method requires numerical integration of the vertical profiles of temperature and vertical profiles of reciprocal temperature in the integrals defined as I_1 and I_2:

$$I_1 = \int_0^H T(z)\,dz \tag{4.1}$$

$$I_2 = \int_0^H \frac{1}{T(z)}\,dz \tag{4.2}$$

The upper layer interface height and temperature are defined as follows:

$$z_{\text{int}} = \frac{T_l(I_1 I_2 - H^2)}{I_1 + I_2 T_l^{\,2} - 2T_l\ H} \tag{4.3}$$

$$(H - z_{\text{int}})T_u = I_1 - Z_{\text{int}} T_l = \int_{z_{\text{int}}}^H T(z)\,dz \tag{4.4}$$

where T_l is the lower layer temperature and H is the compartment height. Following reference 21, T_l was taken as the value at the lowest temperature measurement location. The algebra in the uncertainty analysis is complicated, as error is propagated through the many terms that involve I_1 and I_2 and that present themselves in the determination of T_u and z_{int} (see Eqs. 4.3 and 4.4). The propagation of error analysis considered uncertainty in both the local temperature

measurement (see Table 4.1) and its location. The latter term has two components, one associated with the uncertainty in the location of the TC [taken as 0.02 m (0.07 ft)] and the other associated with the distance between TCs (which varied from experiment to experiment), both of which impact the accuracy of the calculation. A linear fit to the data in Table 4.1 was used to describe the uncertainty in the local temperature. The numerical analysis of the integrals I_1 and I_2 (Eqs. 4.1 and 4.2) used the measured temperature profiles. In those profiles, the number of TCs and the physical distance between TCs differed for each of the tests, varying from 9 TCs separated by 0.3 m (12 in) in the NBS test series to 3 TCs separated by about 1.9 m (75 in) in BE #4. Uncertainty propagation was calculated using Matlab®, a high-level interactive programming tool, following the rules of propagation of error [12]. Repeatability of the depth determination was investigated for BE #3 by examining the results for the repeat tests. The difference in the calculated upper layer depth and temperature for the four pairs of repeat measurements was about 1%, on average, a negligibly small contribution to the overall uncertainty. It was assumed that the repeatability in the other tests was similar to that determined in BE #3.

Table 4-2 summarizes the results of the uncertainty estimate calculations. The table lists the estimated relative expanded measurement uncertainties, U_E, for the HGL layer depth and temperature rise associated with each of the experiments considered in this report. The calculated HGL depth varied from about 1 m (40 in) to 5 m (200 in) for the experiments considered here, and the relative expanded uncertainties in the values of the HGL depth varied from about 8% to 35%, whereas relative expanded uncertainties in the upper layer temperature varied from about 4% to 25% as seen in Table 4-2. The largest uncertainties were associated with experiments that had relatively coarse instrumentation density (e.g., FM/SNL and BE #4). The value of U_E does not accurately account for radiative exchange in NBS Test 100A, in which natural gas was the fuel, and where the assumption of an optically thick upper layer is inappropriate, and the value of U_E is likely small.

Table 4-2: The Relative Expanded Uncertainties ($\tilde{U}_E$) Associated with the Measured HGL Depth and Temperature Rise

Series	$\tilde{U}_E$ (%)	
	HGL Depth	HGL Temperature Rise
NBS	13	10*
FM/SNL	35	16
BE #2	6	6
BE #3	9	5
BE #4	33	25
BE #5	8	4

* Value of $\tilde{U}_E$ does not accurately account for radiative exchange in Test 100A, in which natural gas was the fuel; its value is likely small (see text).

4.2 Ceiling Jet and Plume Temperatures

Ceiling jet measurements were conducted in BE #3 and the FM/SNL tests, in which the temperatures were measured using bare bead and aspirated TCs, respectively. Temperatures in the plume were measured in BE #2 and the FM/SNL tests, in which the temperatures were measured using bare bead and aspirated TCs, respectively. Because the ceiling jet is located high in the hot smoky upper layer, radiative exchange effects on TCs should be minimal and the results are treated in the same way as the bare bead TCs in the upper layer.

Repeatability of the ceiling jet temperatures was investigated for BE #3 by examining the results of the repeat tests. The difference between the repeat measurements was about 8%, on average. The difference in the repeatability of the FM/SNL tests was assumed to be small, since radiative exchange effects were negligible with the use of aspirated TCs in the relatively low temperature environment. The values of U_E for the ceiling jet varied from 4% to 12% as seen in Table 4-3 for the two test series considered here.

Assessment of the uncertainty of the plume temperature measurements is more problematic. In this case, the bare bead TC results are treated in the same manner as the bare bead TC results for measurements in an upper layer. The repeatability of the BE #2 measurements was assumed to equal 8%, the same as the ceiling jet measurements in BE #3. Still, the value of U_E is probably too small in the lower part of the plume for BE #2, which was not in a well-developed smoky upper layer. The values of $\tilde{U}_E$ for the plume varied from 4% to 11% as seen in Table 4-4 for the two tests considered here.

Table 4-3: The Relative Expanded Uncertainties ($\tilde{U}_E$) Associated with the Measured Ceiling Jet Temperature Rise

Series	$\tilde{U}_E$ (%)
	Ceiling Jet Temperature Rise
BE #3	12
FM/SNL	4

Table 4-4: The Relative Expanded Uncertainties ($\tilde{U}_E$) Associated with the Measured Plume Temperature Rise

Series	$\tilde{U}_E$ (%)
	Plume Temperature Rise (°C)
BE #2 upper	9
BE #2 lower	11 *
FM/SNL	4
* the value of U_e is too small in the lower part of the plume in BE #2, which was not in a well-developed smoky upper layer.	

4.3 Gas Species Volume Fraction

The volume fractions of the combustion products, carbon monoxide (CO) and carbon dioxide (CO_2), were measured using gas sampling in conjunction with non-dispersive infrared analyzers, while the oxygen (O_2) volume fraction was typically measured using a paramagnetic analyzer. Gases were extracted through stainless steel or other types of lines and were pumped from the compartment and passed through the analyzers. For several reasons, water in the sample was typically filtered, so the reported results are denoted as "dry" and comparison with model results must be corrected. Analyzers were calibrated through the use of standard gas mixtures, with low relative uncertainties. Problems with the technique may involve instrument drift, analyzer response, incomplete and partial drying of sample gases, or (in the case when drying is not used) undetermined amounts of water vapor in the oxygen cell, which result in inaccurate readings.

Measurements of gas species volume fractions are considered for BE #3 and BE #5. Specifically, in BE #3, the species were measured at a single location in both the upper and lower layers. The relative expanded uncertainty in the measured values in BE #3 were about 3% for both the O_2 depletion and the CO_2 measurements. The largest contributors were the uncertainty in the composition of the calibration gas and the possibility of an undetermined amount of water vapor in the sample. Repeatability of the gas measurements was investigated for BE #3 by examining the results for the repeat tests. The difference between the repeat measurements was about 2%, on average, for both the O_2 depletion and the CO_2 measurements. Combining the uncertainties, the relative expanded uncertainty was typically 4% for measurements of both the O_2 depletion and the CO_2 gain. The uncertainty in BE #5 was assumed to be similar to that determined in BE #3. The relative expanded uncertainties are listed in Table 4-5.

Table 4-5: Summary of the Relative Expanded Uncertainties Associated with the Oxygen and Carbon Dioxide Concentrations

Series	$\tilde{U}_E$ (%)		
	HGL CO_2 Concentration	**HGL O_2 Concentration Decrease**	**LGL O_2 Concentration Decrease**
BE #3	4	4	4
BE #5	4	4	4

4.4 Smoke Concentration

The mass-based smoke concentration was measured in BE #3. In that experiment, smoke was measured using laser transmission at 632.8 nm. The reported mass concentration of smoke, M_s, was computed using the following expression:

$$M_s = \frac{\ln(I_0 / I)}{\phi_s L} \tag{4.5}$$

where L is the path length, I and I_o are the laser signal and reference signal, respectively, and ϕ_s is the specific extinction coefficient, which has a nearly universal value of 8.7 m^2/g ±5% for hydrocarbons [32]. Other uncertainties in the measurement were attributable to errors in the path length, L, and the light attenuation, I_0 / I. In BE #3, reference 4 reported the expanded uncertainty of the M_s measurement as 18%, with the dominant contribution to the uncertainty coming from drift in the laser measurement. Repeatability of the smoke measurement was investigated for BE #3 by examining the results for the repeat tests. The mean difference between the measurements was about 21%. Therefore, a combined expanded experimental uncertainty of 28% is suggested.

Table 4-6: The Relative Expanded Uncertainties ($\tilde{U}_E$) Associated with the Measured Smoke Concentration and the Compartment Pressure

Series	$\tilde{U}_E$ (%)	
	Smoke Concentration	**Pressure**
BE #3	28	27

4.5 Pressure

The compartment pressure was measured only in BE #3. The uncertainty in pressure measurements is typically small, but depends on the sensor type and calibration. In BE #3, the differential pressure gauge used was temperature compensated, highly linear, and very stable. A conservative estimate of the expanded measurement uncertainty led to a value of 1%. Repeatability of the pressure measurement was investigated for BE #3 by examining the results for the repeat tests. The average difference between the repeat measurements was about 27%. Compartment leakage is a likely explanation for this large difference between repeat tests. An expanded uncertainty value of 27% is suggested in Table 4-6.

4.6 Heat Flux

Measurements of heat flux were considered for BE #3, BE #4, and BE #5. Heat flux gauges were used to measure the transport of radiant energy or the combination of radiation and convection. Several types of gauges were used, and different types of instrumentation and procedures were used to calibrate the gauges. In BE #3, four types of gauges were used, including those that measured total heat flux or just radiative heat flux. In BE #4 and BE #5, total heat flux gauges were used.

The uncertainty associated with a heat flux measurement depends on many factors, including gauge characteristics, the calibration conditions and accuracy, as well as the incident flux modes (convective, radiative, conductive) and their magnitudes in the actual measurement situation [33]. Reference 34 reported two rounds of an international round-robin test of heat flux gauges, in which five fire laboratories performed independent calibrations of two sets of Gardon and Schmidt-Boelter total heat flux gauges. The results showed that the calibrations agreed to within about 5%. Typically, the reported expanded uncertainties of heat flux gauges varies from about 5% to 10%, with the measurement uncertainty typically dominated by uncertainty in the calibration and repeatability of the measurement. Reference 33 suggests that much higher values may be more realistic, depending on the exact nature of the fire conditions and the type of gauge. Repeatability of the various heat flux measurements in BE #3 was determined by examining measurements by the same instruments for different pairs of repeat tests. The difference between the measurements was about 7%, on average, for both the radiative flux measurements and the total flux measurements. In this report, an expanded uncertainty value of about 10% is suggested based on the BE #3 measurement repeatability and calibration uncertainties. It is assumed that the measurement uncertainty in BE #4 and BE #5 was similar to BE #3, as listed in Table 4-7.

Table 4-7: Summary of the Relative Expanded Uncertainties Associated with the Measured Target Heat Flux and Target Temperatures

Series	$\tilde{U}_E$ (%)	
	Total Heat Flux to Targets	**Rise in Target Surface Temperature**
BE #3	10	1 – 7
BE #4	10	1 – 2
BE #5	10	4

4.7 Surface/Target Temperature

Bare bead TCs were used to measure the temperature of targets and compartment surfaces. A typical method is to "peen" the TC into surface, that is, to bend and effectively spring-load the metal TC until physical contact with the surface or target occurs. Heating of the TC can cause it to undergo a shape change, which can cause a "peened" TC to have poor physical contact with a surface. Another method pulls on the leads of a TC with a small gravity load, forcing it to make physical surface.

The inherent expanded uncertainty associated with a Type K TC is approximately 2 °C (4 °F) for temperatures below 200 °C (390 °F) [30]. Repeatability of the surface and cable temperature measurements was investigated in BE #3 by examining the measurements of the same instruments for different repeat tests. The difference between the measurements was about 8% and 7%, on average, for the cable and wall surface measurements, respectively. Combining the inherent TC uncertainty and the repeatability yields uncertainty on the order of 10% for the TC surface measurements. The measurement uncertainty in BE #4 and BE #5 was assumed to be similar to that in BE #3. The relative expanded uncertainties for both surface heat flux and temperature are listed in Table 4-8.

Table 4-8: Summary of the Relative Expanded Uncertainties Associated with the Surface Heat Flux and Temperatures

Series	$\tilde{U}_E$ (%)	
	Total Heat Flux	**Rise in Surface Temperature**
BE #3	10	10
BE #4	10	10
BE #5	10	10

4.8 Summary

In general, measurement uncertainty depends on many issues, including the exact type of instrumentation, the experimental procedure, and the details of the measurement scenario. Because uncertainty was not documented for most of the experiments considered in this report, engineering judgment was used to provide estimates of measurement uncertainty for each of the parameters of interest. This information on *measurement uncertainty* is combined with *the model input uncertainty* in Chapter 6 to provide a basis for the evaluation of the fire models, as described in Volumes 3 through 7 of this report.

5
SENSITIVITY OF MODEL RESULTS TO UNCERTAINTY IN MEASURED INPUT PARAMETERS

This chapter quantifies the sensitivity of model results to uncertainty in measured input parameters, referred to here as the *model input uncertainty* ($\tilde{U}_M$). This could be achieved in a number of ways. A sensitivity analysis for the models could have been performed by running many calculations and determining the variation of a calculated output parameter as a function of the change in one or more input parameters. This is a brute force approach, which provides relevant information, but is labor intensive and does not necessarily offer physical insight. In addition, such an approach would be model specific. Rather than a brute-force method, the approach presented here is based on empirical closed-form expressions, which provides estimates on the effect of experimental uncertainty on the model output results, in a consistent and accepted manner for all of the models.

For each parameter of interest, a simple analytic description of the sensitivity of that parameter to the fire $\dot{Q}$ is given. For example, the nature of the hot gas layer (HGL) is largely a function of the fire size, and the uncertainty in the $\dot{Q}$ measurement for the various experiments ranged from 15% to 25%. The dependence has been quantified based on results documented in the technical literature, in which simple analytical relationships or *correlations* have been developed from measurements made in many compartment fire experiments performed over several decades. Using the empirical correlations, it is possible to estimate how the uncertainty in the specified $\dot{Q}$ influences the various parameters of interest. The magnitude of this uncertainty ($\tilde{U}_M$) plays an important role in the evaluation of model accuracy through consideration of Eq. 1.4 in Chapter 1. The remainder of this chapter discusses the sensitivity of model output parameters to the model input parameters.

5.1 Hot Gas Layer and Ceiling Jet Temperatures

According to an empirical correlation by McCaffrey, Quintiere and Harkleroad (MQH) [35], the HGL temperature is proportional to the heat release rate raised to the two-thirds power:

$$T_g - T_\infty = 6.85 \left(\frac{\dot{Q}^2}{A_0 \sqrt{H_0} h_k A_T} \right)^{1/3} \tag{5.1}$$

where $\dot{Q}$ is the heat release rate in kW, A_0 is the area of the opening, H_0 is the height of the opening, $h_k = k/\delta_w$ is the heat transfer coefficient, k is the thermal conductivity (kW/m/K), δ_w is the wall thickness (m), and A_T is the total compartment surface area (m^2). Although the MQH correlation has limitations, it encapsulates a set of observations that give insight into trends associated with HGL temperature. The uncertainty in the $\dot{Q}$ measurement for the various

experiments ranged from 15% to 25%. The uncertainty in the HGL temperature *prediction* varies, therefore, by two-thirds from the uncertainty in the $\dot{Q}$ *measurement*.

According to the empirical ceiling jet correlations by Alpert [36], the temperature within the ceiling jet is also proportional to the $\dot{Q}$ raised to the two-thirds power; thus, the same sensitivity to the $\dot{Q}$ should apply for the ceiling jet temperature as for HGL temperature.

5.2 Hot Gas Layer Depth

The location of the HGL is relatively insensitive to the $\dot{Q}$ of the fire. According to the correlation of Heskestad and Delichatsios [40], the layer height, *z*, is given by the following function:

$$\frac{z}{H} = 1.11 - 0.28 \ln\left(t\, \dot{Q}^{1/3} \frac{H^{\frac{4}{3}}}{A/H^2} \right) \tag{5.2}$$

which can be rewritten as follows:

$$\frac{z}{H} = 1.11 - 0.28 \ln\left(kt\ \dot{Q}^{1/3}\right)$$

where t is time and $k = \left(\frac{H^{-4/3}}{A/H^2} \right)$. Taking the derivative leads to the following expression:

$$\frac{\delta z}{H} = -(\frac{0.28}{3})\left(\frac{\delta \dot{Q}}{\dot{Q}} + 3\frac{\delta t}{t} \right) \tag{5.3}$$

Dividing through by Eq. 5.2 leads to the following equation:

$$\frac{\delta z}{z} = \frac{-(\frac{0.28}{3})\left(\frac{\delta \dot{Q}}{\dot{Q}} + 3\frac{\delta t}{t} \right)}{\left(1.11 + [0.28/\ln(kt\dot{Q}^{\frac{1}{3}})] \right)} \tag{5.4}$$

As t becomes large, the (1/t) term and the second term in the denominator become small, and Eq. 5.4 takes the following form:

$$\frac{dz}{z} = -\frac{0.28\frac{\delta \dot{Q}}{\dot{Q}}}{3(1.11)} = -0.084\frac{\delta \dot{Q}}{\dot{Q}} \tag{5.5}$$

and a 15% or 25% increase in the $\dot{Q}$, leads to a 1% to 2% decrease in the layer height.

For fire scenarios with open doors or windows, the layer height is largely affected by the position of the soffit. Empirical correlations relating the sensitivity of the layer height to the $\dot{Q}$ were not found in the literature. To confirm the weak dependence of the HGL depth to the $\dot{Q}$, a sensitivity analysis was conducted using CFAST for Test 3 of BE #3. The HGL depth in CFAST is not a result of a simple correlation from the fire literature, but is a product of the solution of the energy and mass conservation equations. The CFAST results confirm that the dependence of the HGL depth on the $\dot{Q}$ is weak, but non-zero. The reason for this likely involves a balance between the increasing HGL temperature and decreasing density and the balance of flows in and out of the compartment.

5.3 Plume Temperature

The plume temperature is mainly a function of the $\dot{Q}$. According to McCaffrey's correlation of fire plume temperature and velocity [36], the centerline temperature is approximately proportional to the $\dot{Q}$ to the two-fifths power for positions a distance above the fuel surface and below the mean flame height, whereas at heights greater than the mean flame height, the temperature rise is proportional to the two-thirds power, just like the HGL relationship. A similar argument can be made for the sensitivity of the fire plume temperature rise to $\dot{Q}$ as that for the HGL temperature rise.

5.4 Flame Height

According to the empirical correlation by Heskestad [37, 38], flame height, *L*, is related to the $\dot{Q}$ and the "diameter" of the fire via the expression:

$$\frac{L}{D} = 3.7\,\dot{Q}^{*2/5} - 1.02 \quad ; \quad \dot{Q}^{*} = \frac{\dot{Q}}{\rho_{\infty} c_p T_{\infty} \sqrt{gD} D^2} \tag{5.4}$$

which is valid for values of $\dot{Q}^{*}$, such that $0.12 < \dot{Q}^{*} < 1.2 \cdot 10^{4}$. Evaluating the constants, Heskestad [37] gives an expression that is approximately valid for most types of hydrocarbon pool fires:

$$L = -1.02\,D + 0.235\,\dot{Q}^{2/5} \tag{5.5}$$

From this relationship, the sensitivity of the flame height to the $\dot{Q}$ can be inferred. Considering a small change in L, denoted as δL, leads to the following expression:

$$\frac{\delta L}{L} = \frac{2}{5}(1 + 1.02\,D/L)\,\frac{\delta \dot{Q}}{\dot{Q}} \tag{5.6}$$

For the experiments considered in this report, a representative relation between *D* and L is D ~ $\frac{1}{3}L$, so Eq. 5.6 is approximately equivalent to the following:

$$\frac{\delta L}{L} \sim \frac{1}{2} \frac{\delta \dot{Q}}{\dot{Q}} \tag{5.7}$$

and an uncertainty of 15% or 25% in the $\dot{Q}$, leads to an uncertainty of about 8% or 13%, respectively, in the flame height.

5.5 Gas Concentration

Most fire models assume that combustion product gases, once generated in the fire, are passively transported throughout the compartment. The major products of combustion, like CO_2 and water vapor, plus the major reactant, O_2, are generated, or consumed, in direct proportion to the burning rate, which is directly proportional to the $\dot{Q}$. The mass fraction of any species in the HGL is related to its yield times the mass entrained into the upper layer [39]:

$$Y_i = \frac{y_i \dot{m}}{\dot{m}_e} = \frac{y_i \dot{Q}}{\chi_a H_c \dot{m}_e} \tag{5.8}$$

where $\dot{m}$ is the fuel mass burning rate (equal to $\frac{\dot{Q}}{\dot{m}\chi_a H_c}$), and $\dot{m}_e$ is the mass entrained into the upper layer, which is approximately equal to the air entrained into the upper layer [39]):

$$\dot{m}_e = 0.0059 \dot{Q}\ Z/L \tag{5.9}$$

where *Z* is a vertical location above the surface of the fire below which air entrainment occurs and *L* is the flame height (for a fire burning in the open). Here, *Z* is taken as the location of the HGL, which can be approximated as the position the soffitt in a compartment fire with natural ventilation, and Z is always less than or equal to L by definition.

$$Y_i = \frac{y_i L}{0.0059 Z \chi_a H_c} \tag{5.10}$$

From this relationship, the sensitivity of Y_i to the HRR can be inferred. The terms other than *L* in the above equation represent parameters that are assumed to be constants for the ventilated compartment fire experiments that represent most of the experiments considered in this report. In fact, the combustion efficiency and the values of y_i are functions of fire conditions in the compartment, particularly when the fire is under-ventilated. Considering a small change in Y_i, denoted as δY_i, leads to the following expression:

$$\frac{\delta Y_i}{Y_i} = \frac{\delta L}{L} \approx \frac{1}{2} \frac{\delta \dot{Q}}{\dot{Q}} \tag{5.11}$$

and from Eq. 5.11, the uncertainty in the change of a gas species in the HGL is can be related to the uncertainty in $\dot{Q}$. An uncertainty of 15% in the HRR, leads to a change of about 8% in the CO_2 and O_2 volume fractions.

5.6 Smoke Concentration

Smoke, or soot, is a product of incomplete combustion. Once formed, the smoke is transported with other combustion products. Smoke particulate is not a gas, but a complex solid, of which the form and concentration depend on the type of fuel and ventilation conditions within the compartment. Nonetheless, a simple assumption used in many zone and field fire models is that smoke is transported in the same way as gas products. The soot generation rate or soot *yield per unit fuel mass,* y_s, is difficult to predict, and the fire models are subject to error attributable to uncertainty in the prescribed soot yield. The soot yield for BE #3 was reported as 1.5 ±18% for heptane [5]. This uncertainty, however, is a measurement uncertainty and omits changes in chemistry that may occur, for example, during an underventilated compartment fire. In the upper layer of a compartment fire, the mass of soot per unit volume, M_s, is equal to the product of the mass fraction of soot (Y_s) and the density (ρ) of the HGL:

$$M_s = \rho Y_s \tag{5.12}$$

Considering a small change in M_s, denoted as δM_s, and using the chain rule:

$$\frac{\delta M_s}{M_s} = \frac{\delta \rho}{\rho} + \frac{\delta Y_s}{Y_s} \tag{5.13}$$

The relation between $\frac{\delta Y_i}{Y_i}$ and $\frac{\delta \dot{Q}}{\dot{Q}}$ is given by Eq. 5.11. A term for the uncertainty in the soot yield ($\frac{\delta y_s}{y_s}$), which arises from Eq. 5.10 must also be considered. The relation between the change in the density and the HRR is determined from the ideal gas law, as follows:

$$\frac{\delta \rho}{\rho} \sim \frac{\delta (1/T)}{(1/T)} = - \frac{\delta T}{T} \tag{5.14}$$

From Eq. 5.1, $\delta T \approx 2/3\ \dot{Q}^{-1/3}\ \delta \dot{Q}$, so the following relationship exists:

$$\frac{\delta T}{T} = 2/3\ (1 - \frac{T_\infty}{T_g})\ \frac{\delta \dot{Q}}{\dot{Q}} \tag{5.15}$$

Substituting Eqs. 5.11, 5.14, and 5.15 into 5.13 yields the following relationship:

$$\frac{\delta M_s}{M_s} = [\ 2/3\ \frac{T_\infty}{T_g} - 1/6]\ \frac{\delta \dot{Q}}{\dot{Q}} + \frac{\delta y_s}{y_s} \tag{5.16}$$

An uncertainty in $\dot{Q}$ leads to an uncertainty in M_s that is dependent on the ratio of the (absolute) ambient temperature to the gas temperature. For T_g equal to 200 °C (473 K), an uncertainty of 15% in $\dot{Q}$ leads to an uncertainty of about 4%, in M_s. In this example, a value of 200 °C (473 K) was selected for T_g, because it represents a typical HGL temperature during the BE #3 tests. The uncertainty attributable to heat release rate is, therefore, small, and the dominant contributor is uncertainty in the soot yield.

5.7 Pressure

In a closed compartment, the average pressure, p_0, is governed by the following equation:

$$\frac{dp_0}{dt} = \frac{\gamma - 1}{V}\left(\dot{Q} - \dot{Q}_{\text{loss}}\right) - \frac{\gamma\, p_0}{\text{V}}\left(\dot{V}_{\text{out}} - \dot{V}_{\text{in}} + \dot{V}_{\text{leak}}\right) \tag{5.17}$$

Here, γ is the ratio of specific heats (about 1.4), V is the volume of the enclosure, $\dot{Q}_{\text{net}} = \dot{Q} - \dot{Q}_{\text{loss}}$ is the net rate of energy heating up the gases in the compartment, and the $\dot{V}$ terms are the volume flow out of the compartment attributable to the exhaust, the volume flow into the compartment caused by a fan, and the leakage, respectively. The volume flow rate attributable to leakage is as follows:

$$\dot{V}_{\text{leak}} = A_{\text{leak}} \sqrt{\frac{2\,(p_0 - p_\infty)}{\rho_\infty}} \tag{5.18}$$

where A is the leakage area. The maximum compartment pressure is achieved when the pressure rise in Eq. 5.17 is set to zero. Rearranging terms, the maximum pressure in the compartment can be estimated as follows:

$$(p_0 - p_\infty)_{\max} \cong \frac{\rho_\infty}{2}\left(\frac{(\gamma - 1)\,\dot{Q}_{\text{net}} - \gamma\, p_\infty \dot{V}_{\text{vent}}}{A_{\text{leak}}\, \gamma\, p_\infty}\right)^2 \tag{5.19}$$

The term $\dot{V}_{\text{vent}}$ is the net ventilation volume flow. The expression for the maximum pressure can be used to estimate the uncertainty in the model prediction to changes in the measured HRR, net ventilation volume flow, and leakage area.

The compartment pressure was considered using data from BE #3 only. The uncertainty in A_{leak} for the open-door experiments was very small; however, for the closed door tests, an uncertainty of 10% to 15% is expected [5]. The uncertainty in $\dot{Q}_{net}$ is dominated by uncertainty in $\dot{Q}$. In the absence of forced ventilation, an uncertainty of 15% in the $\dot{Q}$ leads to an uncertainty of 30% in pressure. For the closed door tests with ventilation, the uncertainty in $\dot{V}_{\text{vent}}$ is difficult to characterize because the mechanical flows were generally not well-characterized in the experiments. It is estimated that an uncertainty of 30% is not unreasonable, leading to an uncertainty of about 75% in pressure for the closed-door vented condition.

5.8 Heat Flux

5.8.1 Emitted by the Fire

The total radiative emission from a fire can be related to the fire heat release rate ($\dot{Q}$) and its radiative fraction ($\chi_{rad;}$ see Eq. 3.2). At a distance greater than five fire base diameters away from the fire, the radiative heat flux ($\dot{q}''$) onto surfaces oriented in a direction normal to the fire can be estimated using the point source approximation, as follows:

$$\dot{q}'' = \chi_{rad}\, \dot{Q} / 4\pi r^2 \tag{5.20}$$

where r is the distance from the target to the center of the fire. Considering Eq. 5.20, the change in $\dot{q}''$ is related to the following expression:

$$\delta\dot{q}'' = \delta(\chi_{rad}\, \dot{Q} / 4\pi r^2) \tag{5.21}$$

and the fractional change in ($\frac{\delta\dot{q}''}{\dot{q}''}$) becomes the following:

$$\frac{\delta\dot{q}''}{\dot{q}''} = \frac{\delta\dot{Q}}{\dot{Q}} + \frac{\delta x_{rad}}{x_{rad}} - 2\frac{\delta r}{r} \tag{5.22}$$

In the near-field, Eq. 5.20 would be modified by a constant, depending on the view factor, and Eq. 5.22 would be unaffected. An expanded relative uncertainty of 16% to 30% is typical for χ_r (see Table 2-1), and an uncertainty in r is relatively small, typically less than 1%. The total uncertainty is taken as the quadrature of its components, so an uncertainty of 15% in $\dot{Q}$ and 16% in χ_{rad} leads to a combined expanded uncertainty of about 22% in $\dot{q}''$.

5.8.2 Emitted by a Hot Upper Layer

In a large compartment at distances far from the fire, the radiative heat flux ($\dot{q}''$) would become small because of the ($1/ r^2$) term in Eq. 5.20. Then, the radiative flux emitted by the hot upper layer of a fire would become relatively more important. The radiative heat flux onto surfaces in the upper layer is nearly equal to $\varepsilon\, \sigma\, T_g^4$, where ε is the effective emissivity of the upper layer, $\sigma = 5.67 \times 10^{11}$ kW/m^2/K^4, and T_g is the upper layer gas temperature in Kelvin. Considering a small change in the flux, $\dot{q}''$, denoted as $\delta\dot{q}''$, leads to the following:

$$\delta\dot{q}'' = 4\, \varepsilon\sigma T^3\, \delta T \tag{5.23}$$

The fractional change in $\dot{q}''$, ($\frac{\delta\dot{q}''}{\dot{q}''}$) is expressed as follows:

$$\frac{\delta\dot{q}''}{\dot{q}''} = 4\, \frac{\delta T_g}{T_g} = 8/3\, \frac{\delta\dot{Q}}{\dot{Q}} (1 - \frac{T_\infty}{T_g}) \tag{5.24}$$

so an uncertainty of 15% in $\dot{Q}$ leads to an uncertainty of about 15% in $\dot{q}''$ for T_g equal to 200 °C (473 K), typical of the HGL temperature during the BE #3 tests. For BE #4, the temperature was much higher (~1000 K), and the 25% uncertainty in the $\dot{Q}$ leads to an uncertainty of about 50% in $\dot{q}''$.

5.9 Wall/Target Surface Temperature

The surface temperature of the walls and targets is a function of the heat flux, the thermophysical and optical properties of the material, and its temperature. A simplistic approach to uncertainty considers a well-insulated wall or ceiling surface in the optically thick HGL of a compartment fire. After steady-state is reached, uncertainty in the $\dot{Q}$ leads to uncertainty in the HGL temperature, which translates into uncertainty of the surface or target temperature. An uncertainty in the $\dot{Q}$ of 15% corresponds to uncertainties of 10% in the upper layer and wall temperatures.

5.10 Summary

The empirical correlations described in this chapter provide insights for calculating the uncertainty in the model outputs resulting directly from the uncertainty in key input parameters. For example, a two-thirds power dependence of HGL temperature on the $\dot{Q}$ means that the uncertainty in the predicted HGL temperature is about two-thirds the uncertainty in the measured $\dot{Q}$. This uncertainty does not include the measurement uncertainty. For example, it does not include whatever error is associated with the TC itself. For many of the measured quantities under consideration, the *model input uncertainty* is greater than the *measurement uncertainty* as discussed in the next chapter.

Table 5-1 lists the measured quantities, along with the parameters by which they are most influenced. The last column in the table lists the uncertainties in the given quantity based on the combined uncertainty of the key parameters. For illustrative purposes, the propagated model input uncertainty results, U_m, shown in the table is based on an expanded (2σ) uncertainty of 15% for the $\dot{Q}$, although this value actually varied from 15% to 25% for the six test series (see Table 2-1). The resulting values of the propagated uncertainty for the various parameters should be regarded as the expanded value.

Table 5-1: Summary of the Model Sensitivity, $\tilde{U}_M$, to Uncertainty in the Heat Release Rate ($\dot{Q}$)

Quantity	Input Parameter	Power Dependence	Expanded Uncertainty, $\tilde{U}_M$ (%)
HGL Temperature, T_g	$\dot{Q}$	$2/3$	10
HGL Depth, z	$\dot{Q}, A, H$	Eq (5.4)	-1
Ceiling Jet Temperature	$\dot{Q}$	$2/3$	10
Plume Temperature	$\dot{Q}$	$2/5 \quad 1.3 < z/D^* < 3.3$ $2/3 \quad 3.3 < z/D^*$	6 10
Flame Height	$\dot{Q}$, D	½	8
Gas Concentrations	$\dot{Q}$	½	8
Smoke Concentration	$\dot{Q}$, y_s	Eq (5.16), 1	18 **
Pressure	$\dot{Q}$, A_{leak}, $\dot{V}_{vent}$	2, 2, 2	no forced ventilation: 30 with ventilation: 75
Heat Flux, $\dot{q}''$	$\dot{Q}$, χ_{rad}	from fire: Eq. 5.22 from upper layer: Eq. 5.24	22 15 **
Surface/Target Temperature	$\dot{Q}$	2/3	10

* actual uncertainty in the $\dot{Q}$ varied from 15% to 25% among the experiments, and there was also some variation among the tests for a single experimental series (see Table 2-1 and text).

** with T_g = 200 °C (392 °F).

6
REPRESENTATIVE UNCERTAINTIES

6.1 Summary of the Estimated Measurement Uncertainty and Subsequent Model Input Uncertainties

This section summarizes the estimated measurement and model input uncertainties. The uncertainties for each of the parameters of interest in each of the experimental series are listed in Tables 6-1 through 6-7. Each table contains information on the expanded (2σ) relative measurement uncertainty ($\tilde{U}_E$), the expanded (2σ) relative model input uncertainty associated with model input uncertainty ($\tilde{U}_M$), and the combined relative expanded (2σ) uncertainty (U_c), defined in Eq. 1.3 as $U_c = U_\varepsilon = (\tilde{U}_E{}^2 + \tilde{U}_M{}^2)^{½}$. The values of $\tilde{U}_E$ are taken from Tables 4-2 through 4-8. The values of $\tilde{U}_M$ are calculated using the formulas provided in Chapter 5 (e.g., Table 5-1). The values of the $\dot{Q}$ uncertainty for each experiment, which are used to determine $\tilde{U}_E$ and $\tilde{U}_M$, are taken from Table 2-1.

Table 6-1: Summary of the Relative Expanded Uncertainties Associated with the HGL Depth and Temperature Rise

Series	HGL Depth			HGL Temperature Rise		
	$\tilde{U}_E$ (%)	$\tilde{U}_M$ (%)	U_c (%)	$\tilde{U}_E$ (%)	$\tilde{U}_M$ (%)	U_c (%)
NBS	13	2	13	10 *	10	14
FM/SNL	35	2	35	16	13	21
BE #2	6	2	6	6	10	12
BE #3	9	2	9	5	11	12
BE #4	33	2	33	25	17	30
BE #5	8	2	8	4	10	11

* the value of $\tilde{U}_E$ does not accurately account for radiative exchange in Test 100A, in which natural gas was the fuel; its value is likely small (see text in Section 3.2.3).

Table 6-2: Summary of the Relative Expanded Uncertainties Associated with Ceiling Jet Temperatures

Series	Ceiling Jet Temperature Rise		
	$\tilde{U}_E$ (%)	$\tilde{U}_M$ (%)	U_c (%)
BE #3	12	11	16
FM/SNL	4	13	14

Table 6-3: Summary of the Relative Expanded Uncertainties Associated with Plume Temperatures

Series	Plume Temperature Rise (°C)		
	$\tilde{U}_E$ (%)	$\tilde{U}_M$ (%)	U_c (%)
BE #2 upper	9	10	14
BE #2 lower	11 *	10	15
FM/SNL	4	13	14
* the value of $\tilde{U}_E$ does not accurately account for radiative exchange; its value is likely small (see text).			

Table 6-4: Summary of the Relative Expanded Uncertainties Associated with HGL Carbon Dioxide and Oxygen Concentrations

Series	HGL CO_2 Concentration			HGL O_2 Concentration Decrease			LGL O_2 Concentration Decrease		
	$\tilde{U}_E$ (%)	$\tilde{U}_M$ (%)	U_c (%)	$\tilde{U}_E$ (%)	$\tilde{U}_M$ (%)	U_c (%)	$\tilde{U}_E$ (%)	$\tilde{U}_M$ (%)	U_c (%)
BE #3	4	8	9	4	8	9	4	8	9
BE #5	4	8	9	4	8	9	4	8	9

Table 6-5: Summary of the Relative Expanded Uncertainties Associated with Smoke Concentration and Compartment Pressure

Series	Smoke Concentration			Compartment Pressure		
	$\tilde{U}_E$ (%)	$\tilde{U}_M$ (%)	U_c (%)	$\tilde{U}_E$ (%)	$\tilde{U}_M$ (%)	U_c (%)
BE #3	28	20	33	27	30 (no vent) 75 (vent)	40 (no vent) 80 (vent

Table 6-6: Summary of the Relative Expanded Uncertainties Associated with Total Heat Flux to Targets and Rise in Target Surface Temperature

Series	Total Heat Flux to Targets			Rise in Target Surface Temperature		
	$\tilde{U}_E$ (%)	$\tilde{U}_M$ * (%)	U_c (%)	$\tilde{U}_E$ (%)	$\tilde{U}_M$ (%)	U_c (%)
BE #3	10	16	19	10	11	14
BE #4	10	47	48	10	13	16
BE #5	10	13	17	10	10	14

* $\tilde{U}_M$ is determined using Eq. 5.24, as this represents a smaller value, which is conservative in terms of model evaluation (see Chapter 5).

Table 6-7: Summary of the Relative Expanded Uncertainties Associated with Total Heat Flux and Rise in Surface Temperature

Series	Total Heat Flux			Rise in Surface Temperature		
	$\tilde{U}_E$ (%)	$\tilde{U}_M$ (%)	U_c (%)	$\tilde{U}_E$ (%)	$\tilde{U}_M$ (%)	U_c (%)
BE #3	10	16	19	10	11	14
BE #4	10	47	48	10	13	16
BE #5	10	13	17	10	10	14

6.2 Representative Uncertainties

Using engineering judgment, a weighted expanded combined uncertainty, U_{cw}, representative of the uncertainty for each of the parameters was estimated:

$$U_{cw} = \frac{1}{\sum_{i=1}^{6} n_i} \sum_{i=1}^{6} U_c \, n_i \qquad (5.1)$$

where the weighted average used the combined expanded uncertainties (U_c listed in Tables 6-1 through 6-6), and was based on the sum of the number of tests (n_i) (see Table 1-1) for the parameters of interest for each of the six test series (i). A weighted average based on the number of experimental tests was used (rather than some other weighting approach), because the model evaluation considered each of the 26 tests as independent trials (see Chapter 6 in Volumes 2 through 6). The number of experiments (and the associated number of tests) varied for each parameter. The weighted expanded combined uncertainty, U_{cw}, and the total number of tests ($\sum_{i=1}^{6} n_i$) for each of the parameters is shown in Table 6-8. Many of the tests were from BE #3 and, in this sense, the results from BE #3 strongly influenced the results.

Table 6-8: The Weighted Combined Expanded Uncertainty, U_{cw}, Determined from Eq. 5.1 and Tables 6-1 through 6-7

Quantity	Number of Tests	Weighted Expanded Combined Uncertainty, U_{cw} (%)
HGL Temperature Rise, T_g	26	14
HGL Depth, z	26	13
Ceiling Jet Temperature	18	16
Plume Temperature	6	14
Gas Concentrations	16	9
Smoke Concentration	15	33
Pressure	15	40 (no forced ventilation) 80 (with forced ventilation)
Heat Flux, $\dot{q}''$	17	20
Surface/Target Temperature	17	14

6.3 Conclusions

This evaluation used fire experiments as a way of establishing confidence in model predictions, and considered the effect of experimental uncertainty on both models and measurements. A literature search was also conducted to select experiments that would allow evaluation of key aspects of fire models. In general, the reports of experiments did not adequately address measurement uncertainty.

There may be many reasons for this, but one important reason is that the expense of performing a comprehensive uncertainty analysis is often larger than the cost of the measurement itself.

Without such analysis, however, the accuracy of fire measurements is unlikely to improve. Experimental design and execution must carefully address measurement uncertainty and, in particular, attempt to reduce the uncertainty in key experimental parameters, most notably the fire $\dot{Q}$. The ability to accurately and precisely measure $\dot{Q}$ requires a significant institutional investment, as a facility must be well-instrumented, its performance characterized, and the uncertainties analyzed and documented.

Because of the time and expense involved in conducting large-scale fire experiments, there is often a desire by the test laboratory to include as many measurements as possible. Unfortunately, much of the data go unanalyzed, either because the sponsoring organization needs only a relatively small subset of the data, or because the budget for the project is exhausted in preparing and executing the experiments. In any event, there is a tremendous amount of fire test data that has never been thoroughly analyzed or used for V&V. It should be noted that the number of measurements is less important than selecting the right measurements and ensuring that those measurements are of high quality (that is, accurate with well-characterized uncertainties).

In this study, measurement uncertainty was estimated for the experiments of interest using engineering judgment. The importance of the uncertainty in the $\dot{Q}$ was emphasized in this study, because this parameter drives the thermal environment in the model calculation results, and the calculation results are sensitive to the uncertainty of this parameter. Quantifying the uncertainty in $\dot{Q}$ provides a basis for understanding model sensitivity to this parameter, taken here as a representation of model input uncertainty.

To date, few fire model V&V studies have been based on ASTM E 1355, and even fewer have used experimental uncertainty as part of the analysis. The uncertainty in model output was assessed through consideration of the uncertainty in measured quantities that are used as input for the models. Both measurement uncertainty and model input uncertainty are found to be important and both contribute to the combined uncertainty. The information from this volume is used as a basis for the model evaluation, as discussed in Volumes 3 through 7 of this report.

7
REFERENCES

1. *Standard Guide for Evaluating the Predictive Capability of Deterministic Fire Models*, ASTM E 1355-05a, American Society for Testing and Materials, West Conshohocken, PA, 2005.
2. Nowlen, S.P., *Enclosure Environment Characterization Testing for the Base line Validation of Computer Fire Simulation Codes*, NUREG/CR-4681, SAND86-1296, U.S. Nuclear Regulatory Commission, Washington, DC, March 1987.
3. Peacock, R.D., S. Davis, and B.T. Lee, *Experimental Data Set for the Accuracy Assessment of Room Fire Model*, Report NBSIR 88-3752, National Bureau of Standards, Gaithersburg, MD, April 1988.
4. Hostikka, S., M. Kokkala, J. Vaari, "Experimental Study of the Localized Room Fires," NFDC2 Test Series, VTT Research Notes 2104, 2001.
5. Hamins, A., A. Maranghides, E. Johnsson, M. Donnelly, J. Yang, G. Mulholland, and R. Anleitner, *Report of Experimental Results for the International Fire Model Benchmarking and Validation Exercise #3*, NIST Special Publication 1013-1, National Institute of Standards and Technology, Gaithersburg, MD, 2005.
6. Klein-Heßling, W., and M. Röwenkamp, *Evaluation of Fire Models for Nuclear Power Plant Applications: Fuel Pool Fire Inside a Compartment*, Gesellschaft für Anlagen-und Reaktorsicherheit (GRS), Köln, Germany, May 2005.
7. Riese, O., and D. Hosser, *Evaluation of Fire Models for Nuclear Power Plant Applications: Flame Spread in Cable Tray Fires*, Draft Version, Revision 1, Institut für Baustoffe, Massivbau und Brandschutz (iBMB), Braunschweig, Germany, June 2004.
8. *Guide to the Expression of Uncertainty in Measurement*, International Organization for Standardization, Geneva, Switzerland, 1993.
9. Taylor, B.N., and C.E. Kuyatt, *Guidelines for Evaluating and Expressing the Uncertainty of NIST Measurement Results*, NIST Technical Note 1297, National Institute of Standards and Technology, Gaithersburg, MD, 1994.
10. Lopez-Droguett, E., A. Mosleh, *Methodology for the Treatment of Model Uncertainty*, Technical Research Report, Center for Technology Risk Studies, University of Maryland, College Park, MD, April 2002
11. Bevington, P.R., *Data Reduction and Error Analysis for the Physical Sciences*, McGraw-Hill, NY, NY, 1969.
12. Coleman, H.W., and F. Stern, "Uncertainties and CFD Code Validation," *J. Fluids Eng*., 119:795–803, 1997.

13. Hogg, R.V., and E.A. Tannins, *Probability and Statistical Inference*, 2nd Ed., MacMillan, 1983.

14. NUREG/CR-5384, "A Summary of Nuclear Power Plant Fire Safety Research at Sandia National Laboratories, 1975–1987," U.S. Nuclear Regulatory Commission, Washington, DC, December 1989.

15. Nowlen, S.P., "Enclosure Environment Characterization Testing for the Base line Validation of Computer Fire Simulation Codes," NUREG/CR-4681, SAND86-1296, U.S. Nuclear Regulatory Commission, Washington, DC, March 1987.

16. Tewarson, A., *Prediction of Fire Properties of Materials*, Part 1, NBS-GCR-86-521, National Bureau of Standards, Gaithersburg, MD, December 1986.

17. Tewearson, A., Chapter 4, Section 3, "Generation of Heat and Chemical Compounds in Fires," *The SFPE Handbook of Fire Protection Engineering*, 3rd Ed. (P.J. DiNenno, D. Drysdale, C.L. Beyler, and W.D. Walton, eds.), National Fire Protection Association and The Society of Fire Protection Engineers, Quincy, MA, 2003.

18. Hamins, A., M. Maranghides, and G. Mulholland, *The Global Combustion Behavior of 1 MW to 3 MW Hydrocarbon Spray Fires Burning in an Open Environment*, Internal Report NISTIR 7013, National Institute of Standards and Technology. Gaithersburg, MD, June 2003.

19. Hamins, A., M. Klassen, J. Gore, and T. Kashiwagi, "Estimate of Flame Radiance via a Single Location Measurement in Liquid Pool Fires," *Combust. Flame*, 86:223–228. 1991.

20. *Fire Modeling Code Comparison*, TR-108875, Electric Power Research Institute, Palo Alto, CA.

21. McGrattan, K.B., and G.P. Forney, "Fire Dynamics Simulator (Version 4): User's Guide," Internal Report NISTIR 1019, National Institute of Standards and Technology, Gaithersburg, MD, March 2006.

22. Hamins, A., T. Kashiwagi, and R. Buch, "Characteristics of Pool Fire Burning," *Fire Resistance of Industrial Fluids*, ASTM STP 1284, Publication Number 04-012840-12 (G. Totten and J. Reichel, eds.), American Society for Testing and Materials, West Conshocken, PA, pp. 15–41, 1995.

23. Bryant, R., T. Ohlemiller, E. Johnsson, A. Hamins, B. Grove, W.F. Guthrie, A. Maringhides, and G. Mulholland, "The NIST 3 Megawatt Quantitative Heat Release Rate Facility - Procedures and Guidance," NIST Special Publication 1007, National Institute of Standards and Technology, Gaithersburg, MD, December 2003.

24. Axelsson, J., P. Andersson, A. Lonnermark, P. VanHees, and I. Wetterlund, *Uncertainties in Measuring Heat and Smoke Release Rates in the Room/Corner Test and the SBI*, SP Report 2001:04 SP Swedish National Testing and Research Institute, Boras, Sweden, 2001.

25. Enright, P.A., and Fleischmann, C.M., "Uncertainty of Heat Release Rate Calculation of the ISO5660-1 Cone Calorimeter Standard Test Method," *Fire Technology*, 35:153–169, 1999.

26. Yeager, R.W., "Uncertainty Analysis of Energy-Release Rate Measurement for Room Fires," *J. Fire Sciences*, 4:276–296, 1986.

27. Janssens, M.L., *Variability in Oxygen Consumption Calorimetry Tests*, (1427), American Society for Testing and Materials, pp. 147–162, 2002.

28. Blevins, L.G., *Behavior of Bare and Aspirated Thermocouples in Compartment Fires*, Proceedings of the 33rd National Heat Transfer Conference, Albuquerque, NM., August 15–17, 1999.

29. Pitts, W.M., E. Braun, R.D. Peacock, H.E. Mitler, E.L. Johnsson, P.A. Reneke, and L.G. Blevins, *Temperature Uncertainties for Bare-Bead and Aspirated Thermocouple Measurements in Fire Environments*, Internal Report NISTIR 6242, National Institute of Standards and Technology (NIST), Gaithersburg, MD, October 1998.

30. Appendix B, "Thermocouple Characteristics," *The Temperature Handbook*, OMEGA Engineering Inc., 2000.

31. Hamins, A., A. Maranghides, K. McGrattan, T. Ohlemiller, and R. Anleitner, *Federal Building and Fire Safety Investigation of the World Trade Center Disaster: Experiments and Modeling of Multiple Workstations Burning in a Compartment*, NIST Special Publication NCSTAR 1-5E, National Institute of Standards and Technology, Gaithersburg, MD, June 2005.

32. Mulholland, G.W., and C. Croakin, "Specific Extinction Coefficient of Flame Generated Smoke," *Fire and Materials*, 24:227–230, 2000.

33. Bryant, R., C. Womeldorf, R. Johnsson, T. and Ohlemiller, "Radiative Heat Flux Measurement Uncertainty," *Fire and Materials*, 27:209–222, 2003.

34. Pitts, W.M., A.V. Murthy, J.L. de Ris, J.-R. Filtz, K. Nygård, D. Smith, and I. Wetterland, *Round Robin Study of Total Heat Flux Gauge Calibration at Fire Laboratories*, Special Publication 1031, National Institute of Standards and Technology, Gaithersburg, MD, October 2004.

35. Walton, W.D., and P.H. Thomas, Chapter 6, Section 3, "Estimating Temperatures in Compartment Fires," *The SFPE Handbook of Fire Protection Engineering*, 3rd Ed. (P.J. DiNenno, D. Drysdale, C.L. Beyler, and W.D. Walton, eds.), National Fire Protection Association and The Society of Fire Protection Engineers, Quincy, MA, 2003.

36. Alpert, R.L., Chapter 2, Section 2, "Ceiling Jet Flows," *The SFPE Handbook of Fire Protection Engineering*, 3rd Ed. (P.J. DiNenno, D. Drysdale, C.L. Beyler, and W.D. Walton, eds.), National Fire Protection Association and The Society of Fire Protection Engineers, Quincy, MA, 2003.

37. Heskestad, G., Chapter 1, Section 2, "Fire Plumes, Flame Height and Air Entrainment," *The SFPE Handbook of Fire Protection Engineering*, 3rd Ed. (P.J. DiNenno, D. Drysdale, C.L. Beyler, and W.D. Walton, eds.), National Fire Protection Association and The Society of Fire Protection Engineers, Quincy, MA, 2003.

38. Heskestad, G., "Luminous Heights of Turbulent-Diffusion Flames," *Fire Safety J.*, 5:103–108, 1983.

39. Milke, J.A., Chapter 13, Section 4, "Smoke Management in Covered Malls and Atria," *The SFPE Handbook of Fire Protection Engineering*, 3rd Ed. (P.J. DiNenno, D. Drysdale,

C.L. Beyler, and W.D. Walton, eds.), National Fire Protection Association and The Society of Fire Protection Engineers, Quincy, MA, 2003.

A TIME AVERAGING

Figure A-1 shows various periods used to time-average heat flux data acquired at 1 Hz for Gauge 9 during Test 13 of BE #3. The time response of the measurement itself is on the order of 1 s. The data used in this report were averaged over a 10 s period. Time averaging the data over too long a period may cause the loss of legitimate data and valuable information. No time-averaging at all, causes signal noise to play a role in the determination of peak values. This issue would have less significance if there had been many report experiments, and a statistically large number of peak values had been determined for one set of experimental conditions, but this was not the case. The selection of a 10 s averaging period is a compromise, but appears to be reasonable for the types of measurements considered in this report.

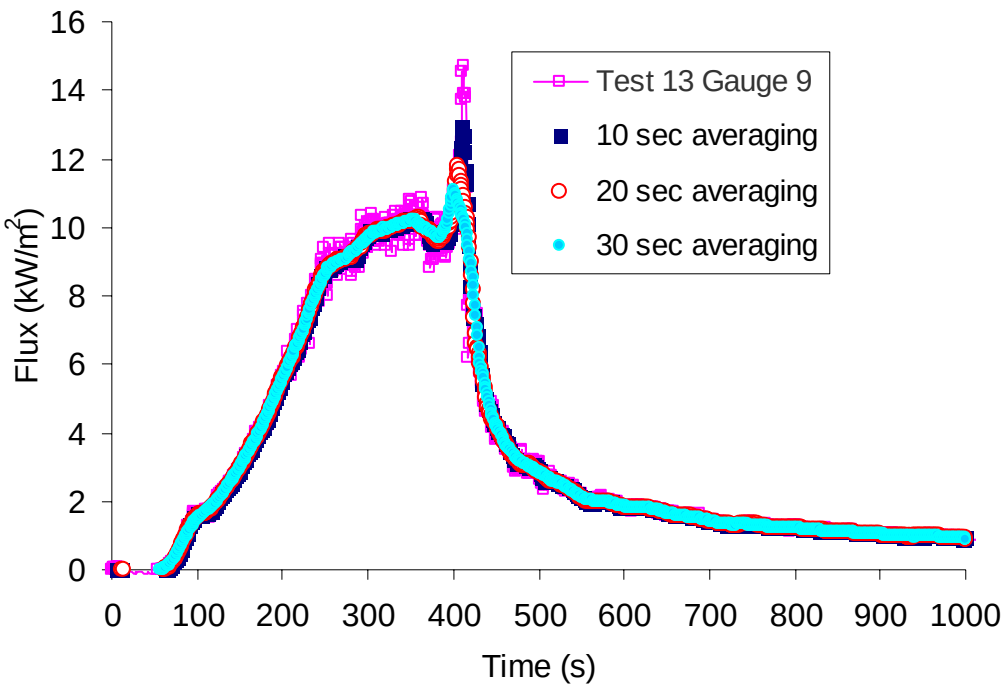

Figure A-1: Various Periods Used To Time Average Heat Flux Data Acquired at 1 Hz for Gauge 9 During Test 13 of BE #3